CHALMERS
UNIVERSITY OF TECHNOLOGY

Exploratory approach to examination of synthetic clay tennis courts properties

Master Thesis

PANAGIOTA PAPADOPOULOU

Department of Industrial and Materials Science
CHALMERS UNIVERSITY OF TECHNOLOGY
Gothenburg, Sweden 2017

MASTER THESIS IN PRODUCT DEVELOPMENT

Exploratory approach to examination of synthetic clay tennis courts properties

DEPARTMENT OF INDUSTRIAL AND MATERIALS SCIENCE
CHALMERS UNIVERSITY OF TECHNOLOGY
GÖTEBORG, SWEDEN

SEPTEMBER 2017

Abstract

Tennis is a racquet sport introduced in 1873 by Walter Clopton Wingfield. It can be played on various types of surfaces with the most popular being clay, grass and hard courts. Each surface provides a distinct response and playing characteristics with clay court being among the most preferable surfaces due to its lower rate of injury reports. However, its high maintenance demands and dependence of playability on climate conditions, have led to the creation of synthetic clay courts, which consist of a carpet base with infill material on top. Synthetic clay tennis court properties need to be examined and modified to converge towards playing characteristics of natural clay tennis court.

This thesis was conducted in collaboration with Chalmers Sports and Technology and aimed to enhance understanding of synthetic clay courts behaviour and to investigate their compressive and frictional properties. Three distinct carpets and ceramic sands were tested under cyclic loading to identify differences between various carpet-material combinations. The specimens were uniaxially compressed up to 2 kN at 200-400 N/s loading rates and at different number of cycles. Energy transformation, strain accumulation, step of strain accumulation and moduli of each surface combination were calculated. Results supported that measurements were affected by loading rate and that carpet modification influenced energy transformation and strain accumulation, while material change affected additionally moduli of the system.

Additionally, repetitive sliding movements, in a synthetic clay tennis court, were recorded by Xsens motion capture system and data was used to identify kinematic characteristics of the sliding movement and to program a robot to imitate that motion. The sliding motion was evaluated both in a whole and in a cut shoe sample, at various initial normal loads, velocity patterns and volume of ceramic sand. Results showed that forces developed and utilized coefficients of friction were affected by those parameters' changes and further investigation is needed to identify how they correlate. An interview with Magnus Gustafsson, who is a former professional tennis player, contributed to the connection of results and player's perspective.

This Thesis is an initial approach to clay courts investigation and provides information on how surface responds when the carpet and/or the infill material are modified. The results could be used to identify differences between surfaces, interpret the player's perception with quantitative data and contribute to the initial modelling of the synthetic clay surface.

Keywords: tennis, clay court, compression, friction, motion capture system, robot

Contents

Acknowledgements

First of all, I would like to thank my supervisors Associate Professor Dr. Erik Hulthén and Associate Professor Dr. Magnus Karlsteen for giving me the opportunity to participate in the tennis project and supporting me throughout the process.

I would also like to thank Marcus Johansson who helped me and participated in the experiments. I wish to thank to Magnus Gustafsson (Unisport) and Marius Malek (PlayItGlobal) for providing the testing materials and Magnus Gustafsson for his active participation in the biomechanical tests.

Thanks to Associated Researcher Johannes Quist for his ideas and support during the conduction of the compression experiments, and to Phd student Ilker Erdem for his help with the friction test and for borrowing me his force sensor for the tests. Thanks to Research Engineer Hans Sjöberg for creating the necessary equipment for the friction test and to Research Engineer Per Nyqvist who set up and handled the robot arm throughout the experiments. Without him the friction test would not be possible.

Thanks to my family, and especially my grandma, who believed in me and supported me throughout my studies and to Rostyk for his support and help.

Panagiota Papadopoulou

Gothenburg 2017

1. Introduction

1.1 Tennis

Tennis was introduced in its recent form in 1873 by Walter Clopton Wingfield while there are references for a similar game in France in the 12th century. Tennis is played in a rectangular court, which can exhibit many possible types of upper surface, and it includes a net and boundary lines. The necessary equipment consists of a racquet and a ball. Tennis can be played by one player or a team of two players, whose purpose is to win points by hitting the ball with their racquet over the net to the opponent's territory without them being able to return the ball within the set boundaries [1]. The winner of the match is whoever reaches first 2 (best of 3) or 3 sets (best of 5) depending on the tournament type.

International Tennis Federation (ITF) is the governing body of tennis and it is responsible to develop the rules and specifications of the game and contribute to its improvement. The court's dimensions and the racquet's and ball's characteristics (shape, dimensions, weight, and technology) are regulated by ITF and they are described in the "ITF Rules of Tennis" manual [2].

In Sweden, the Swedish Tennis Association was formed in 1906 and is in charge of the conduction and development of tennis in the country. Tennis is very popular with 506765 recreational players, 440 clubs and 4400 courts registered in the whole country [3]. In 2016, there were 11546 licensed players, 6687 juniors and 4859 seniors, of which 7609 were active. The female proportion of players was just over 28% (28.51) [4]. Due to weather conditions in Sweden, tennis is mostly played in indoor courts and outdoor courts are mainly used during summer. Each tennis court's type exhibits different playing attributes and maintenance needs and research should be conducted to understand and regulate the properties of the courts and to assure the desirable conditions at the right time.

1.2 Tennis Court Classification

The variety of tennis surfaces which present different playing characteristics, led to the need of a classification system. ITF categorizes tennis courts based on the type (Table 1) and the Court Pace Rating (CPR). The CPR is extracted according to the coefficient of friction (COF) and the coefficient of restitution (COR) and based on that the court is categorized as slow, medium-slow, medium, medium-fast, and fast [2]. The most commonly used surfaces on tournaments are grass, clay and acrylic courts.

Table 1. ITF Court type characterization [2].

Type	Description
Acrylic/Polyurethane	Textured, pigmented, resin-bound coating.
Artificial clay	Sand-dressed and/or rubber-dressed surface with the appearance of clay.
Artificial grass	Synthetic surface with the appearance of natural grass.
Asphalt	Bitumen-bound aggregate.
Carpet	Textile or polymeric material supplied in rolls or sheets of finished product.
Clay	Unbound mineral aggregate.
Concrete	Cement-bound aggregate.
Grass	Natural grass grown from seed.
Hybrid clay	Clay-dressed systems supported by a carpet matrix.
Other	E.g. modular systems (tiles), wood, canvas.

Clay court (Figure 1) is classified as the slowest court, producing the longest rallies compared to the other types. The lowest injury rates reported on it, make it a desirable surface for both professional and recreational players [5]. Clay courts have three possible variations, the natural clay court consisting of unbound mineral aggregate, originally crushed bricks, and two synthetic, the hybrid clay and the artificial clay which use a carpet base, dressed with clay and sand (and/or rubber), respectively. The benefit of the synthetic clay courts is their combination of lower maintenance costs with playability in all weather conditions.

Figure 1. Clay Tennis court [6].

In Figure 2, the layered structure of a synthetic clay court is presented. The base, which can be porous concrete or draining asphalt, an adhesive layer, the carpet and the infill material with the lines. The carpet is produced in rolls and it is glued on top of the base and then rolling is performed to obtain a higher quality result.

Figure 2. The synthetic clay court's components [6].

The main two components of the synthetic clay court which can be altered, influencing the court's properties, are the carpet and the infill material. The main characteristics of the carpet are its material, the pattern of the surface and whether and how it is glued or not. As far as the infill material is concerned, its type (mineralogy) and its particles' size, distribution and shape are parameters that should be considered.

Multiple carpets can be used in synthetic clay courts. Each carpet contributes differently to the behaviour and response of the court during dynamic tennis movements. In Figure 3, the three specific carpets examined in this thesis are presented, which exhibit varying patterns and way of gluing.

(a)

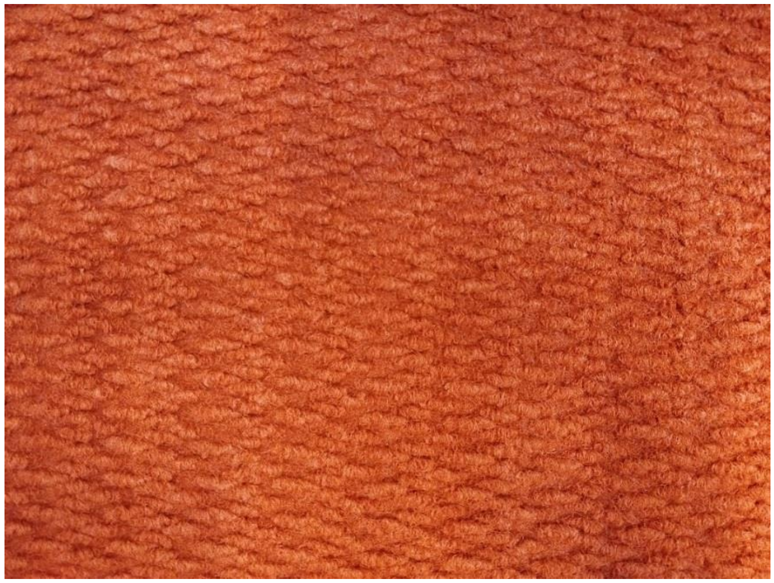

(b)

(c)

Figure 3. Three different carpets used in clay tennis courts. (a) Partially glued with swiss cross pattern, (b) fully glued with fishbone pattern, (c) locally glued with oval diagonal pattern.

The infill material is poured upon the carpet, and then it is distributed evenly throughout the court, so that a surface with similar playing characteristics will be produced. In Figure 4, the carpet material combination and the way shoe marks are formed during playing are shown.

Figure 4. Tennis Carpet with material on top.

1.3 Design and maintenance of tennis courts

Design

The design of a synthetic clay court should be examined around three main aspects [7]:

- Surface functionality
- Athlete's protection
- Technical characteristics of the court

The surface functionality refers to the optimal player-surface and ball-surface interaction. The player-surface interaction can be described by the shock absorption, the deformation and the friction of the surface, whereas the ball-surface interaction examines the ball rebound, roll and spin in order to follow the ITF Standards. The protection of the athlete refers to the choice of materials that do not subject the player to excessive forces, slip or premature fatigue and limit the risk of injuries while maintaining the performance of the surface. The technical characteristics of the surface analyse the court evenness, drainage, slope and planarity as well as the maintenance procedures in order to assure uniformity on the court and long term usage [7].

Maintenance

From the maintenance perspective, the courts which are filled with normal clay [6]:

- They should be brushed at least once per day, so that the infill material will be distributed evenly and all leaves and dirt will be removed.
- Their moisture content should be controlled and the court should be kept damp for optimal playing conditions.
- Additional material may be required according to the court's usage, the players' preferences and the weather conditions (wind, rain, humidity).

- After 3-5 years parts of the infill material may need renewal which can be conducted by high pressure machines and the placement of new material.

When the court is filled with ceramic sand, maintenance needs are almost zero.

1.4 Unisport and Play it Global

The project was carried out with the assistance of Magnus Gustafsson and Marius Malek, who represent Unisport and Play It Global companies, respectively. Their role was to assist with the evaluation of the clay court from the player's perspective and from the installation and maintenance point of view, and to provide information regarding the synthetic clay courts they produce. They also provided the carpets, the infill material, and the tennis shoes for the testing.

Unisport was founded in 1993 and it is a market leader in sports facilities in the Nordic countries. In the tennis field, they offer consultancy, installation of new tennis courts or renovation of existing ones. Play it Global is the international distributor of Play it s.r.l., which was established in 1996 and it refers to tennis court surfaces.

1.5 Problems encountered in tennis courts

Problems in clay tennis courts can be categorised as design and as maintenance problems.

A) The **design** issues may refer to:

1) the choice of materials which lead to:

- Excessive slipperiness or grip of the surface, jeopardizing the safety of the athlete
- Excessive stiffness or compliance of the surface, where the athlete experiences higher peak loads or muscles' fatigue, respectively, and the ball's bounce may not be optimal.

2) construction issues which can cause court's unevenness and inadequate drainage, which could be a major issue in the rainy climate of Sweden

B) The **maintenance** issues may refer to:

- Excessive or inadequate watering of the surface
- Quick wear of the carpet
- Excessive compaction of the surface

2. Objectives

2.1 Research Outline

The purpose of this project is to understand the behaviour of the synthetic clay courts and to investigate their compressive and frictional properties. A three point exploratory approach was used by conducting lab experiments to the infill material and the carpet-material system, alongside with biomechanical testing in full scale courts.

The synthetic clay tennis court project was implemented within Chalmers Sports & Technology and it was a Master Thesis work carried out over an 8-month period. The project's design and formulation were performed based on parts of "The Value Model" method [8] and its objective was to evaluate the response of different carpet-material combinations considering the player-surface interactions and the maintenance aspects, based on an experimental data and interview with an expert.

2.2 Research Questions

Three research questions were formed based on the research outline of the thesis.

- What are the parameters that influence the compressive behaviour of the clay court?
- Is it possible to quantify the compressive behaviour of the clay court with cyclic axial compression tests?
- What are the parameters that influence the frictional behaviour of the clay court?
- In it possible to measure the frictional properties of the clay court by using a robot?
- How does the carpet-material combination affect the response of the court and is it possible to choose the best combination from player's perspective?

2.3 Limitations

This project did not consider:

- Construction issues
- Weather effects such as response of the court with varying moisture content
- Wear of the carpet

The approach to the project is also exploratory, which means it is dependent upon test equipment available.

3. Literature Review

The synthetic clay court surface consists of two components, the carpet and the material. The parameters that should be considered regarding the material selection are the type (mineralogy), the particle size, the particle size distribution, the shape and the infill volume. As far as the carpet is concerned, its material, pattern and the used adhesions should be examined. In order to characterize a clay court, its stiffness and frictional properties should be analysed.

The impact absorption of sport surfaces has been previously studied by performing both mechanical and biomechanical tests. Mechanical tests include the Artificial Athlete Berlin, ASTM Standard test and Clegg Impact Hammer [9]. Artificial Athlete Berlin aims to simulate the impact forces a person experiences during a vertical jump [10]. A 20 kg mass is dropped on a spring and the exerted force is applied on a test foot which impacts on the testing surface. Peak impact force is measured and values are compared with the respective values of a rigid concrete surface [11, 12]. Tests on tennis court showed that it is not a reliable test method due to inconsistencies with the actual forces experienced by the athlete [13], whereas the ASTM test [14] for a given shoe-surface combination was proven reliable [15]. However, drop tests have as disadvantages that the results can depend on the test setting (dropping mass and dropping height and contact area) [16] and that they usually report only peak magnitudes and do not provide a complete view of the force-deflection curve [17]. This deficiency is being confronted with cyclic loading tests which examine the stress- strain curve of the material with applications in field hockey [18] and in natural turf sports surfaces [19]. The drawbacks with those methods are the restricted loading rates due to machinery limitations. In order to examine the surface under real circumstances a biomechanical approach has been proposed [20]. However, biomechanical testing are difficult to replicate and reproduce. Every method has benefits and disadvantages and they should be combined to get more accurate and representative results.

The frictional properties of clay courts have been previously measured with mechanical devices in conjunction with biomechanical tests and perception analyses [21-28]. Indicative devices used for the calculation of the surface's static and dynamic coefficients were the pendulum device, the Crab III device developed by the ITF and bespoke sled devices. However, the different applied loads and mechanism of the tests render the comparisons between the results untrustworthy [21, 23]. The biomechanical trials accompanied by the perception questionnaires aimed to quantify the sliding distance and velocities of the player in real tennis conditions and the variations in the slipperiness of surfaces [23]. Additionally, force data collection during in court movements, enabled the inspection of the loads and loading rates developed on the athlete during playing on surfaces with different friction characteristics [22, 24-27].

In Table 2, the biomechanical data for a specific tennis movement, running forehand (Figure 5), are examined.

Figure 5. Running forehand with sliding. Picture in article by John Evert [29].

Table 2. Biomechanical data for the forehand movement in different clay surfaces.

Parameters/movement type	Running Forehand		
	Carpet + Clay	Carpet + Sand	Clay
Peak Vertical GRF (N)	1824±393 [27] 1288±375 [30] 1331±365 [25]	1237±351 [25]	1351±379 [30]
Peak Horizontal GRF (N)	742±288 [27] 520±135 [25]	487±85 [25]	
Sliding Distance (m)			0.48±0.16 [23] 0.74±0.13 [23]
Utilized COF	0.53±0.13 [27] 0.46±0.04 [30] 0.42±0.04 [25]	0.42±0.02 [25]	0.46±0.04 [30]

It can be noticed that for every court type, the vertical forces developed were significantly higher than the horizontal. Later in this report values from the above table were used as reference to the experiments' set up. The less favourable scenario was adopted and therefore the vertical force was chosen to be 2 kN.

From the literature review, it can be mentioned that the majority of the impact tests were performed in athletic tracks, artificial turf and acrylic surfaces and there were very little information regarding the synthetic clay courts. Additionally, it was observed that there were scarce descriptions of the carpets used for testing and no reference on the influence of carpet's change on court's response.

4. Theoretical Background

4.1 Particle Size Distribution

A particle size distribution (PSD) analysis represents the analogy of the different particle sizes in the material. The shape of the curve (slopes) illustrates the grading of the granular materials whereas the position of the curve on the horizontal axis is an indicator of how fine or coarse the material is [31].
For coarse-grained soils the following two coefficient are used to describe the grading of the material.
Coefficient of Uniformity (C_U):

$$C_U = \frac{D_{60}}{D_{10}} \quad (1)$$

Coefficient of Curvature (C_c):

$$C_c = \frac{D_{30}^2}{D_{10} \cdot D_{60}} \quad (2)$$

Where D_n refers to the grain diameter at which n% of the material passes through a sieve.

The uniformity coefficient describes the slope of the line between those two points and it is used to describe the wideness of the distribution. The narrowest distribution is when C_U is equal to 1, which means that there is only one particle size in the material. Well graded are considered the sandy soils with $C_U > 4$ and $C_c = 1 - 3$ [32].

4.2 Loading Classification

The loading problems are distinguished into two main categories, the dynamic and the static (Figure 6). The characteristics that distinct them, are the time of loading and the number of the applied cycles [33]. The tests performed in this thesis belong to the quasi-static-regime because the time of loading was between 3-4 seconds and the inertia phenomena can be neglected.

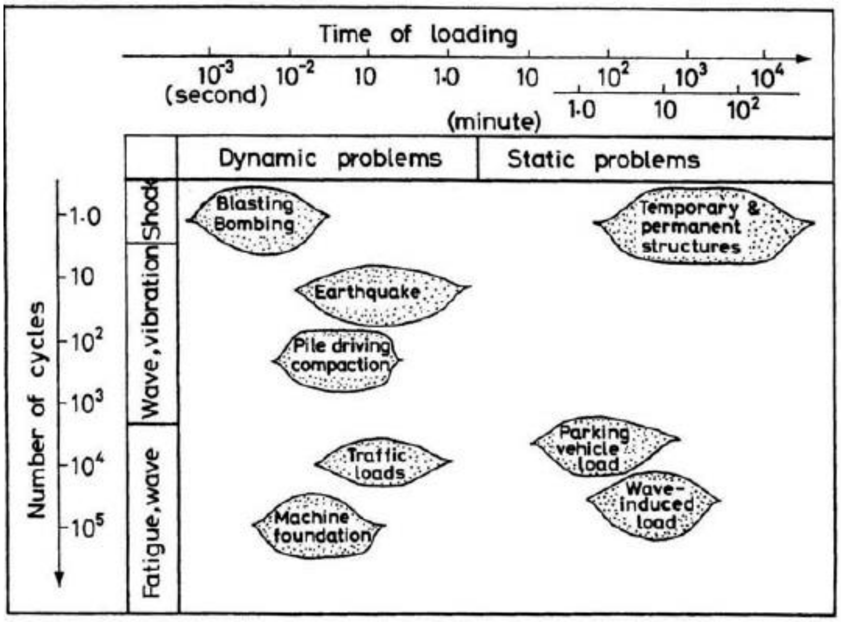

Figure 6. Loading Classification. Figure by Ishihara K. [33].

4.3 Soil Response to Cyclic Loading

The stress-strain response of the granular material under stressed controlled cyclic loading can be expressed in two different ways: adaptation and ratcheting. Adaptation (Figure 7 (a)) refers to the linear response of the material with no energy dissipation in steady state, exclusively for strain amplitudes lower than 1 to $3 \cdot 10^{-5}$ [34]. However, this behaviour is not possible since under dynamic loading a small damping ratio (1%) still exists even at very low strains [35]. Ratcheting is defined as any strain accumulation under cyclic loading which after the initial transient deformation, can be either finite (Figure 7 (b)) or infinite (Figure 7 (c)). In finite ratcheting (accommodation, "plastic shake down"), in steady state, the material develops a closed hysteretic loop. In that state, there is still energy dissipation but no additional plastic deformation. In infinite ratcheting, there is strain accumulation during each cycle which will eventually lead to the collapse of the material. The type of the response depends on the initial conditions and stress amplitude [34, 36, 37].

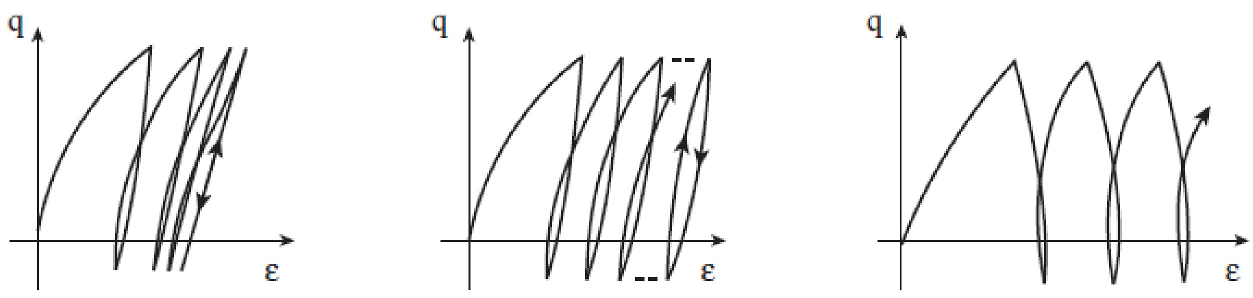

(a) (b) (c)

Figure 7. Cyclic behaviour of sand under stress-controlled testing, (a) adaptation, (b) finite ratcheting, (c) infinite ratcheting. Figures by Rascol Emilie [36].

In terms of stiffness, the material can present either hardening or softening behaviour (Figure 8). Hardening is when the modulus increases and softening is when the modulus decreases with the increasing the number of cycles. This can be detected on a stress-strain graph with an increasing or decreasing inclination of the cycles, respectively [34].

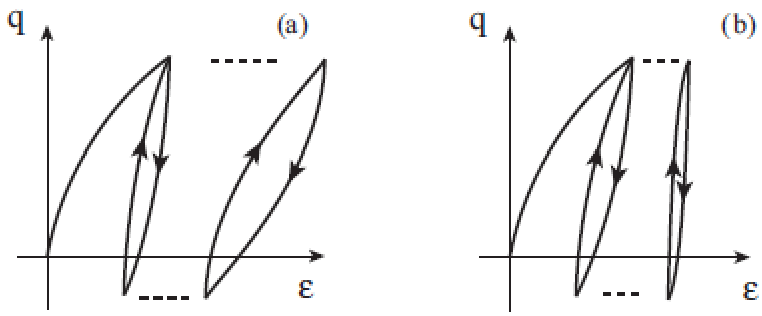

Figure 8. (a) Cyclic softening, (b) cyclic hardening of sand. Figures by Rascol Emilie [36].

When there is stress-control asymmetrical cyclic loading ($\sigma_{max} \neq -\sigma_{min}$) (Figure 9), a mean stress is developed which may cause strain accumulation in the material. The strain accumulation can be calculated from the displacement (Figure 11), if it is divided by the sample height. It increases with the number of cycles and with the increased stress amplitude and it is higher for looser materials [38], while it does not depend on the loading frequency in the range of 0–10 Hz [39]. The step with which the strain is increased, depends on the loading amplitude and the material characteristics and decreases with every cycle [34].

Figure 10 and Figure 11 are representative of the force-displacement correlation and the displacement over time of the sample (carpet-material) in 10 cycles of forced controlled cyclic compression test. The response can be divided into two sections, the first irregular cycle and the rest of the cycles, which present similar behaviour. Those two sections should be studied separately. In this research, the focus was given to the subsequent cycles.

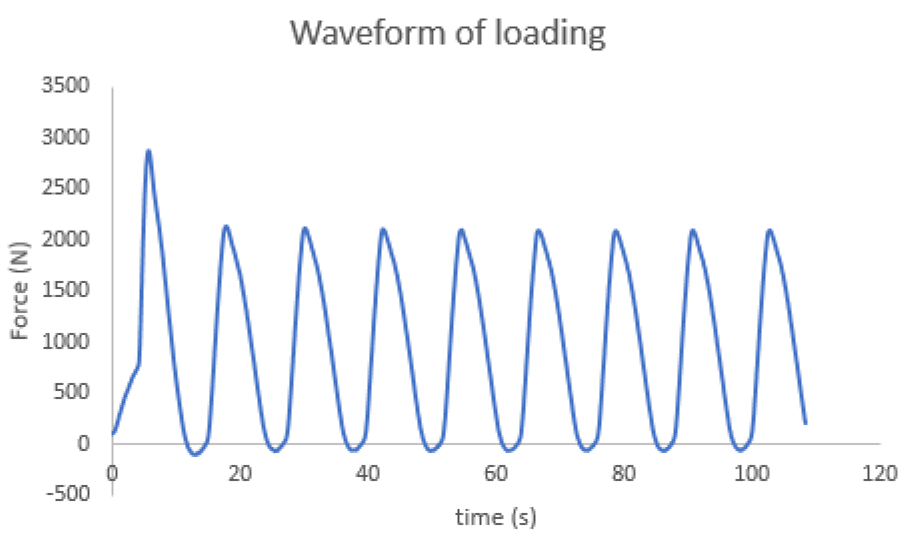

Figure 9. Waveform of loading under force-controlled cyclic loading at 400 N/s loading rate.

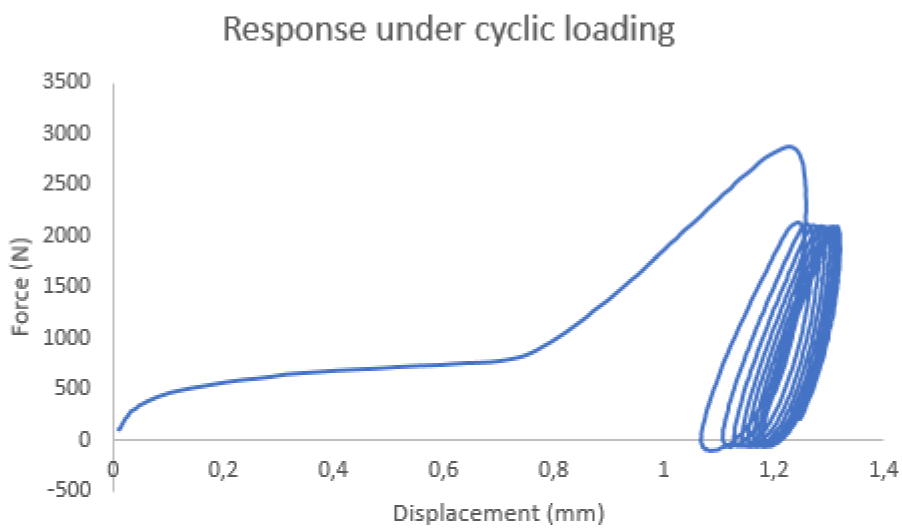

Figure 10. Response under force-controlled cyclic loading at 400 N/s loading rate.

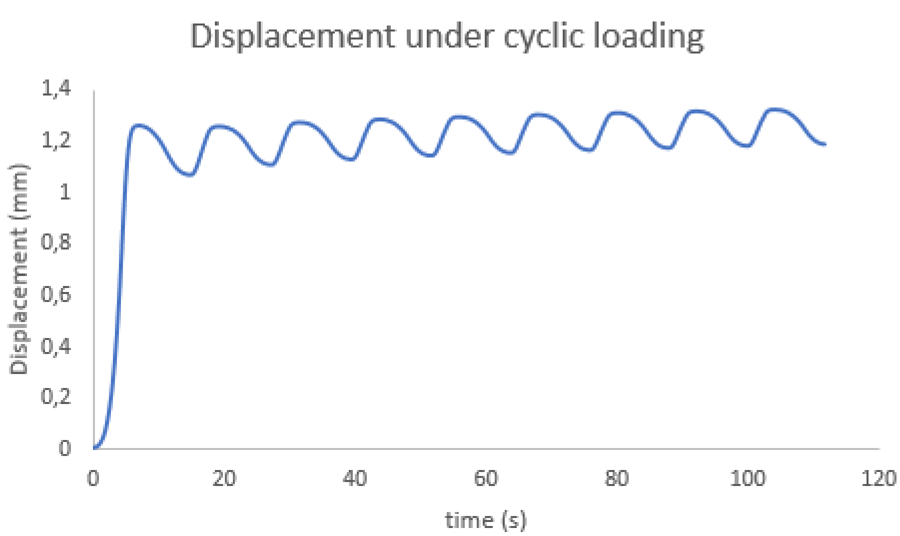

Figure 11. Displacement under force-controlled cyclic loading at 400 N/s loading rate.

4.4 Modulus

If the first irregular cycle of loading is subtracted, the Figure 12 shows a representative stress-strain graph of the carpet-material sample for the remained cycles. Each cycle consists of a compression (positive force) and an extension part (negative force) and each of these parts has a loading and an unloading phase. It can be noticed that the shape and the size of the curves change as the number of cycles rises.

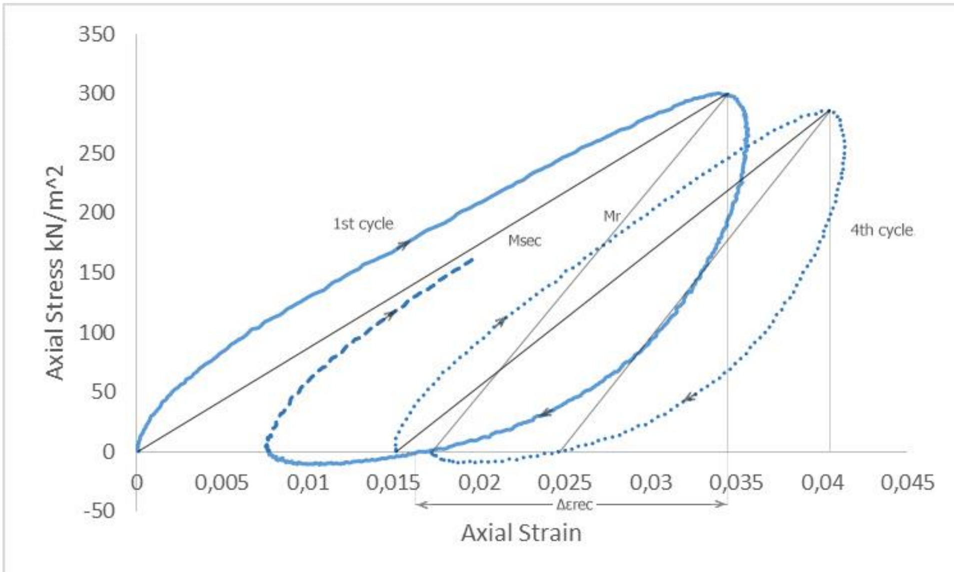

Figure 12. A representative Stress-Stain graph-Modulus definition.

Two types of Modulus, secant and resilient, are used to describe the behaviour of the sample in each cycle (Figure 12). Both of them do not take into consideration the differentiation of the modulus with strain during the loading-unloading cycle but only between the initial and the final state.

Secant Modulus (M_{sec}) is defined as the ratio of the maximum axial stress and the correspondent axial strain, excluding the permanent strain accumulation from previous cycles:

$$M_{sec} = \frac{\sigma_a^{max}}{\varepsilon_a} \quad (3)$$

The Secant Modulus examines the behaviour of the sample in the loading phase and it is an indicator of the strain that is induced to the material under maximum stress. It also describes the overall inclination of the cycle.

Resilient modulus (M_r) is defined as the ratio between the maximum axial stress and the recovered axial strain ($\Delta\varepsilon_{rec}$), which is the difference of the axial strain at maximum stress from the axial strain at the end of the unloading curve of the compression phase.

$$M_r = \frac{\sigma_a^{max}}{\Delta\varepsilon_{rec}} \quad (4)$$

The resilient modulus refers to the response of the sample in the unloading phase and shows the portion of strain that is recovered in the unloading phase. If the extension phase was also included the resilient modulus would be lower. The resilient modulus depends on the loading conditions, the stress history and the material properties (type, particle size and shape, particle size distribution, void ratio and water content) [40] [41]. The loading characteristics are defined by the amplitude, the rate and the direction of the loading. As the stress amplitude increases, the resilient modulus increases, because the grains repack to a denser state [42]. In addition, the resilient modulus is influenced by the stress-path direction [43] but not from the loading rate for low frequencies (0-10 Hz) [41]. Stress history can be described by the number of cycles. As the number of the cycles rises the modulus increases as well [44].

In the scope of the material properties, the coarser granular materials develop higher resilient modulus compared to the finer, if both of them have similar particle size distributions. Regarding the particle size distribution, the well graded material presents higher resilient modulus than the uniform with the influence being more significant with the increase in water content [45]. The increase in water content affects more the well graded materials, in which Mr is decreased, and not at the same extent the uniform ones. In addition, the Mr rises with density, angularity and surface roughness. Among the parameters mentioned above, the stress amplitude, the water content and the density are the parameters that have the higher influence on the resilient modulus [41].

4.5 Energy Transformation

The player-surface interaction includes the energy exchange between the athlete and the surface. When the athlete steps on the surface, energy is transferred on it ($\mathrm{E_{total}}$) and when he lifts his leg a portion of this energy may be returned ($\mathrm{E_{return}}$) to the athlete from the surface [46]. This energy transformation can have a significant impact on the player's performance, which can be enhanced, provided the energy returns at the proper time, location and frequency while minimizing the losses [47]. The right location of the energy return is the position of the athlete's take-off movement and the right timing can be achieved by setting the surface's natural frequency similar to the frequencies produced by the athlete's movements [46]. The equation that describes the energy exchange is the following:

$$E_{return} = E_{total} - E_{dissipated} \quad (5)$$

Characteristic energy values in the vertical direction, reported for a conventional surface using FEM simulation, were 1.085 (J) energy input and 0.01 (J) dissipated energy [13].

A granular material subjected to cyclic loading may develop the hysteresis loop depicted in Figure 13. The loop can be described by its path and shape. In terms of shape, the inclination of the loop changes at every step and a mean value is calculated by the secant modulus. Regarding the width of the loop, it is correlated to the area and the dissipated energy and it can be described by the damping ratio. The dissipated energy increases with the increase of the strain and it is not significantly affected by the strain rate [48]. However, at higher frequency (>2 Hz), the damping appears to rise significantly with the increase of the frequency. Therefore, the approach of the hysteretic nature of damping may introduce significant error and the viscous effect should also be considered [49]. In addition, the damping ratio decreases with the number of cycles [50].

The energy transformation in every cycle was calculated based on the force displacement curve. The hatched (diagonally) area between the loading-unloading curves, is the dissipated energy during the cycle and the hatched (vertically) area under the unloading curve, is the recovered energy (Figure 13). The approach is similar to [19].

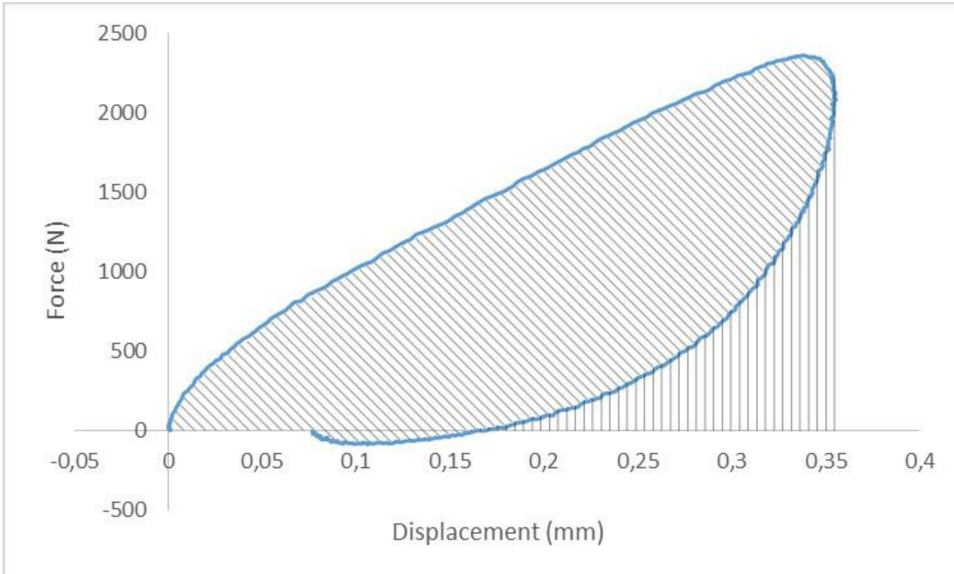

Figure 13. Force-Displacement graph during load-controlled loading of a carpet-ceramic sand sample. The marked area inside the loading-unloading curves corresponds to the dissipated energy due to hysteretic damping of the material and the vertically marked area shows the recovered energy.

4.6 Friction

Sliding, shearing and rolling are the frictional mechanisms which determine the shoe-surface interaction [51]. Sliding (Figure 14 (a)) is the prevalent mechanism for particles with diameter below the threshold of 50-60 μm, under which particles act as a single layer instead of separate units. Above that diameter, rolling of the particles (Figure 14 (b)) is observed leading to lower values of friction and higher slipperiness of the surface. The shearing mechanism (Figure 14 (c)) is developed when the surface's roughness rises. Besides the particle size, the thickness of the material's layer can also influence the response of the surface and which mechanisms will be developed [51].

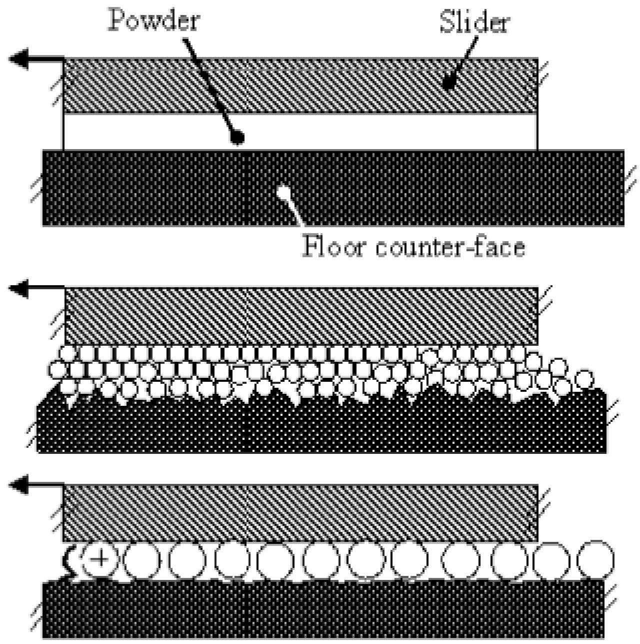

Figure 14. Mechanisms developed during surface-slider contact, (a) sliding, (b) shearing and (c) rolling [51].

The description of the friction mechanisms can be made with the assistance of the friction coefficients. The coefficient of friction (COF) can be defined as:

$$COF = \frac{F_{shear}}{Fz} \quad (6)$$

Where Fz is the force in the vertical direction and F_{shear} is the force in the horizontal direction and it calculated from the following equation:

$$F_{shear} = \sqrt{F_x^2 + F_y^2} \quad (7)$$

The translational coefficient of friction on clay and synthetic clay tennis courts is between 0.5-0.7 [52] and it is affected by the particles' size, the infill volume of the material and the moisture of the surface. Higher coefficients of friction and lower sliding distances compared to material with larger particles are exhibited by materials with smaller particles [23]. In addition, lower initial stiffness is developed in dry conditions by particles with size below the threshold of the 60 μm compared to larger particles, and it is being linearly increased with the normal load [21]. Furthermore, when materials with the same particle size are compared, the initial shear stiffness of the smaller particles is raised by the presence of moisture but it is less influenced by the bigger sand particles [21]. The coefficient of friction is also affected by the infill volume of the material. As the volume of the material is being raised the static coefficient of friction is being decreased [24]. Moreover, the peak friction force and the average dynamic force are influenced both by the infill volume of the material and the moisture content [28].

5. Methods

5.1 Compression Test

5.1.1 Tested Material

The materials examined were three different carpets and three different ceramic sands with different particle size distributions. All testing materials were provided by Magnus Gustafsson and Marius Malek. The carpets had varying patterns and way of gluing and they are depicted in Figure 15. The first carpet (S) had a "Swiss Cross" pattern and it was glued superficially, Figure 15 (a, b). The second carpet (F) had a "Fishbone" pattern and it was fully glued through a glue bath, Figure 15 (c, d). The third carpet "Topsand" (T) had oval formations placed diagonally and it was glued locally, Figure 15 (e, f).

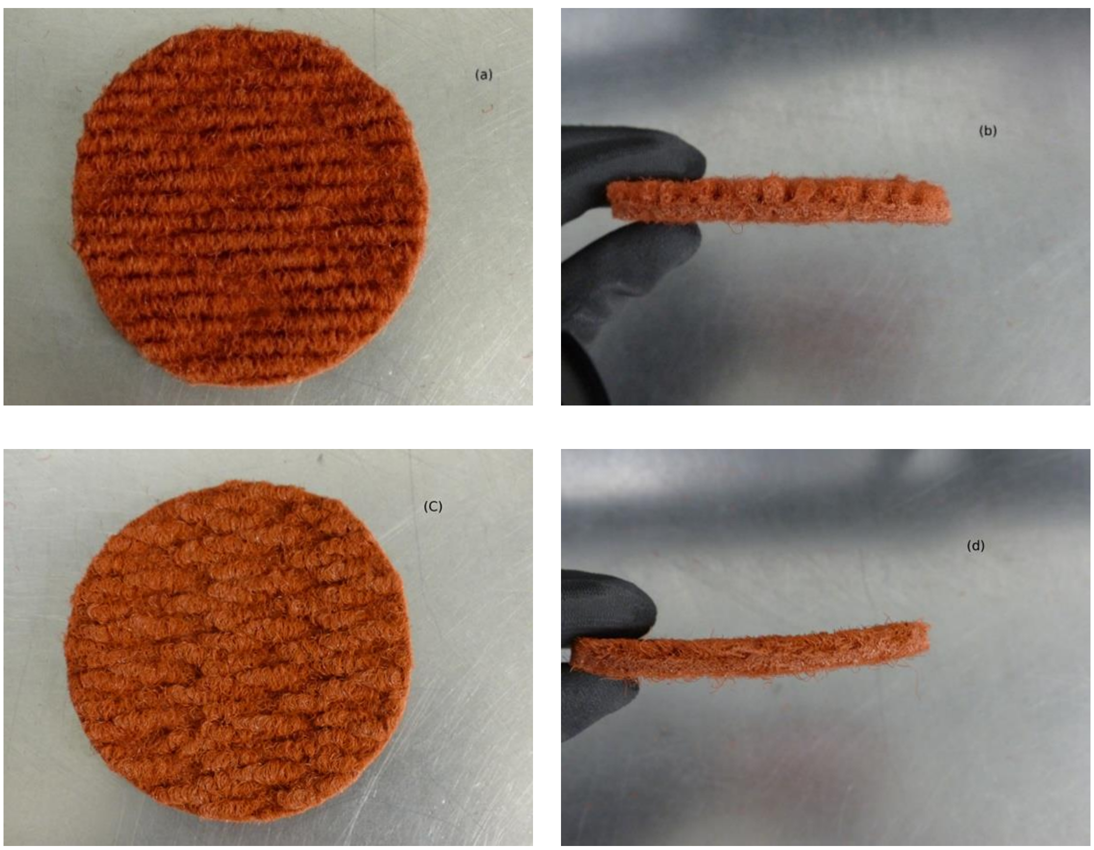

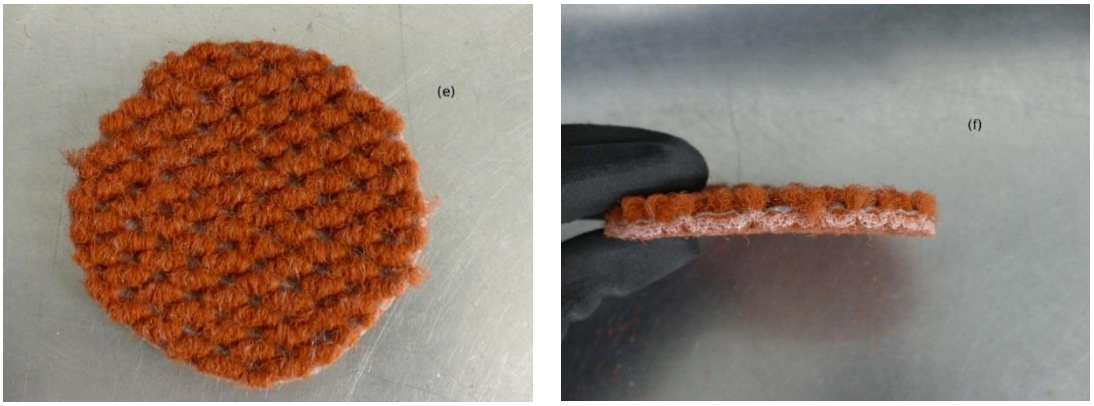

Figure 15. Three distinct types of carpets cut in circles with 100 mm diameter. In pictures (a), (b), there is the partially glued (NFG) carpet with the Swiss Cross pattern. In pictures (c), (d), there is the fully glued carpet (FG) with the fishbone pattern and in pictures (e), (f), there is the locally glued carpet with the oval diagonal pattern.

The ceramic sands were produced by two different producers and they had different particle size distributions (Figure 17). In Figure 16 (a), it is the 0.3-0.9 sample (C), in Figure 16 (b), the 0.4-0.8 sample (M) and in Figure 16 (c), the finer 0.1-0.3 sample (F). Ceramic sands M and F had the same producer and similar texture, whereas ceramic sand C had a different producer and different texture potentially due to varying ways of production and processing of sand between the producers.

Figure 16. Wet material in picture (a) there is the ceramic sand 0.3-0.9, in picture (b) there is the ceramic sand 0.4-0.8 and in picture (c) there is the ceramic sand 0.1-0.3.

The moisture content for each distribution of sand was calculated (Table 3). 1 kilogram of wet material, in 5x200 g batches, was dried in the oven at 110 ∘ C for 1 hour. The batches were weighed again and the water content of each material was calculated. Then, 100 g of the dried material were sieved in a standard sieving equipment according to SS-EN 933-1 Standard [53] and the particle size distribution was calculated (Figure 17). All tests were performed with the dried ceramic sand.

Table 3. Moisture content of the Ceramic Sand.

Ceramic Sand 0.3-0.9 (C)			
No of sample	Total Wet Mass (g)	Total Dry Mass (g)	Moisture wt.- %
1	200	199.9	0.05%
2	200	199.9	0.05%
3	200	199.9	0.05%
4	200	199.85	0.08%
5	200	199.9	0.05%
Average			0.05%

Ceramic Sand 0.4-0.8 (M)			
No of sample	Total Wet Mass (g)	Total Dry Mass (g)	Moisture wt.- %
1	200	194.75	2.63%
2	200	194.48	2.76%
3	200	194,38	2.81%
4	200	195,25	2.38%
5	200	194,6	2.70%
Average			2.65%

Ceramic Sand 0.1-0.3 (F)			
No of sample	Total Wet Mass (g)	Total Dry Mass (g)	Moisture wt.- %
1	200	197	1.50%
2	200	197.3	1.35%
3	200	196.3	1.85%
4	200	196.5	1.75%
5	200	196	2.00%
Average			1.69%

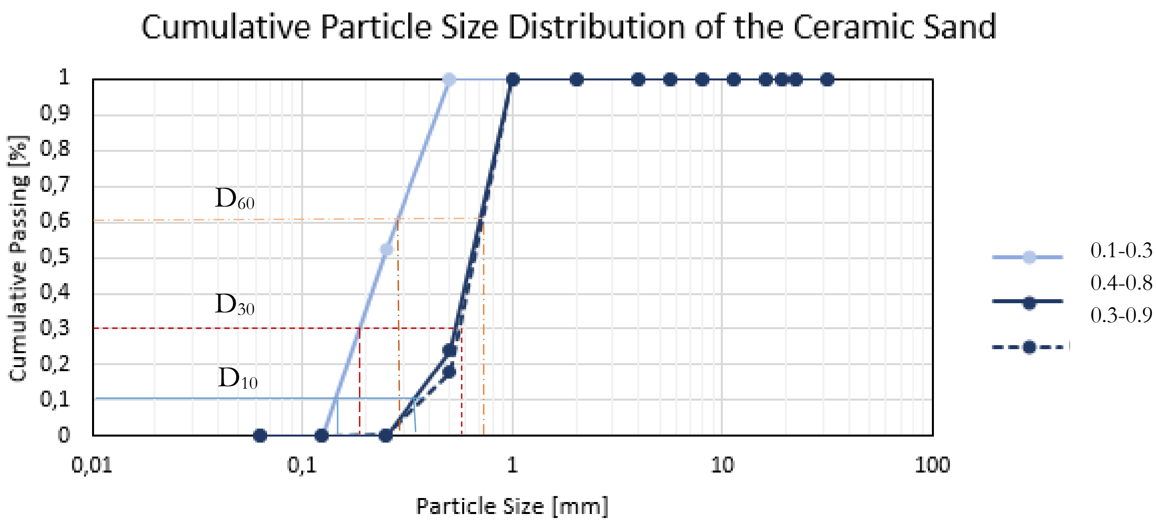

Figure 17. Particle Size Distribution of the Ceramic Sand. The sieving method was used to perform the particle size analysis according to SS-EN 933-1 Standard.

In Table 4, the coefficients of uniformity and curvature, which were calculated for the three ceramic sands from equations (1) and (2), are presented. The values for the equations were taken from the particle size distribution of each ceramic sand (Figure 17). According to Table 4, the sand samples were uniform and narrow graded.

Table 4. Coefficients used to describe the grading of the material. Coefficient of Uniformity (C_U) and coefficient of Curvature (C_c).

	Cu	Cc	D_{50}
0.1-0.3 (F)	1.93	0.83	0.24
0.4-0.8 (M)	2.11	1.13	0.67
0.3-0.9 (C)	2.05	1.16	0.69

5.1.2 Compression Test Procedure

The samples of the compression test consisted of a carpet and infill ceramic sand, while the carpets were also tested with no material addition. In Table 5, there are the combinations of carpet-material that were examined in the compression tests. The ones with the bold **x** refer to combinations that exist in real courts.

Table 5. Material/Carpet Combinations and performed tests.

Type of material / Type of carpet	Partially glued (NFG) with Swiss Cross-pattern (S)	Fully glued (FG) with fishbone pattern (F)	Locally glued (LG) with oval diagonal pattern (T)
Ceramic Sand 0.3-0.9 (C)	x	x	x
Ceramic Sand 0.4-0.8 (M)	**x**		
Ceramic Sand 0.1-0.3 (F)	x	**x**	x
No infill material	x	x	x

Figure 18 and Figure 19 describe the equipment and how the sample is placed into the machine. The samples, carpet and ceramic sand, were placed in a rigid cylinder (100 mm diameter, 105.7 mm height) with a metal base (90 mm diameter and 17.8 mm height) below. The height of the sample ranged between 7 and 12 mm and its preparation included pouring of the material on top of the carpet and brushing it until the surface became even. Subsequently, the piston was placed on top of the sample and then inside the hydraulic compression machine. The sample was cyclic compressed in the vertical direction. Axial displacement and vertical force were measured at 100 Hz. Due to the confinement, the strain was developed only on the vertical direction. The losses from the cylinder's wall were not taken into consideration.

Figure 18. Sample preparation. In picture (a) starting from the left, there is the cylinder where the sample is placed, with 105.7 mm height and 100 mm internal diameter. Next is the piston which is placed on the sample with 96.7 mm height, 100 mm diameter and 5469 g weight. Next is the carpet, which is cut in 100 mm diameter and then the brush which was used to distribute the material. In the end, there is the dried material, here 43.1 g of it. In picture (b) there is the carpet with the base. The base has 17.8 mm height and 90 mm diameter. In picture (c) there is the sample after the brushing procedure (appendix Test 14).

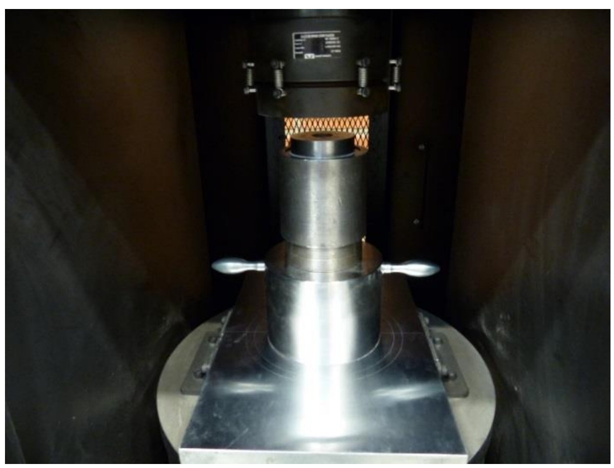

Figure 19. Instron Compression machine with a sample inside. The jog control is 76 mm/min. The preload is 100 N with rate 25 N/s. The preload is used to remove slack in the specimen or compressive load on the specimen due to gripping. During preloading no data are captured.

The testing aims to measure the response of the surface on cyclic vertical loading. The parameters of the experiment were chosen based on biomechanical measurements on tennis players (Table 2). A limitation is that it corresponds only to the vertical direction and omits the horizontal forces. However, as the vertical forces developed are higher, it can be considered as an informative initial approach.

The test was force controlled using a sinusoidal waveform with 200-2000 N range to imitate the movement of a tennis athlete. It corresponds to the repetitive jumping of the athlete on a specific point. The compression phase refers to the duration that the athlete is in touch with the surface and the extension phase to the time that the athlete is on the air. Because of hydraulic function of the machine, the unloading phase was due to gravity and the response relied on the nature of the specimen. The schematic description of the test procedure is presented in Figure 20. The loading rate was set to 0.2-0.4 kN/s. However, the value of the actual loading rate changes with time and it depends on the machine characteristics, jog control speed, and the initial stiffness of the sample. From biomechanical tests on clay court, the peak vertical loading rate was 135.52- 147.67 BW/s and the average mass of the athlete was 66.75 kg, resulting in 88.7-96.7 kN/s loading rate [24]. For the performed tests, the loading rate at maximum force was on average 0.06 kN/s for the 0.2 kN/s target and 0.12 kN/s for the 0.4 kN/s target, being three orders of magnitude lower than the real measurements. The average loading time was 3-4 seconds.

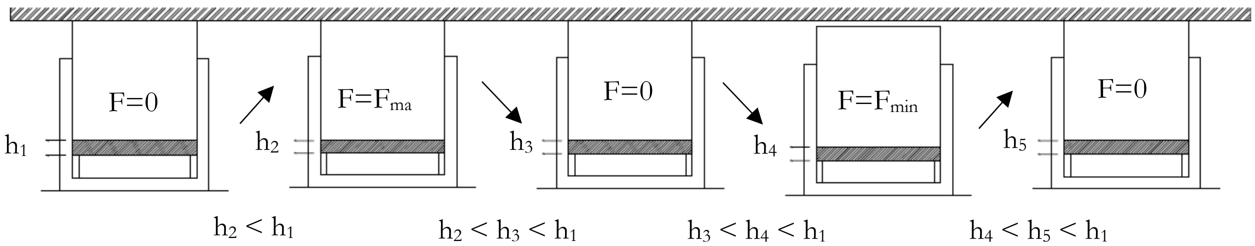

Figure 20. Compression Test description. h_1 is the initial thickness of the sample while h_5 is the final thickness after the compression. The black arrows indicate the increase or decrease of the force and the movement of the hydraulic base.

The quantity of the material was chosen based on the manufacturer's recommendations 5.5 kg/m² and it was kept constant to all the experiments. The number of cycles in each experiment varied in order to investigate the effect of loading history. The data analysis included the examination of the force-displacement curve, the calculation of the energy transformation, the modulus and the strain accumulation of the sample. The parameters of the performed tests are described in the appendix.

5.2 Motion Capture System

The Xsens motion capture system was used to conduct the experiments to analyse the kinematics of a sliding movement. The system consisted of a suit which can be either a full body Lycra suit (MVN Link system) or straps that are placed on the athlete (MVN Awinda) (Figure 21(a)) [54]. The data was collected from 17 motion trackers which were placed on the whole body of the athlete. Each motion tracker had a 3D rate gyroscope inside to measure the angular velocity, a 3D linear accelerometer for the acceleration, a 3D magnetometer for the earth's magnetic field, and a barometer to capture the atmospheric pressure [54].

During the sliding motion experiment both of the systems were used. Marcus Johansson was wearing the MVN Link system and Magnus Gustafsson the MVN Awinda. The performed motion is described in Figure 22. The players started from position 1 and run to position 2 where they slid on the surface, hit the ball and returned to position 1. Before the measurements started the sensors were calibrated using the N-posture (Figure 21 (b)). The Body Dimensions were kept the default except the foot size and the shoe sole height which were measured in each athlete. The data were logged at 60Hz for the Awinda system and at 240Hz for the link system and they were analysed with the MVN Studio BIOMECH- Version 4.4.0 (exported as mvn file) and the MATLAB R2015b (exported as mvnx file) software.

Figure 21. (a) on the left the Link system and on the right the Awinda system. (b) The N-pose for the sensor calibration. Figures by Xsens [54].

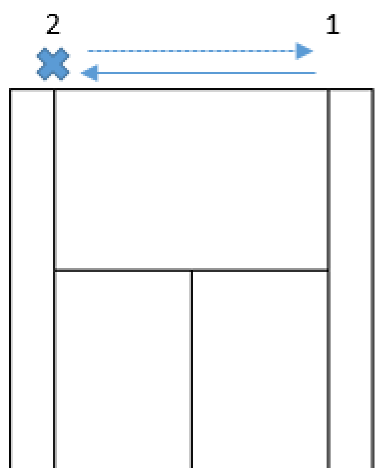

Figure 22. Repetitive sliding movement.

5.3 Friction Test

The friction test rig is depicted in Figure 23. The test was performed by a robot arm, KUKA KR30, which was connected to a controller, KRC2. A tool change adaptor was used to connect the test sample with the robot. The shoe used was a NITRO TEAM CLAY MEN BLFL (size EU 47) produced by HEAD.

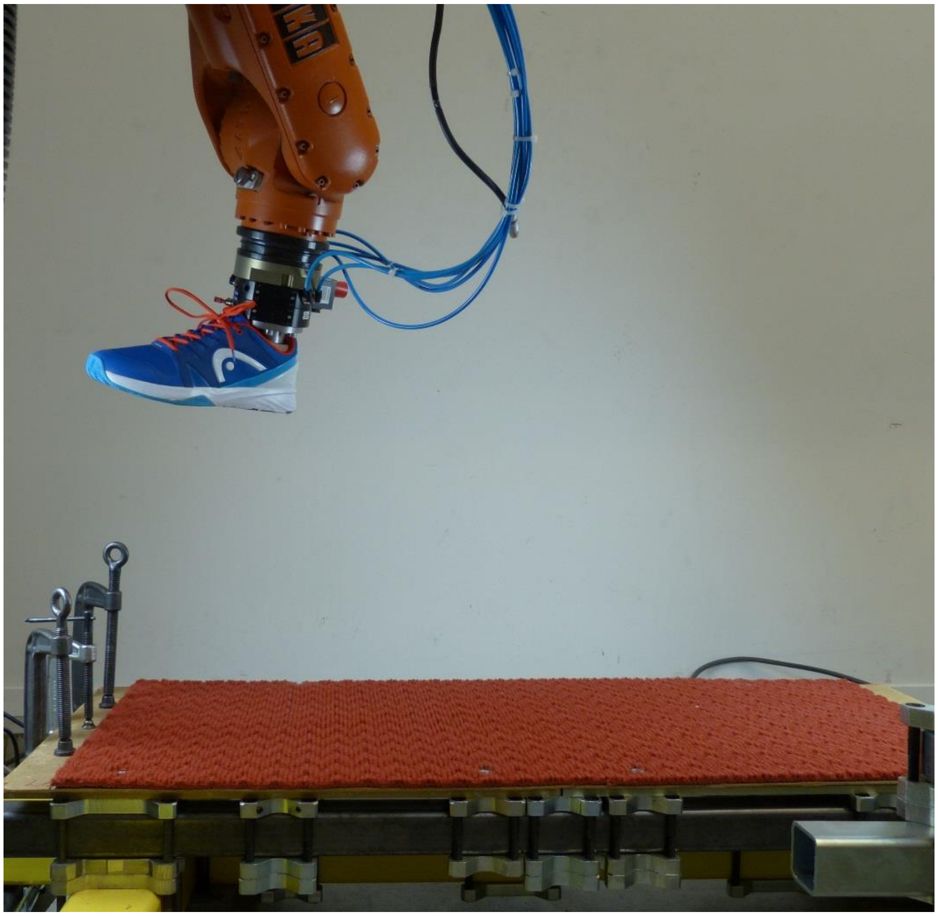

Figure 23. The whole friction test set up. The base with the carpet on it and the robot arm with a tool adaptor in its end. The shoe was placed on the artificial foot and the foot was connected to the robot through the tool.

The carpet was secured on a stiff metallic base which was fixed on a frame. Between the carpet and the base, a wooden thin layer was placed so that the carpet could be changed easier. The carpet and the wooden surface were attached together with a two sided tape and they were secured with the metallic base and the frame through screws. During testing two different tool-shoe samples were used. The first can be noticed in Figure 23 and it consists of a tool connected with an artificial foot and a tennis court's shoe which has been worn on it. The second is depicted in Figure 24 and Figure 25. The shoe sole was cut off the shoe and a circular sample was taken. The cushioning material of the sole was removed and only the thin out layer of the sole with the "z" pattern was used (Figure 25 (b)). In order to receive accurate measurements as close to the shoe surface combination as possible the shoe sample was glued on the force-torque sensor with a two component epoxy glue to ensure stability (Figure 25 (a)).

Figure 24. Tool changer adaptor- Force/Torque Sensor and shoe sample system mounted on the robot.

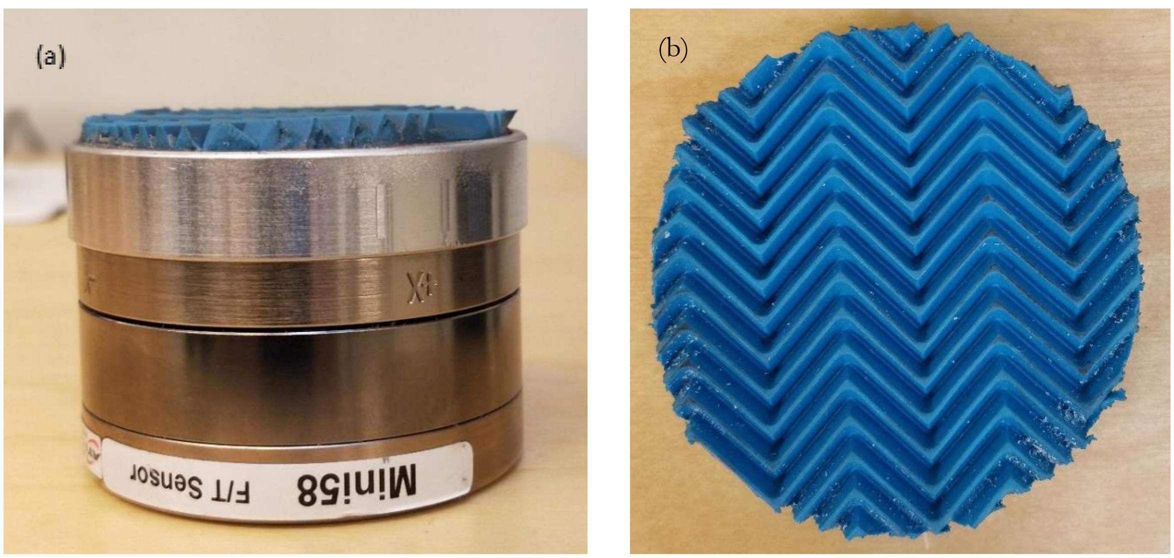

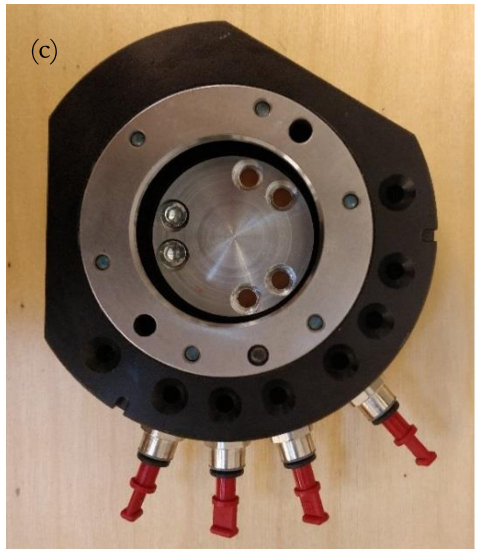

Figure 25. (a) Force-Torque Sensor Mini58 with the shoe sample glued on it. (b) The shoe sample with the z pattern. (c) Tool Changer Adaptor SKUNK.

The friction of the clay court was evaluated during the sliding of the shoe on the surface. Initially, the swiss cross (S) carpet was secured on the base and M (0.4-0.8) ceramic sand was poured on top. The sand was evenly distributed on the carpet with the help of a brush. The sliding movement was programmed in the robot's software based on data from Xsens motion capture system and the restrictions from the sensor's and the robot's limitations. The system was automatically generating traces during the motion. Those were visualised in the WorkVisual 4.0 software provided by KUKA. The movement of the shoe is schematically depicted in Figure 26, where the robot performed a vertical motion in the z-axis (1) and then it started sliding horizontally in the y-axis (2).

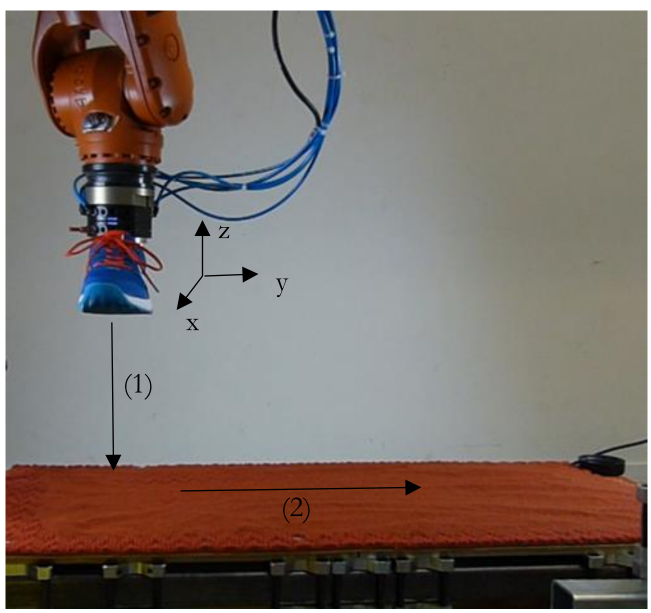

Figure 26. Friction Test, movement description.

The initial measurements were performed with the whole shoe in order to evaluate and adjust the movement. However, since the force sensor had to be placed between the robot and the shoe it was decided to use for the force measurements only the cyclic shoe sample described above for higher precision. Due to a slight inclination of the platform and the coordination system's axes, a calibration method was performed to eliminate the effects. A vertical movement was executed by the robot arm in the starting and in the final position and the measurement of the final force was set to be similar to the force of the starting point by adjusting the lowering depth. The ground reaction forces were measured at 7000 Hz using the F/T Mini 58 sensor. The shear force and the utilized coefficient of friction were calculated for each of the tests.

In Figure 27 and Figure 28 the kinematic data of a linear and a planar movement of the robot arm are depicted respectively. It can be noticed that the displacement in the y-axis was similar to the both cases at 250 mm. In the linear motion the displacement in the x-axis was slight, at 0.2 mm while in the planar motion it reached 2 mm. The main difference between the two movements was the velocity that was developed, which during in the linear motion formed a triangle whereas in the planar motion it shaped a trapezoid with constant speed during the most part of the movement. For both motions the targeted velocity was 1 m/s. However, this was not reached during the linear motion due to the robot's different prioritization, which was for the linear motion to keep the right path instead of reaching the desirable velocity.

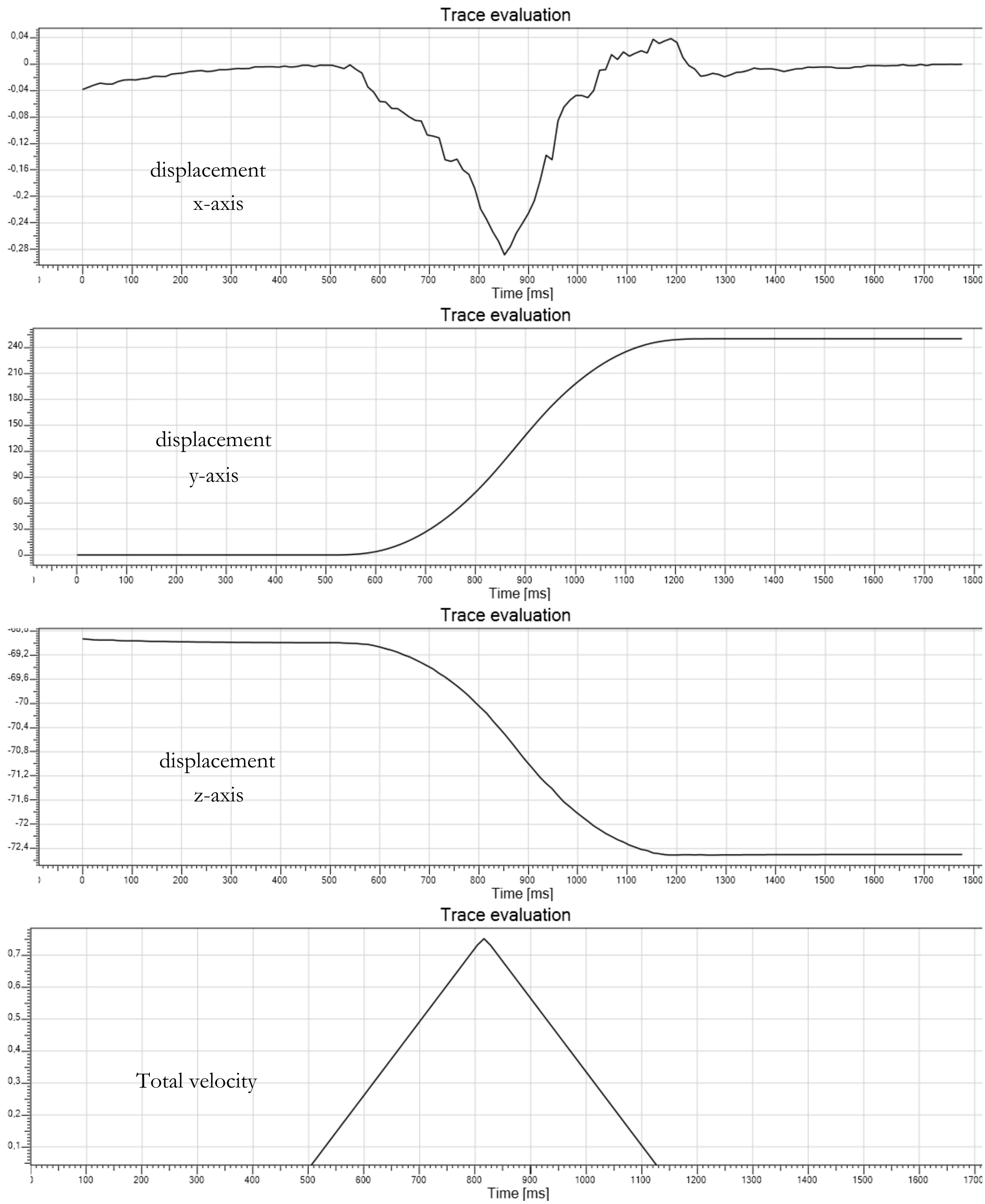

Figure 27. The kinematic data of the linear motion of the robot arm.

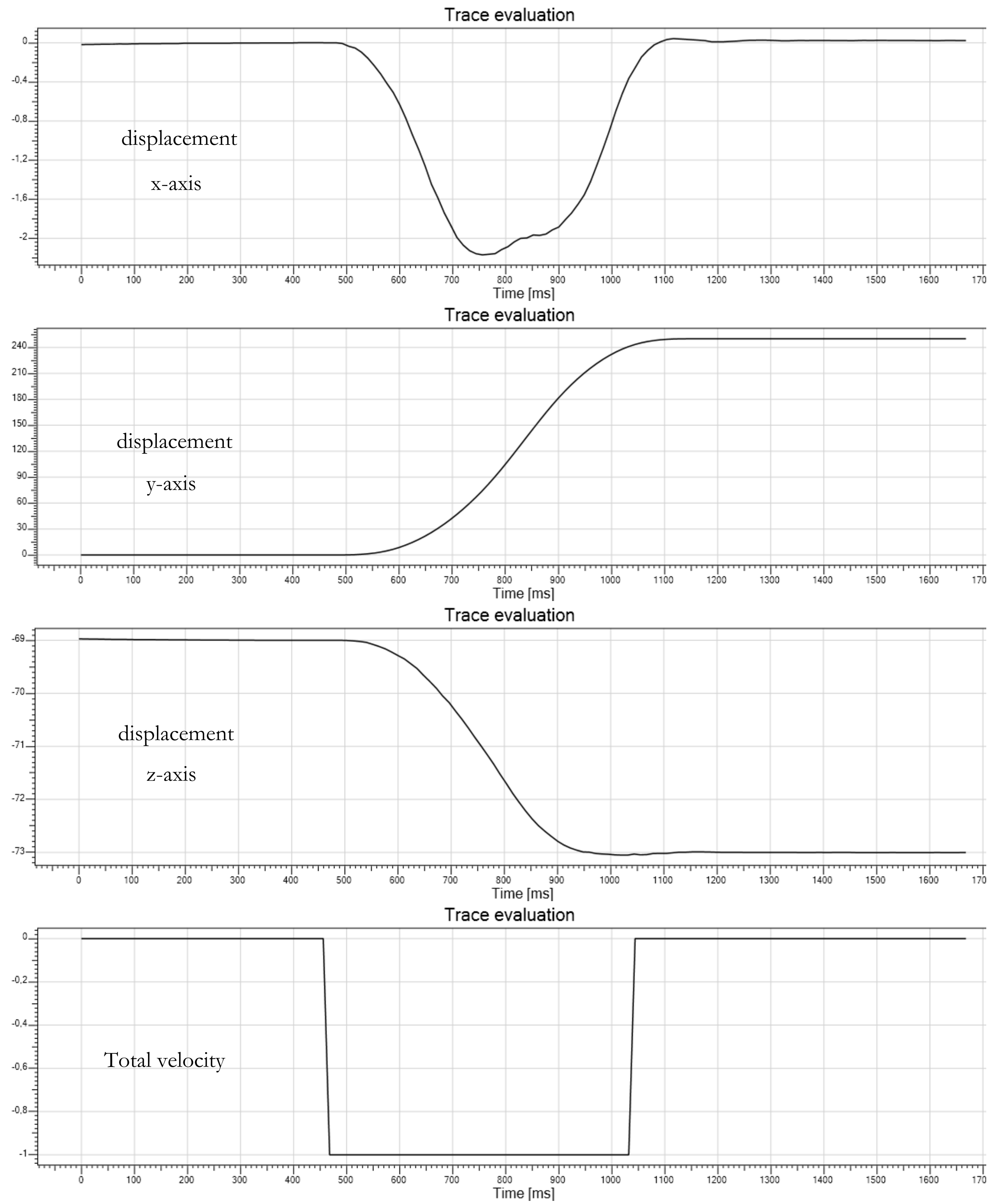

Figure 28. The kinematic data of the planar motion of the robot arm.

5.4 Interview

An interview with Magnus Gustafsson, who is a former professional tennis player, was carried out for the results of the tests and the properties of the court from the player's perspective to be interpreted. A short presentation was given to the player and subsequently he was asked to compare the two courts that were tested and exist in full scale (SM and FF courts) and to list the court's properties based on their importance. In addition, he was asked about the maintenance of the courts and his thoughts on the future research in clay tennis courts. The interview was conducted via email and it was in open question form.

6. Results

6.1 Compression Test

In Figure 29-Figure 42, the force-displacement graph of the performed test is analysed, whereas in Figure 43-Figure 48 it was examined how energy transformation (%), Secant and Resilient Modulus, maximum deflection, strain accumulation (%) and step of strain accumulation were evolved as the number of cycles was increased. In Figure 49 and Figure 50 the correlations among energy dissipation (%), secant modulus and strain accumulation (%) were investigated, when the ceramic sand was kept constant and the carpets changed and vice versa. The test plan can be found in the appendix.

<u>Force-Displacement Correlation</u>

In Figure 29, the response of the S-Carpet with the fine ceramic sand is shown, when the samples had no loading history. In Tests 1 and 2, the ceramic sand was poured on top of the carpet and then it was distributed evenly on it. In Test 3, the sand was brushed on the carpet in order to penetrate more inside it. Both approaches of the initial sample preparation cannot be reproduced in a unique way and they introduce unquantified anisotropy. When the sample was fresh and it had not been compacted the response depended on the initial preparation and it was not similar for the same materials.

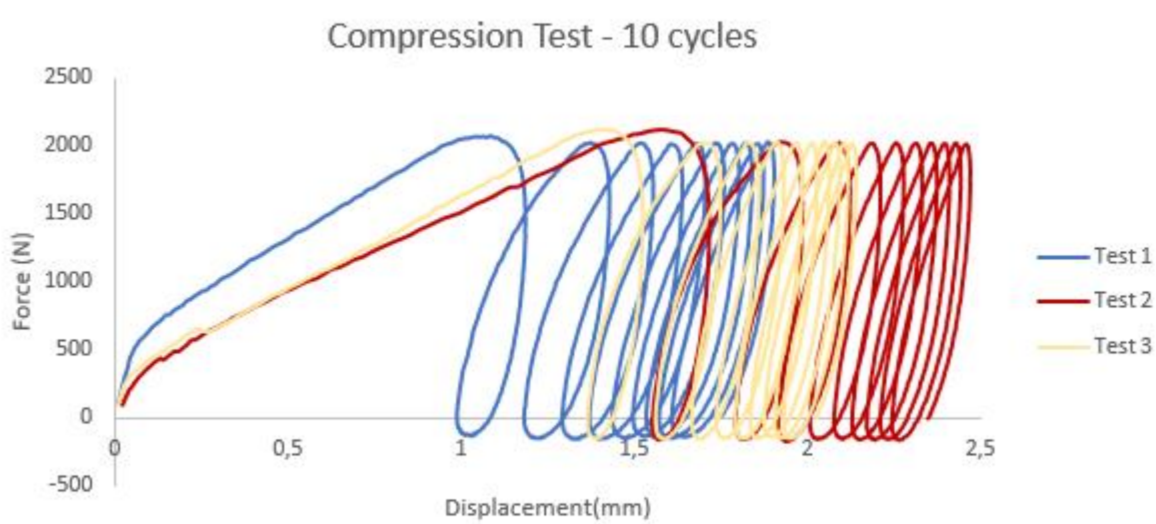

Figure 29. Test 1-3. Force- Displacement graph of Tests 1-3. The carpet was S, the ceramic sand M and the tests were performed at loading rate 200 N/s.

In Figure 30, the response of Tests 1-3 for the cycles 5 to 10 is shown. The Tests were transposed to have a common start in order to be observed how much the following cycles coincide after the first 5 cycles. Based on the graph the cycles were not similar, which means that the influence of the initial sample preparation had not been vanished.

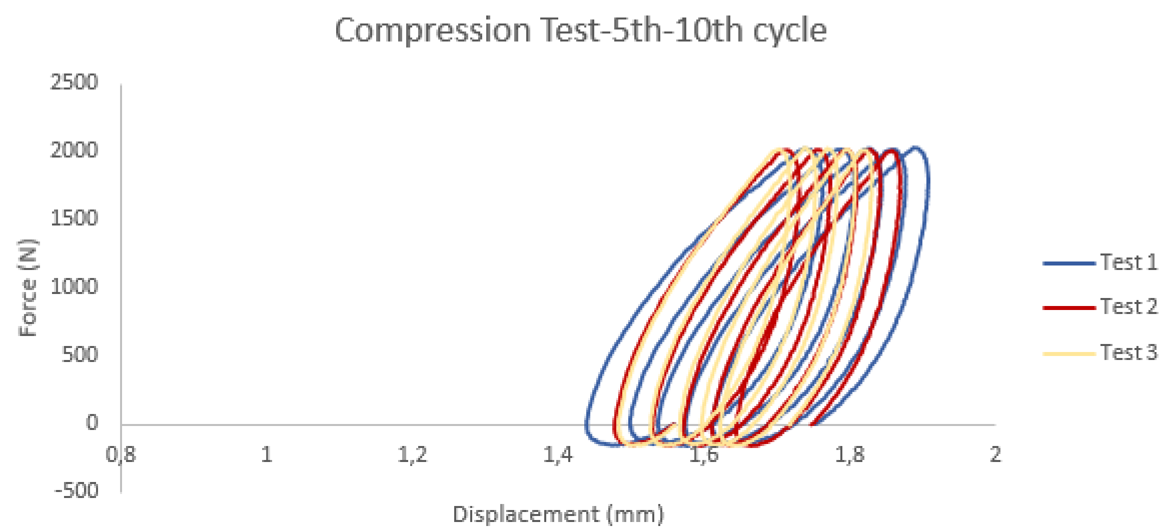

Figure 30. Test 1-3. Force- Displacement graph of Tests 1-3. The first 5 cycles in each test were removed and then, the next 5 cycles of Test 2 and 3 were transposed to have a common start with Test 1.

Tests 4B and 5B (Figure 31) were the second set of tests that were performed on the samples. Initially, the samples were submitted to a set of 5 consecutive loading cycles with the same parameters. The variation of the samples in the first 5 cycles was still significant. In addition, it can be noticed that the total displacement of the samples after 10 cycles was quite lower compared to the Tests 1-3.

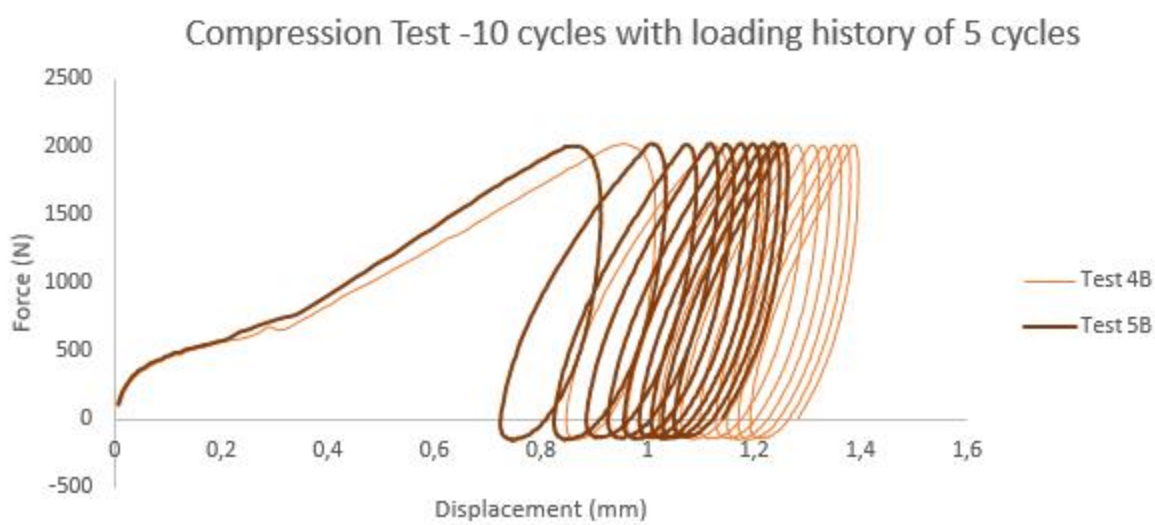

Figure 31. Test 4-5. Force-Displacement graph. The carpet was S, the ceramic sand M and the tests were performed at loading rate 200 N/s. There was a 5 cycle loading history.

If the same method as in Figure 31 is followed, the result is shown in Figure 32. The cycles of the two tests were quite similar with small constant differences in the initial unloading part. The loading history of 5 cycles appeared to be sufficient for the cycles 5-10 to coincide.

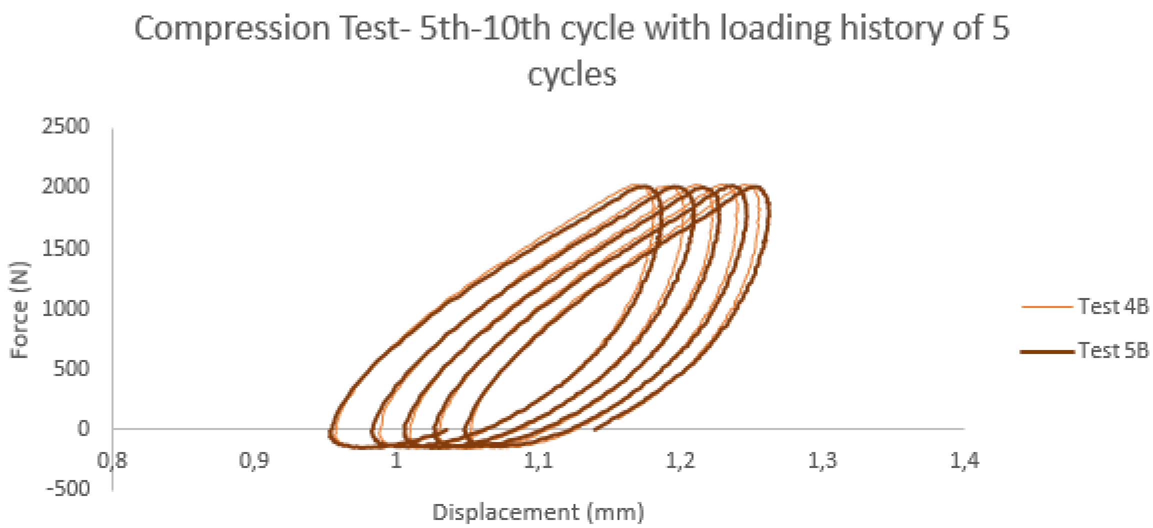

Figure 32. Test 4-5. Force Displacement graph. If the first 5 cycles are removed and the Displacement results of the Test 5B are transposed to have a common start with the correspondent of the Test 4B.

In Figure 33, the samples have a loading history of 15 cycles. Here, the curves were similar for all the 10 cycles. However, this is an exception rather than the rule.

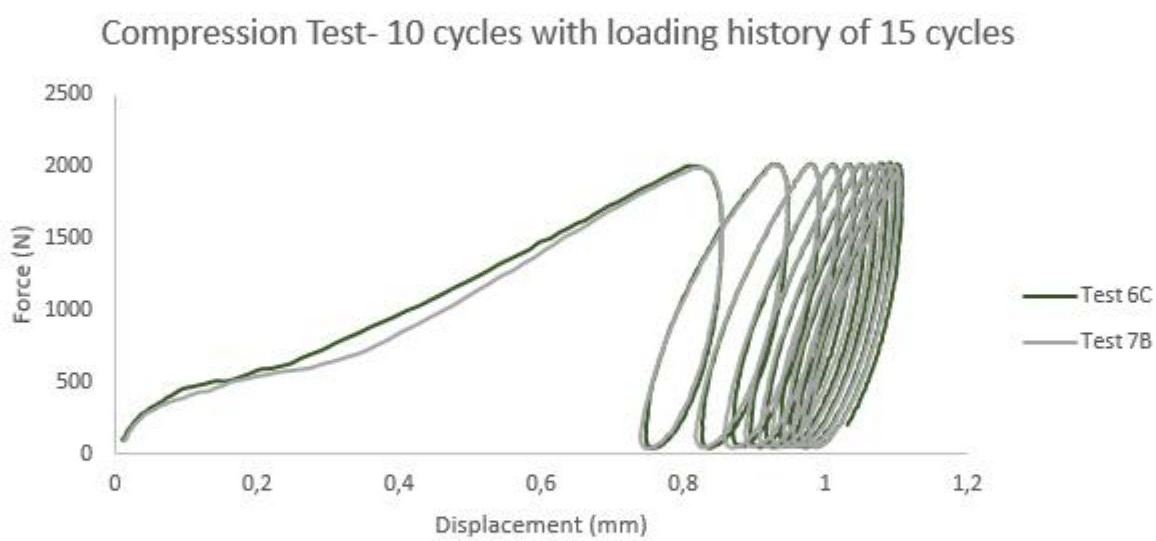

Figure 33. Force-Displacement graph. The carpet was S, the ceramic sand M and the tests were performed at loading rate 200 N/s. Tests 6C and 7B have the same preloading history but in a different way. In test 6C, the preloading history was 5+10 cycles whereas in Test 7B, it was 13 consecutive cycles.

Similarly, it can be noticed that for loading history of 15 cycles the 5th to 10th cycle of the two samples were quite similar with small differences in the loading part and the initial unloading part (Figure 34).

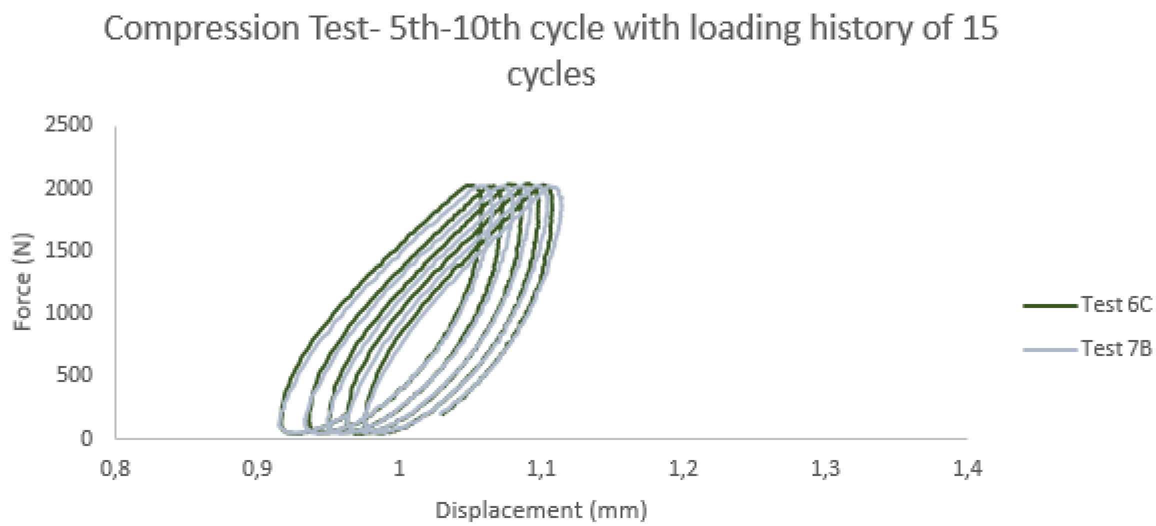

Figure 34. Force- Displacement graph. If the first 5 cycles are removed and the displacement results of Test 7B are transposed to have a common start with the correspondent of Test 6C.

From Figure 35 and Figure 36, for loading history of 10 and 10+10 cycles, similar behaviour of the samples to Tests 4-8 can be observed. It can be assumed from Figure 13-Figure 17 that 5 cycles is the minimum threshold for the samples to present uniform response in the next set of cyclic loading, during the last 5 cycles. This observation refers to the specific carpet material combination (carpet S, ceramic sand M) and at nominal loading rate of 200 N/s.

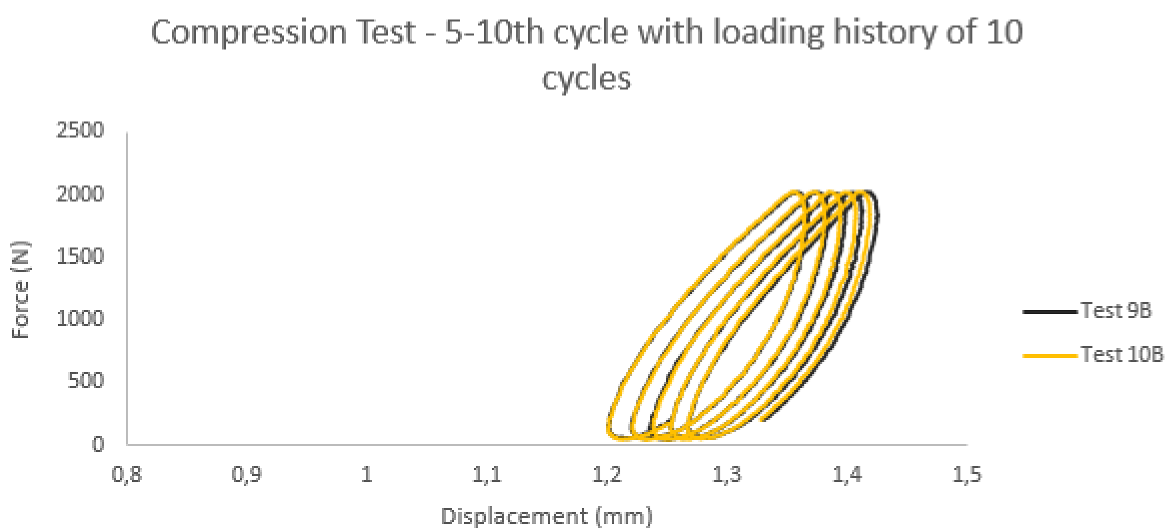

Figure 35. Force-Displacement graph. The carpet was S, the ceramic sand M and the tests were performed at loading rate 200 N/s. In tests 9B and 10B, if the 5th-10th cycles are compared, the results are quite similar with a small constant difference in the initial unloading part.

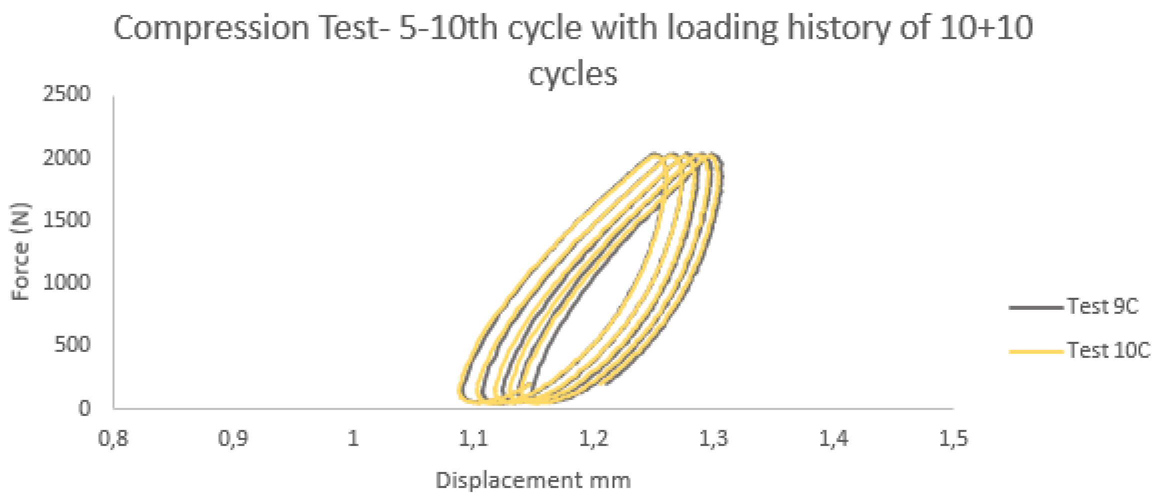

Figure 36. Force-Displacement graph. In tests 9C and 10C if the 5th-10th cycles are compared, the results are quite similar with small constant differences in the initial loading part. Compared to picture 11, the graph is transposed to the left, to lower displacements.

In Figure 37, the response of the sample at 400 N/s is depicted. As the loading rate was raised from 200 N/s to 400 N/s, the first irregular cycle changed its shape compared to Figure 31 and presented a maximum force, which was significantly higher than the 2000 N which was set from the machine. The reason for this abnormal behaviour was not identified and it could be due to the late initial response of the hydraulic machine at a higher loading rate.

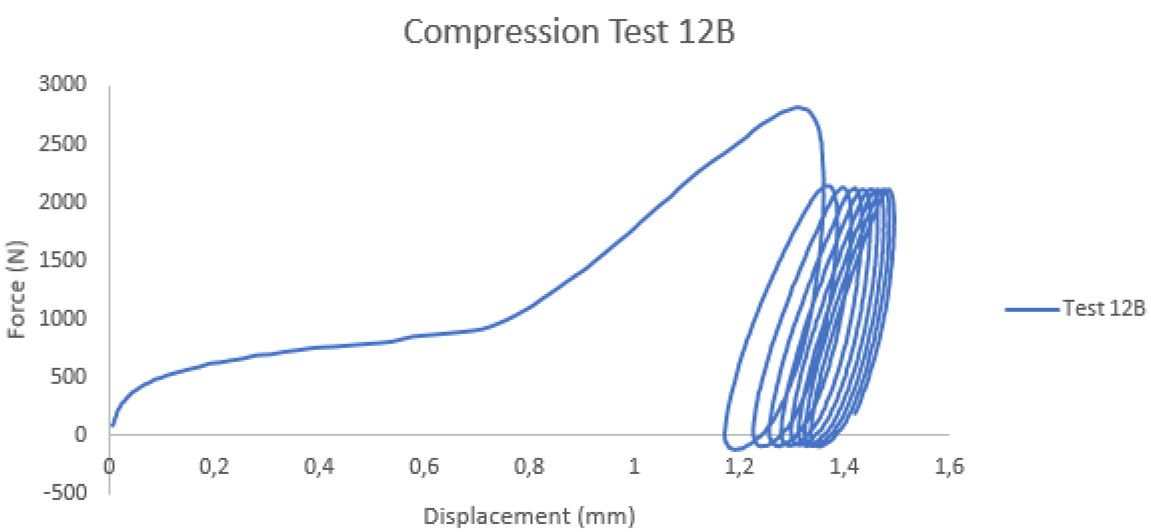

Figure 37. Force Displacement graph. The carpet was S, the ceramic sand M and the tests were performed at loading rate 400 N/s.

In Figure 38, the samples had a higher nominal loading rate of 400 N/s and two different loading histories. The 12B and 13B had 20 cycles of loading history and the 12C and 13C had 20+10. Both pairs presented differences in the initial loading part in one cycle order of magnitude. The C Tests were expected to be in lower displacement values compared to the B Tests due to the higher loading history, which did not happen in that case.

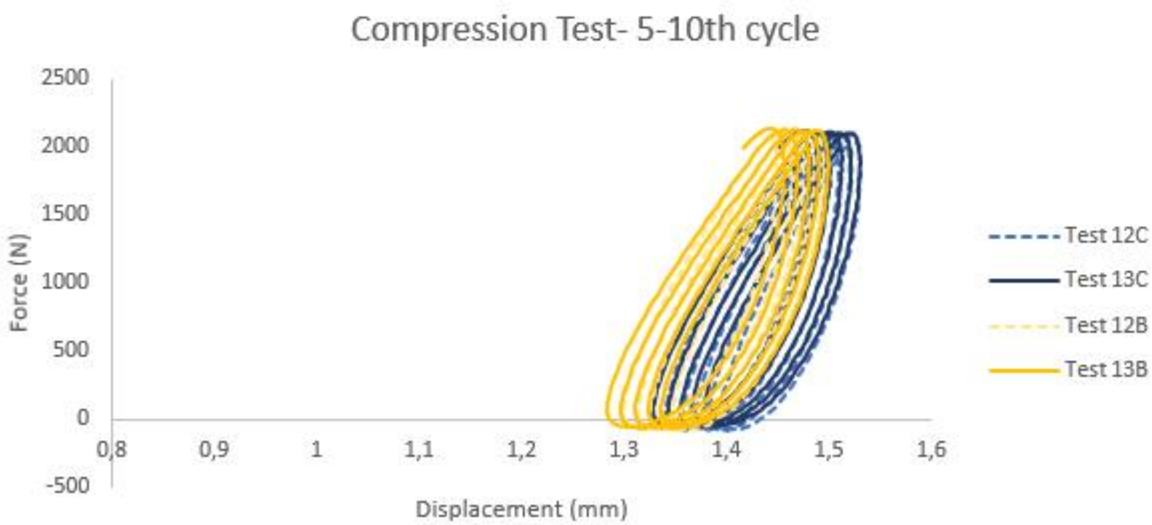

Figure 38. Force Displacement graph. The carpet was S, the ceramic sand M and the tests were performed at loading rate 400 N/s. If the first 5 cycles are removed and the displacement results of the Test 13B and 13C are transposed to have a common start with the correspondent of the Test 12B and 12C, respectively.

In Figure 39, Tests F2 and F3 had the same test parameters as in Figure 38. The only difference was the carpet-material combination, which in this case was F carpet and F ceramic sand. The results were similar, and a difference between the cycles was observed during the loading phase. In this case, the tests with the higher loading history were in lower displacement values, as expected.

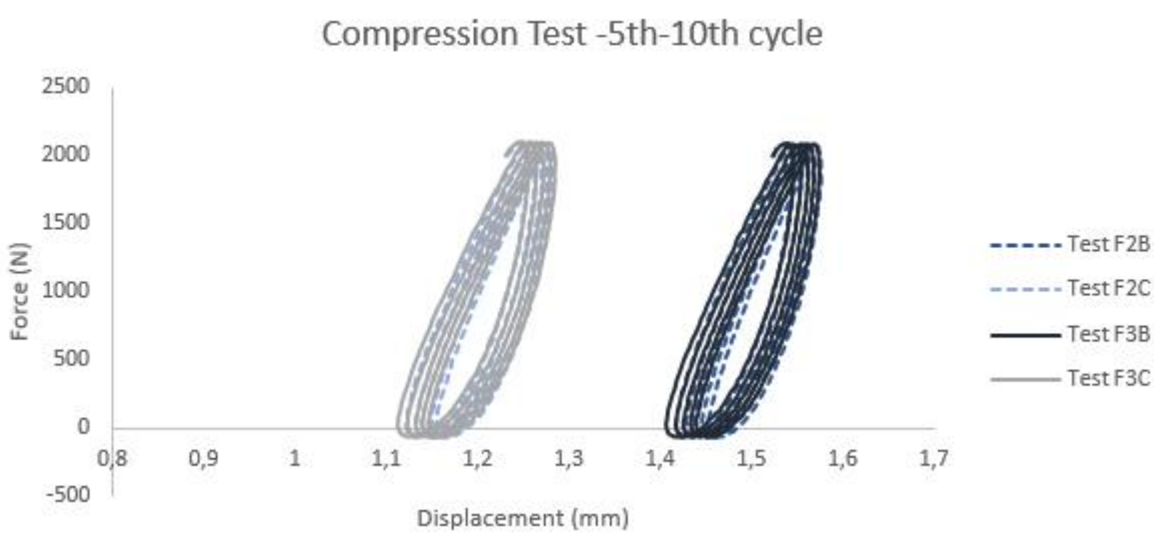

Figure 39. Force-Displacement graph. The carpet was F, the ceramic sand F and the tests were performed at loading rate 400 N/s.

In Figure 40, the same sample after two consecutive sets of cycles was examined. The Test F3B had 20 cycles of loading history whereas the Test F3C had 20+10. The cycles of the two samples after transposition to have the same start, coincided at high percentage.

For the higher nominal loading cycle, it can be noticed from Figure 39 and Figure 40, that the last 5 cycles of a loading set, for two different carpet- material combinations (SM, FF), presented similar behaviour. For both samples, the cycles concurred in the unloading phase with a difference of one cycle being observed during the loading phase Additionally, within the same sample which had been submitted to a previous loading, there was an indication that the last 5 cycles of each cyclic loading set, if they were set to have the same start, coincided at a high percentage.

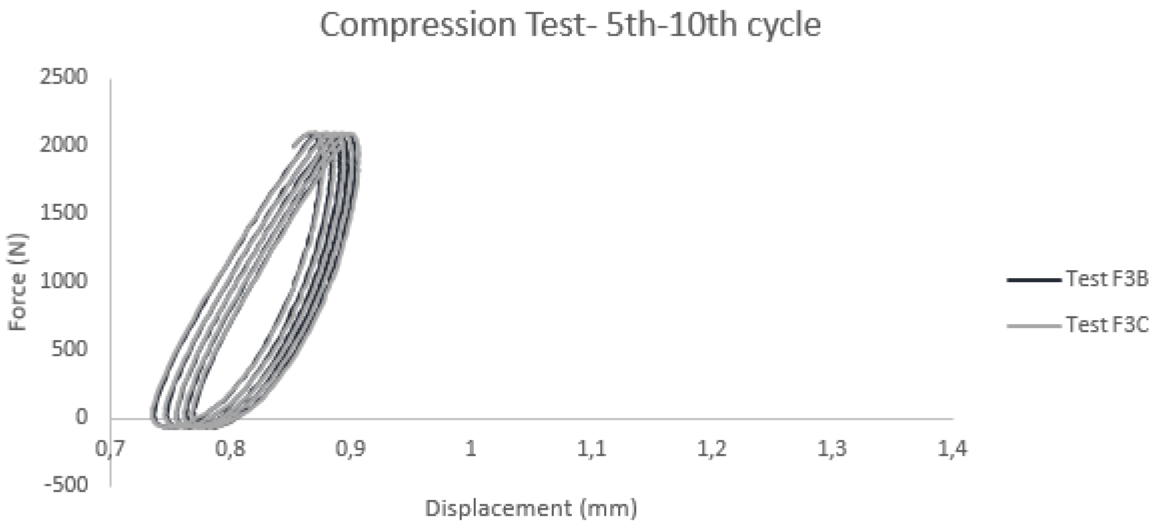

Figure 40. Force-Displacement graph. If the first 5 cycles are removed and the displacement results of Test F3C are transposed to have a common start with the correspondent of the Test F3B.

In Figure 41 and Figure 42, two different carpet-material combinations are analysed. The FF sample had a lower total displacement value and a smaller area between the loading and unloading curves compared to the SM sample for both B and C tests. For the B set, the two samples displayed similar inclinations in the loading phase but different during the unloading phase where the FF sample had steeper slopes especially in the initial unloading phase. In the C set the differences remained but they were reduced.

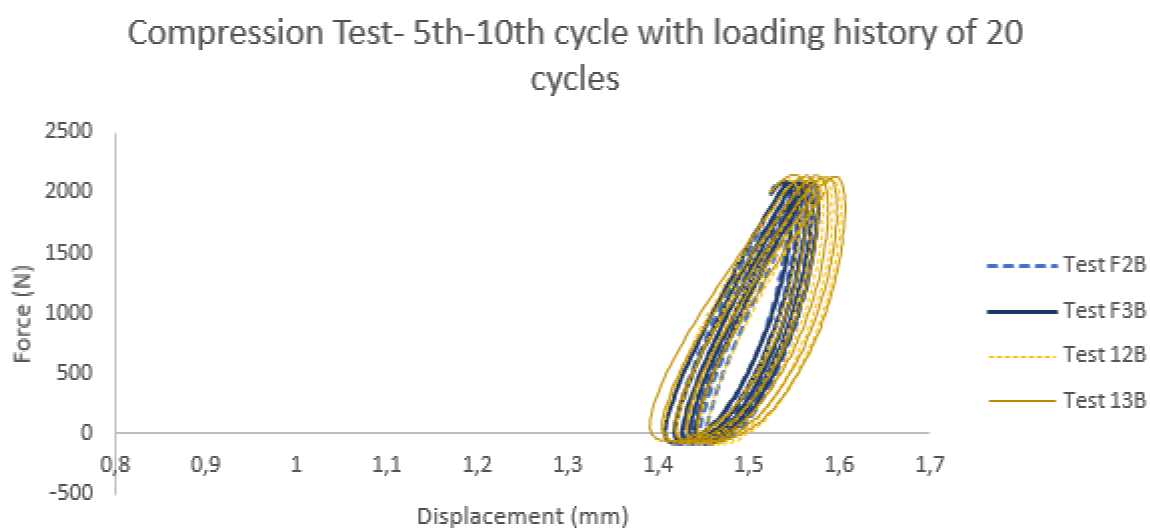

Figure 41. Force-Displacement graph. Two different carpet-material combinations under cyclic loading of 400 N/s were examined. The Tests 12 and 13 had S carpet and M ceramic sand whereas the Tests F2 and F3 had F carpet and F ceramic sand. The loading history of the B Tests was 20 cycles.

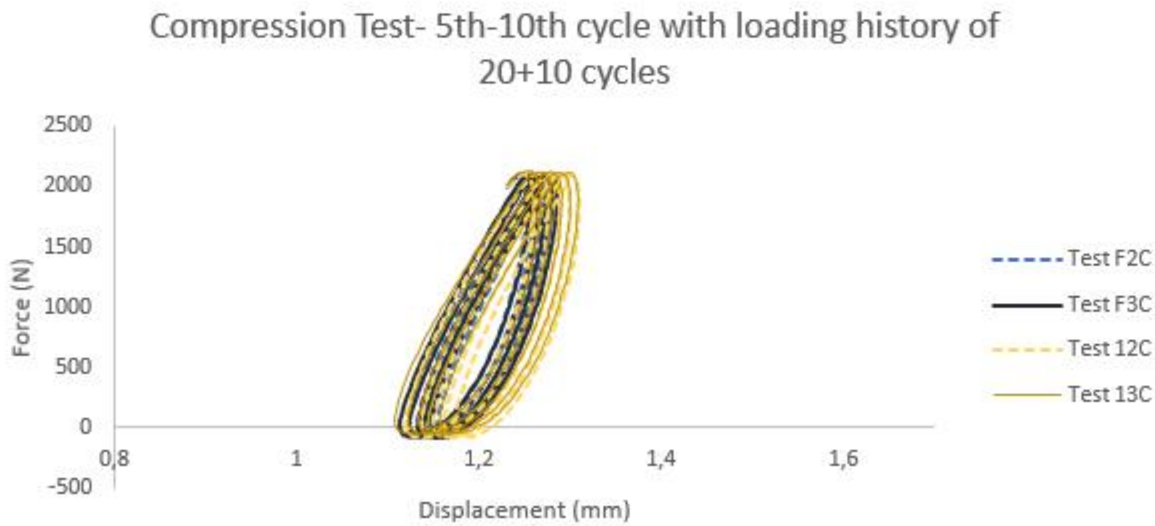

Figure 42. Force-Displacement graph. Two different carpet-material combinations under cyclic loading of 400 N/s were examined. The Tests 12 and 13 had S carpet and M ceramic sand whereas the Tests F2 and F3 had F carpet and F ceramic sand. The loading history of the C Tests was 20+10 cycles.

Loading History effect

The Figure 43-Figure 48 represent the response of various carpet-material combinations during 9 loading cycles with 400 N/s loading rate and 20 cycles loading history. The tests were performed two times and an average value was calculated. In (a), the energy transformation during nine consecutive cycles is illustrated. For all the carpet- material combinations, as the number of the cycles was raised, the percentage of energy dissipation (Ed) was reduced and the percentage of energy recovery (Er) was increased. In (b), the resilient and the secant modulus are examined. The Msec was increased for all the carpet-material combinations with the number of cycles and the Mr either changed slightly or remained constant. In (c), the maximum deflection of the carpet-material combinations in each cycle is presented, which was decreased with the number of cycles. In (d), the percentage of axial strain accumulation is displayed which was increased with the number of cycles for every carpet-material combination. In (e), the step of axial strain accumulation is depicted which was decreased with the number of cycles for carpet-material combination.

In Figure 43, the response of the three different carpets without the addition of ceramic sand was investigated. In (a), all the carpets had similar values but the T carpet had slightly lower Ed and higher Er than the S carpet, resulting in a potential better athlete performance, if the energy is returned under the right circumstances [47]. In (b), the Mr of the S carpet remained constant. Carpets S and T had similar Msec, higher than the F and carpet S had higher Mr than T and F which had similar. In (c), Carpet S showed higher maximum deflection compared to the other two carpets which presented similar values. The response of the S carpet is unexpected because although it had the higher Msec and Mr, it also produced maximum deflections. In (d), Carpet F presented the highest strain accumulation whereas carpet T had the lowest and in (e), during the first two cycles the F carpet had the higher step of strain accumulation and the T carpet the lower. After the fourth cycle all the carpets had similar step. The carpet F might exhibit the highest wear due to vertical loading force.

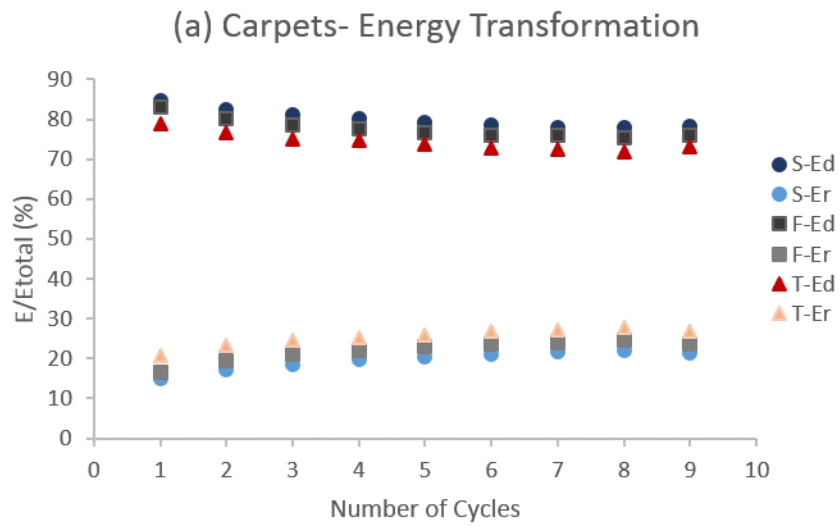
(a) Carpets- Energy Transformation
E/Etotal (%)
Number of Cycles
S-Ed
S-Er
F-Ed
F-Er
T-Ed
T-Er

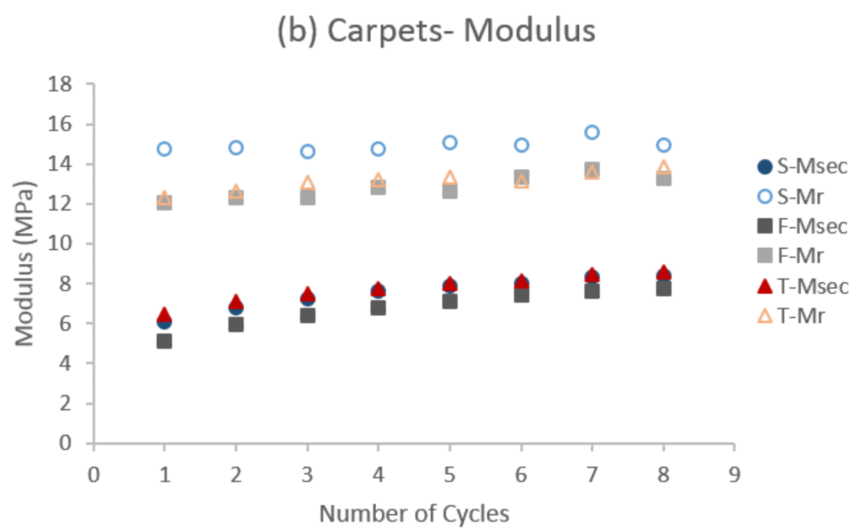
(b) Carpets- Modulus
Modulus (MPa)
Number of Cycles
S-Msec
S-Mr
F-Msec
F-Mr
T-Msec
T-Mr

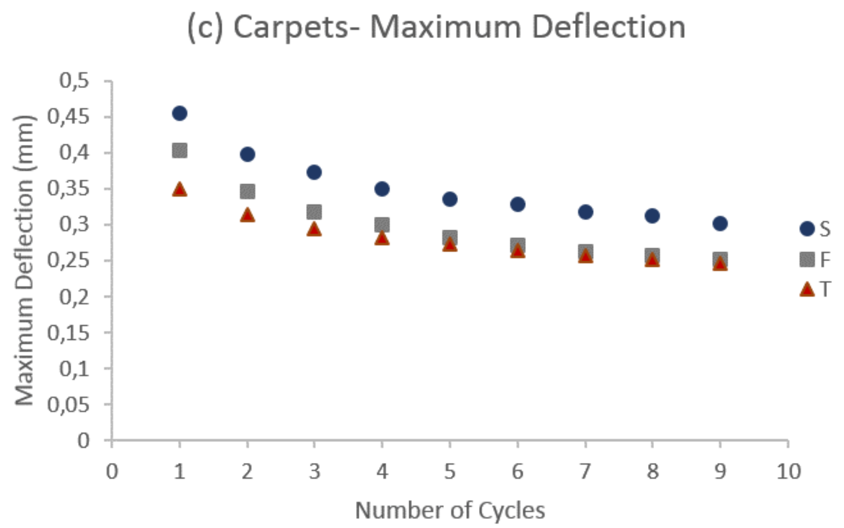
(c) Carpets- Maximum Deflection
Maximum Deflection (mm)
0,5
0,45
0,4
0,35
0,3
0,25
0,2
0,15
0,1
0,05
0
0 1 2 3 4 5 6 7 8 9 10
Number of Cycles
S
F
T

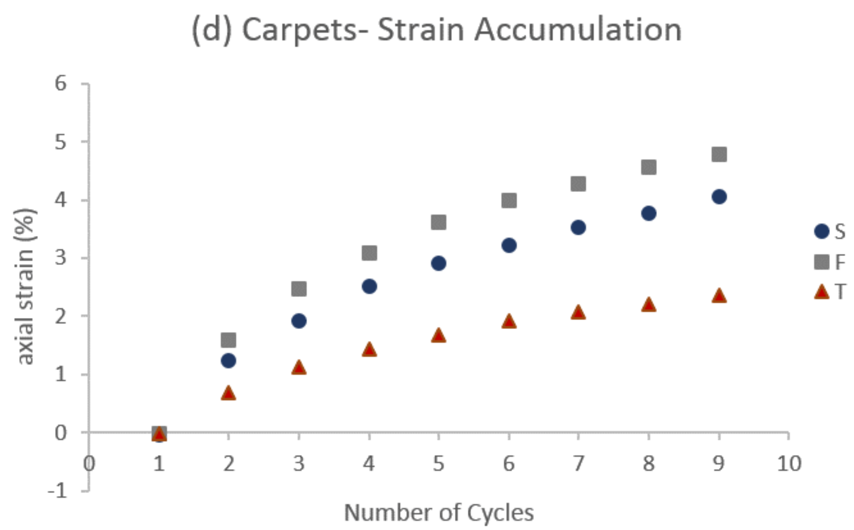
(d) Carpets- Strain Accumulation
axial strain (%)
6
5
4
3
2
1
0
-1
0 1 2 3 4 5 6 7 8 9 10
Number of Cycles
S
F
T

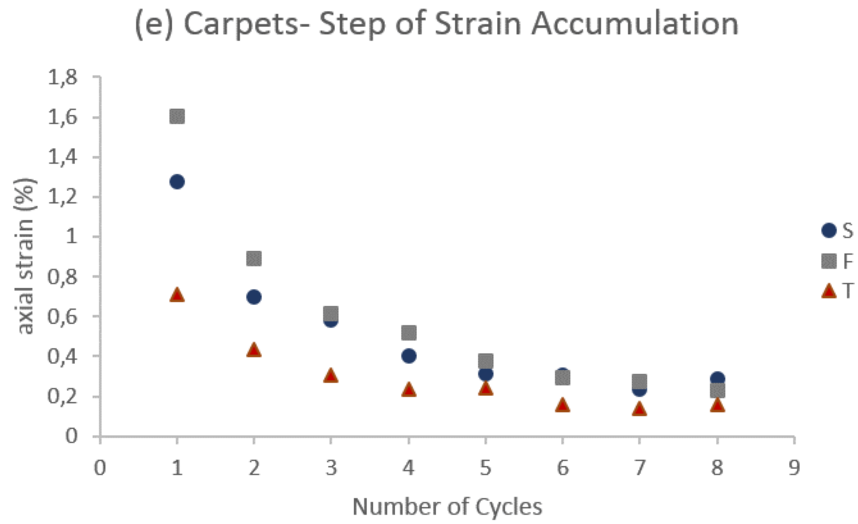

Figure 43. The three different carpets (S, F, T) without any material addition were examined under cyclic loading with 400 N/s loading rate. Figure (a) refers to the percentage of energy transformation, (b) to the Modulus of the material (Secant,Resilient), (c) the maximum deflection, (d) to the percentage of strain accumulation and (e) to the step of percentage strain accumulation.

In Figure 44 the response of the S carpet in combination with the three different ceramic sands C, M, and F was investigated. In (a), the S carpet with the F and M ceramic sand had lower Ed and higher Er than the S carpet without any material. In (b), the addition of the material resulted in higher values of Mr and Msec in all carpet S-material combinations compared to the simple carpet S. The ceramic sand S and M had similar values, higher than the ceramic sand C. This might be explained by the higher density of the F and M ceramic sands compared to the C. However, although S and M have also different densities, their values differentiate only in the first two cycles which may imply that there are additional mechanisms contributing to this behaviour, such as the particle shape, size and texture and/or the way each type of ceramic sand blends in with the carpet. In (c), Carpet S showed the highest maximum deflection and then the carpet S with the C ceramic sand. The F and M ceramic sand had similar lower displacement. In (d), the carpet S and then the C ceramic sand with the carpet S presented the higher strain accumulation. In (e), the S carpet with no material had the highest step of strain accumulation and the S carpet with the M and F ceramic sand the lowest. In this set of tests the carpet S combined with the F or the M ceramic sand had similar response and they were stiffer than the carpet S alone or combined with C ceramic sand. Examples for absolute values of energy transformation are for SF, SC energy lost 0.21 J, 0.27 J and 0.3 J, 0.35 J energy input, respectively. The effect of those values can be examined if the mechanical energy demanded for a vertical movement is provided.

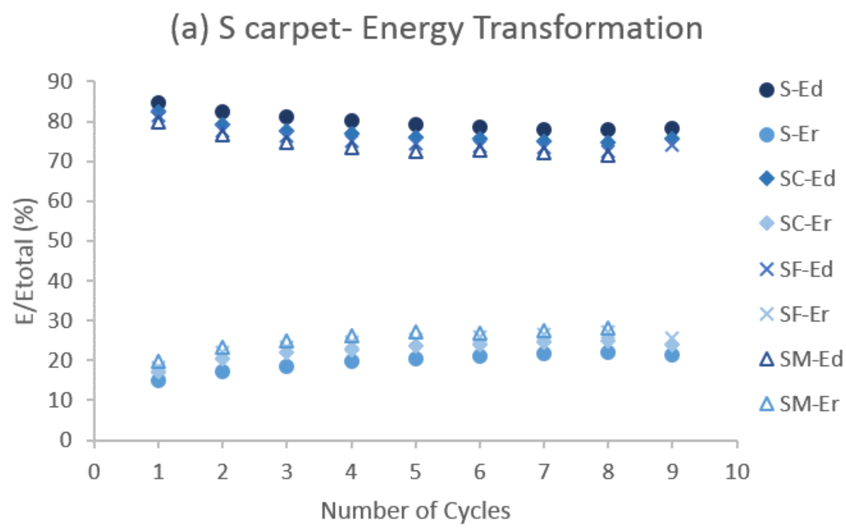
(a) S carpet- Energy Transformation
E/Etotal (%)
Number of Cycles
S-Ed
S-Er
SC-Ed
SC-Er
SF-Ed
SF-Er
SM-Ed
SM-Er

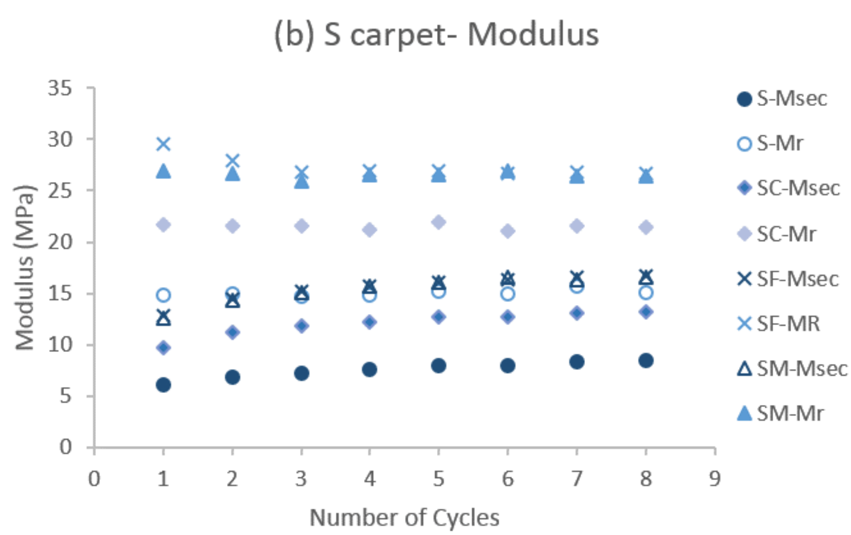
(b) S carpet- Modulus
Modulus (MPa)
Number of Cycles
S-Msec
S-Mr
SC-Msec
SC-Mr
SF-Msec
SF-MR
SM-Msec
SM-Mr

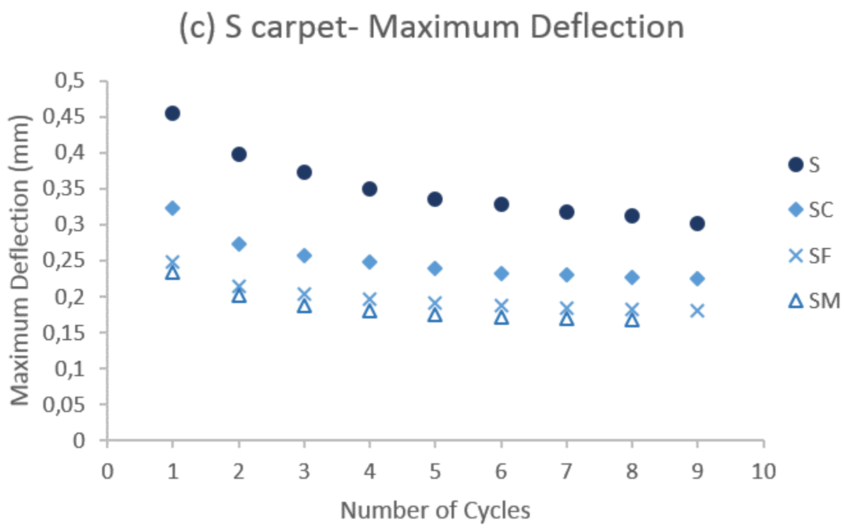
(c) S carpet- Maximum Deflection
Maximum Deflection (mm)
0,5
0,45
0,4
0,35
0,3
0,25
0,2
0,15
0,1
0,05
0
0
1
2
3
4
5
6
7
8
9
10
Number of Cycles
S
SC
SF
SM

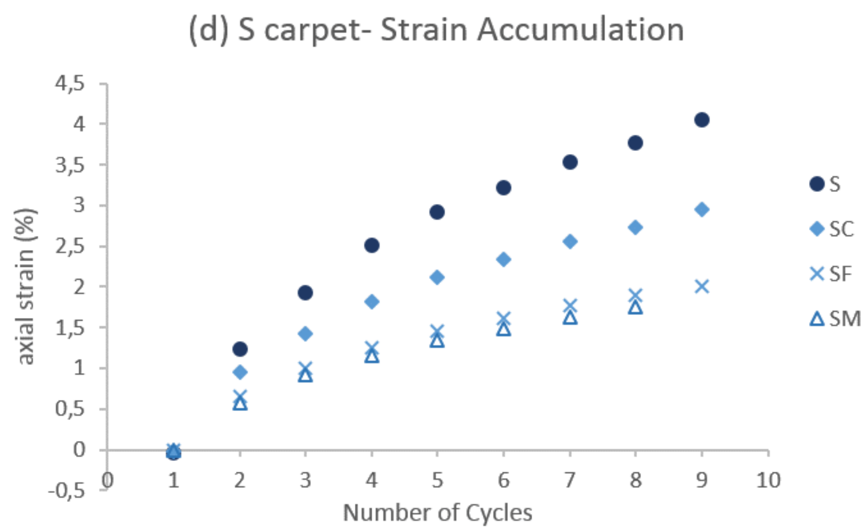
(d) S carpet- Strain Accumulation
axial strain (%)
4,5
4
3,5
3
2,5
2
1,5
1
0,5
0
-0,5
0
1
2
3
4
5
6
7
8
9
10
Number of Cycles
S
SC
SF
SM

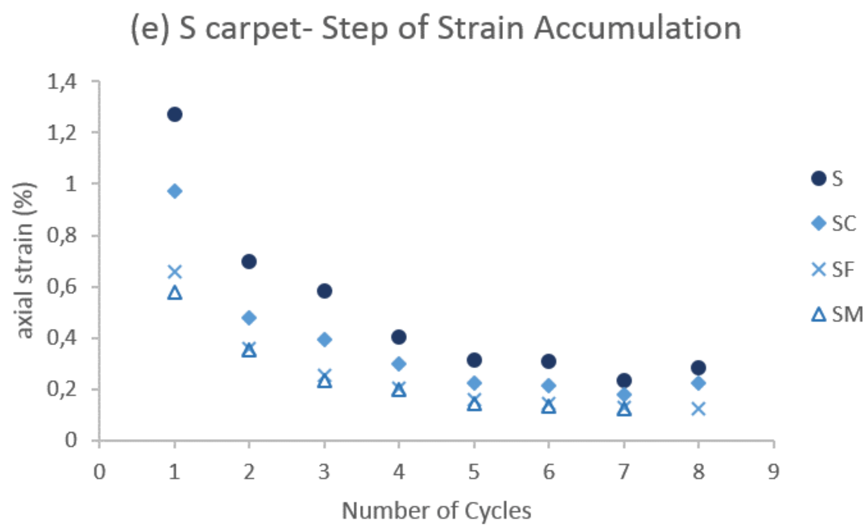

Figure 44. The carpet S with ceramic sand C, M, F were examined under cyclic loading with 400 N/s loading rate. Figure (a) refers to the percentage of energy transformation, (b) to the Modulus of the material (Secant, Resilient), (c) the maximum deflection, (d) to the percentage of strain accumulation and (e) to the step of percentage strain accumulation.

In Figure 45, the response of the F carpet in combination with two different ceramic sands C and F was examined. In (a), the F carpet with the F ceramic sand had lower Ed and higher Er than the F carpet with the F ceramic sand or without any material. In (b), the addition of the material resulted in higher values of Mr and Msec in all carpet F-material combinations compared to the simple carpet S. The carpet F with the ceramic sand S had higher values than with the ceramic sand C, which was similar behaviour with Figure 44 (c). The carpet with the finer material was stiffer than the carpet with the C ceramic sand. In (c), Carpet F showed the highest maximum deflection and then the carpet F with the C ceramic sand, followed by the carpet F with the finer material. In (d), the carpet F and then the C ceramic sand with the carpet F presented higher strain accumulation than carpet F with the F ceramic sand. In (e), the F carpet with no material had the highest step of strain accumulation and the F carpet with the C and F ceramic sand the lowest, differing only in the first cycle. In this set of tests the carpet F combined with the F ceramic sand was stiffer than the carpet F with the C ceramic sand.

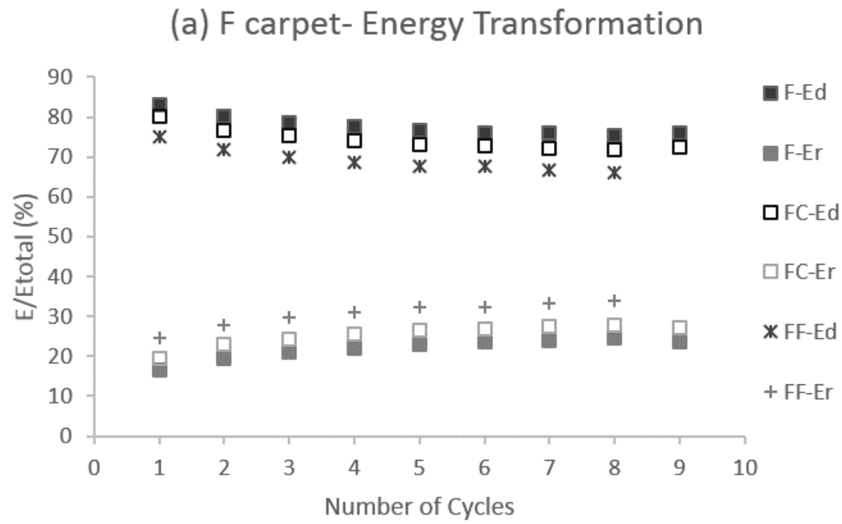
(a) F carpet- Energy Transformation
E/Etotal (%)
Number of Cycles
F-Ed
F-Er
FC-Ed
FC-Er
FF-Ed
FF-Er

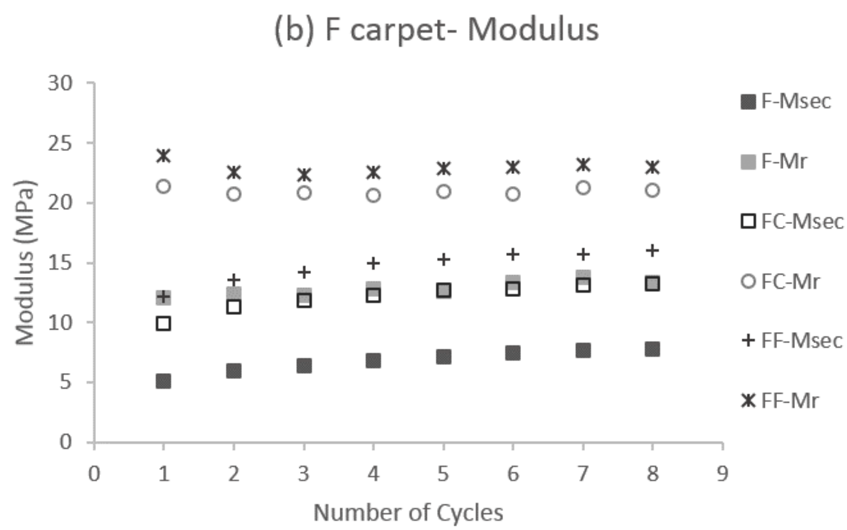
(b) F carpet- Modulus
Modulus (MPa)
Number of Cycles
F-Msec
F-Mr
FC-Msec
FC-Mr
FF-Msec
FF-Mr

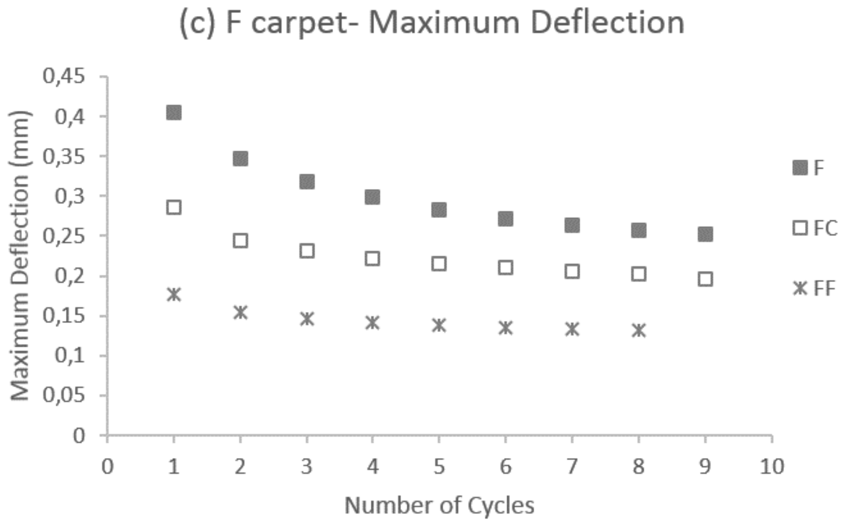
(c) F carpet- Maximum Deflection
Maximum Deflection (mm)
0,45
0,4
0,35
0,3
0,25
0,2
0,15
0,1
0,05
0
0
1
2
3
4
5
6
7
8
9
10
Number of Cycles
F
FC
FF

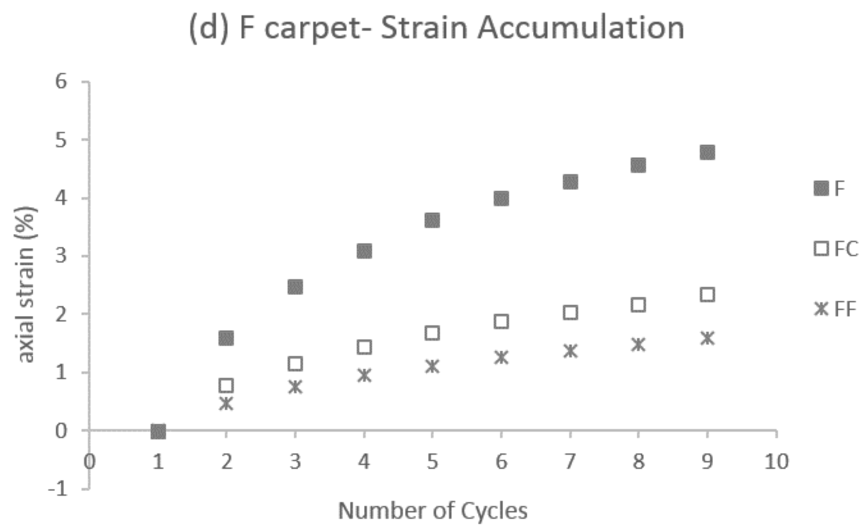
(d) F carpet- Strain Accumulation
axial strain (%)
6
5
4
3
2
1
0
-1
0
1
2
3
4
5
6
7
8
9
10
Number of Cycles
F
FC
FF

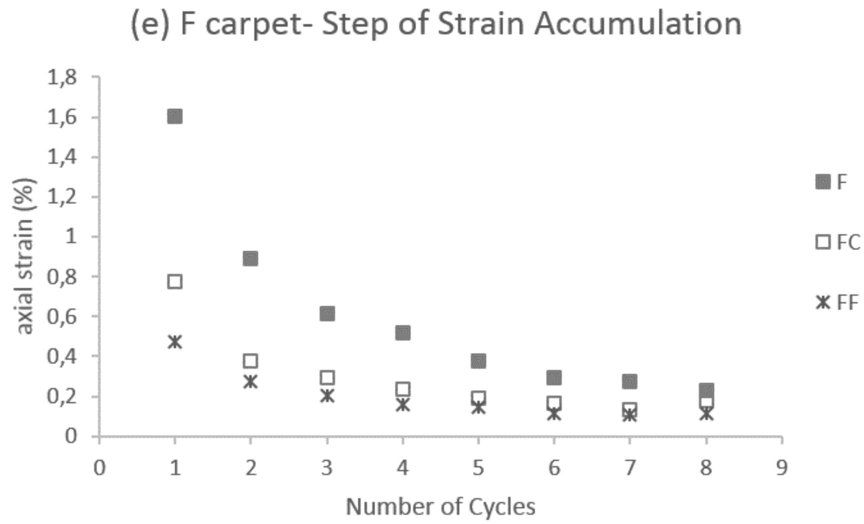

Figure 45. The carpet F with the ceramic sand C and F were examined under cyclic loading with 400 N/s loading rate. Figure (a) refers to the percentage of energy transformation, (b) to the Modulus of the material (Secant, Resilient), (c) the maximum deflection, (d) to the percentage of strain accumulation and (e) to the step of percentage strain accumulation.

In Figure 46, the response of the F ceramic sand in combination with three different carpets S, F and T was examined. In (a), the F ceramic sand with the F carpet had lower Ed and higher Er than the other two combinations. In (b), all the combinations had similar Msec and the F ceramic sand with the S carpet had a higher Mr compared to the other two. In (c), the ceramic sand F with the carpet T showed the highest maximum deflection and the carpet F the lowest. In (d-e), the ceramic sand F with the carpet T and F showed similar strain accumulation, higher the same ceramic sand combined with M carpet, and also higher step of strain accumulation for the first two cycles which became similar for all the three combinations during the following cycles. In the fine ceramic sand- carpet combination, the change in the carpet resulted in lower percentages of energy transformation for the F carpet, similar modulus for all the combinations except the Mr of the S carpet which was higher, and a higher percentage of strain accumulation for the S and T carpets.

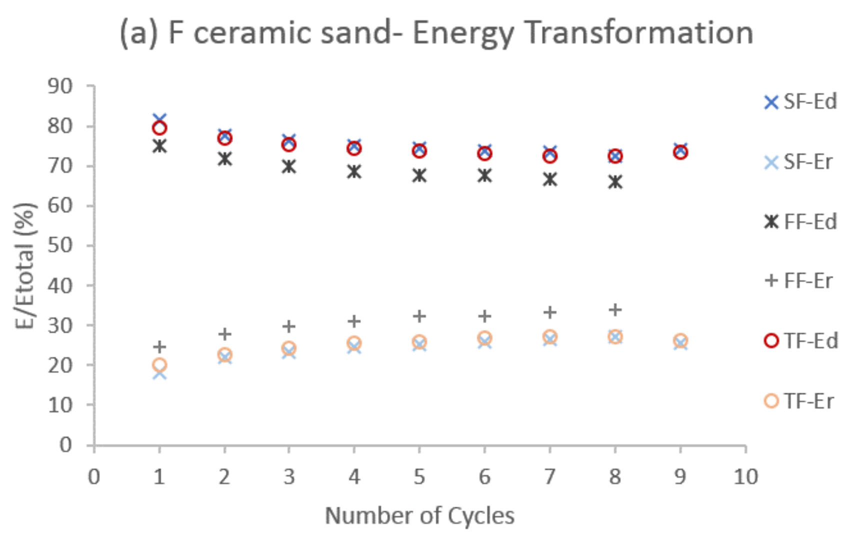

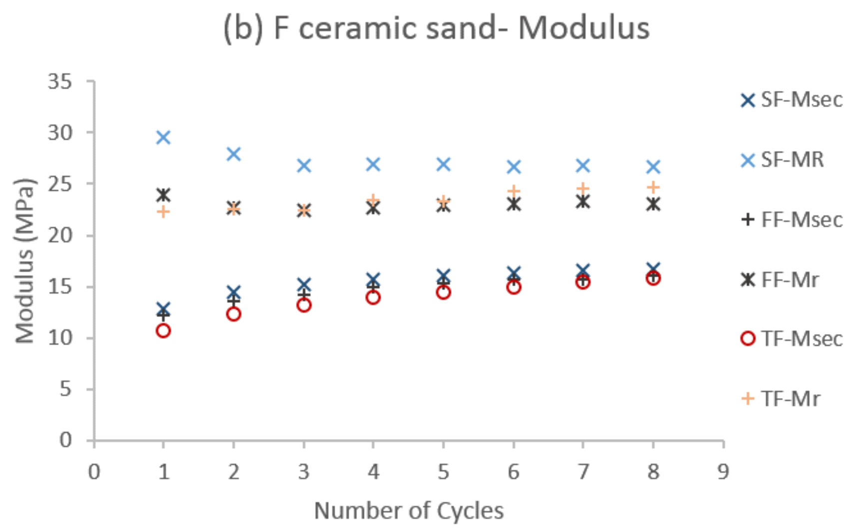
(b) F ceramic sand- Modulus
Modulus (MPa)
Number of Cycles
SF-Msec
SF-MR
FF-Msec
FF-Mr
TF-Msec
TF-Mr
35
30
25
20
15
10
5
0
0
1
2
3
4
5
6
7
8
9

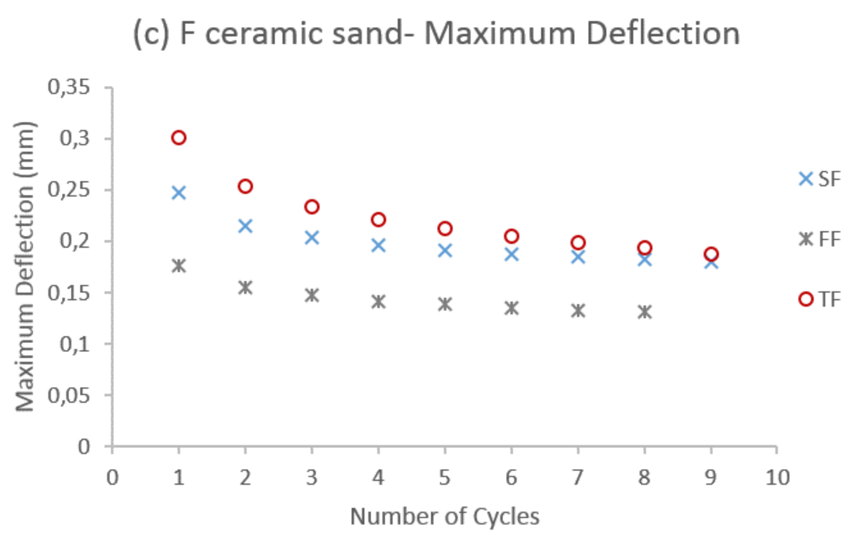
(c) F ceramic sand- Maximum Deflection
Maximum Deflection (mm)
Number of Cycles
SF
FF
TF
0,35
0,3
0,25
0,2
0,15
0,1
0,05
0
0
1
2
3
4
5
6
7
8
9
10

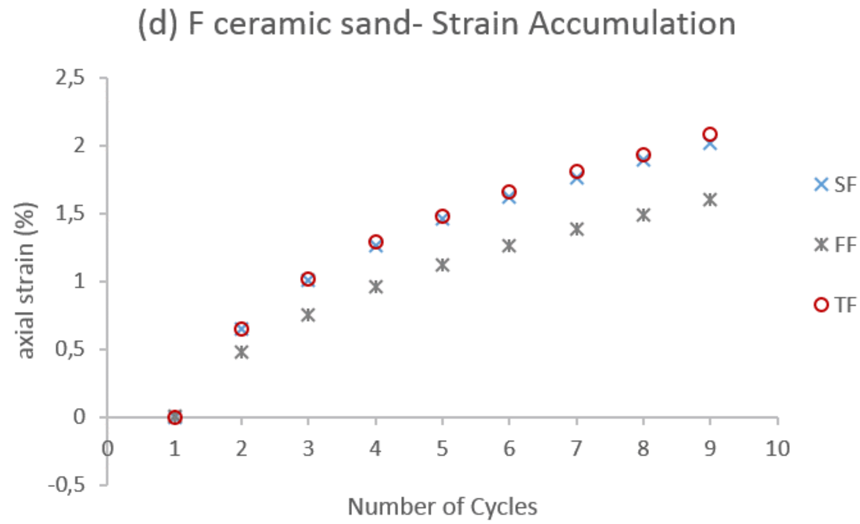

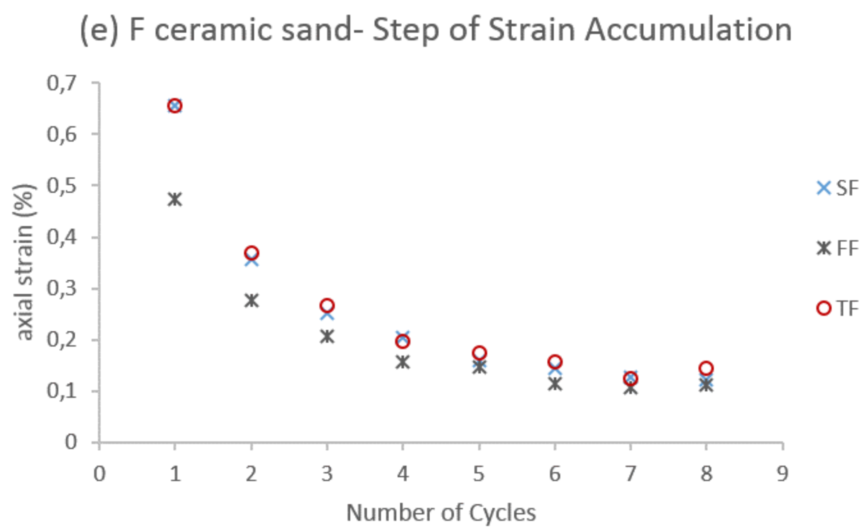

Figure 46. The ceramic sand F with the carpets S, F, T were examined under cyclic loading with 400 N/s loading rate. Figure (a) refers to the percentage of energy transformation, (b) to the Modulus of the material (Secant, Resilient), (c) the maximum deflection, (d) to the percentage of strain accumulation and (e) to the step of percentage strain accumulation.

In Figure 47 , the response of the C ceramic sand in combination with two different carpets S and F was investigated. In (a), the C ceramic sand with the S and F carpet similar Ed and Er and in (b), they have similar Mr and Msec. In (c), the ceramic sand C with the carpet F showed slightly lower maximum deflection compared to the C ceramic sand with the S carpet and in (d-e), it had higher strain accumulation and step of strain accumulation for the first three cycles which became similar for both the combinations during the following cycles. In the coarse ceramic sand-carpet combination, the change in the carpet did not influence the percentage of energy transformation or the modulus of the system, but it was presented a higher percentage of strain accumulation to the S carpet.

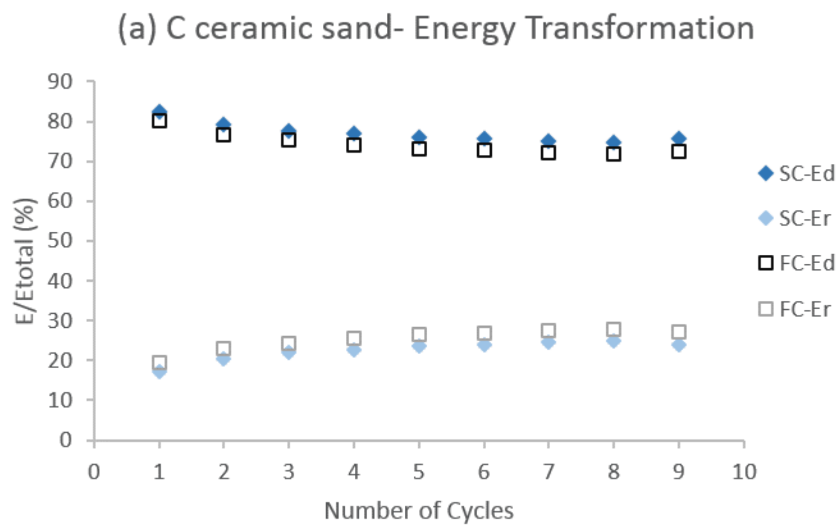

(a) C ceramic sand- Energy Transformation
E/Etotal (%)
Number of Cycles
SC-Ed
SC-Er
FC-Ed
FC-Er

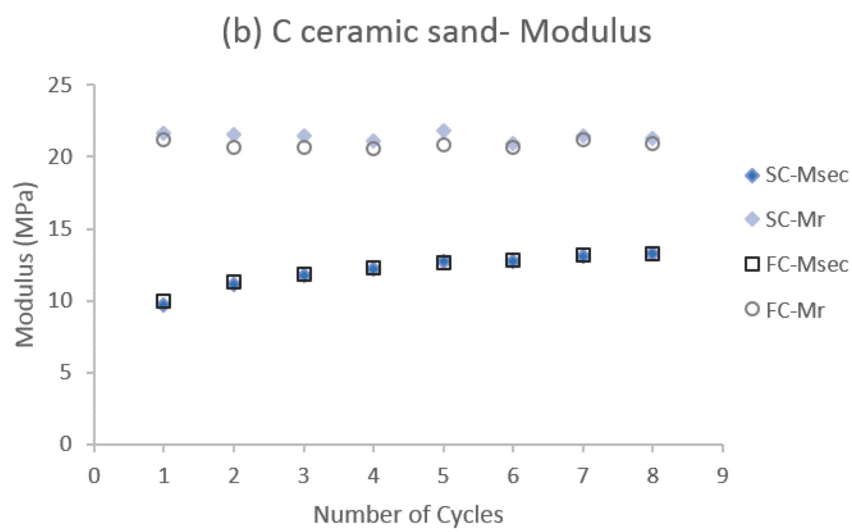

(b) C ceramic sand- Modulus
Modulus (MPa)
Number of Cycles
SC-Msec
SC-Mr
FC-Msec
FC-Mr

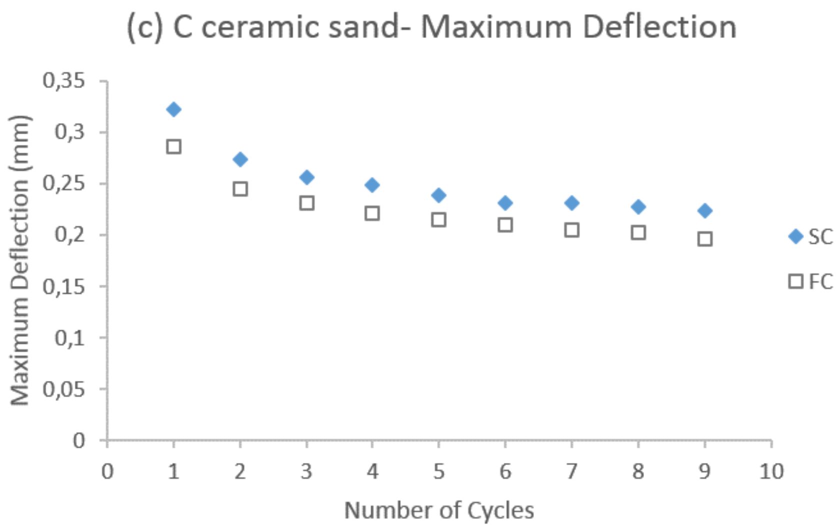
(c) C ceramic sand- Maximum Deflection
Maximum Deflection (mm)
0,35
0,3
0,25
0,2
0,15
0,1
0,05
0
0 1 2 3 4 5 6 7 8 9 10
Number of Cycles
SC
FC

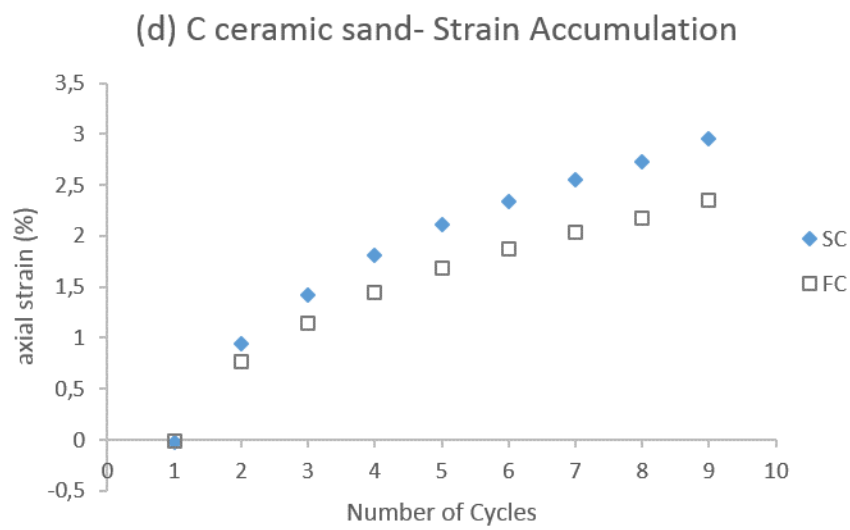
(d) C ceramic sand- Strain Accumulation
axial strain (%)
3,5
3
2,5
2
1,5
1
0,5
0
-0,5
0 1 2 3 4 5 6 7 8 9 10
Number of Cycles
SC
FC

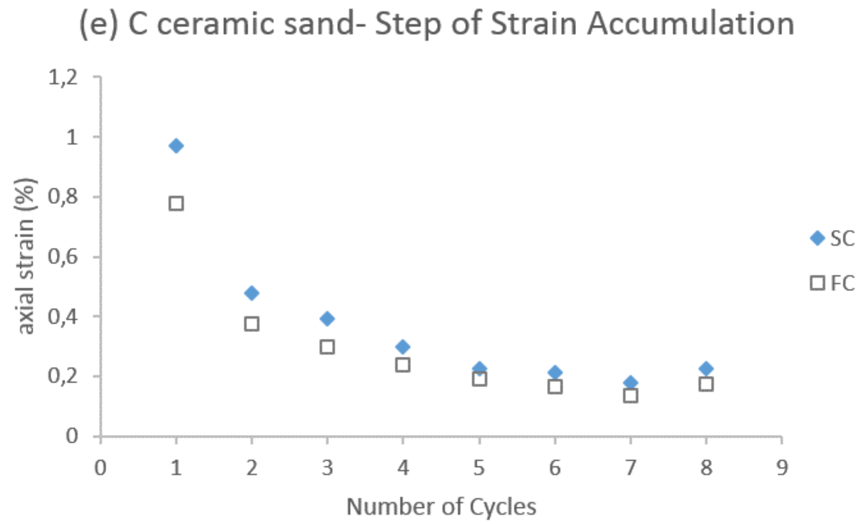

Figure 47. The ceramic sand C with the carpet S and F were examined under cyclic loading with 400 N/s loading rate. Figure (a) refers to the percentage of energy transformation, (b) to the Modulus of the material (Secant, Resilient), (c) the maximum deflection, (d) to the percentage of strain accumulation and (e) to the step of percentage strain accumulation.

In Figure 48, the response of the S carpet with M (SM) ceramic sand and the F carpet with F ceramic sand (FF) was investigated. Those two material-carpet combinations exist in real courts. In (a), the FF combination had lower Ed and Er compared to the FF combination. In (b), both combinations had similar Msec values and the SM had higher Mr. In (c-d), SM showed higher maximum deflection and slightly higher strain accumulation compared to the FF whereas in (e) the step of strain accumulation was slightly higher in the first two cycles for the SM but became similar for both the combinations during the following cycles. Combination FF had a lower percentage of energy losses and lower strain accumulation.

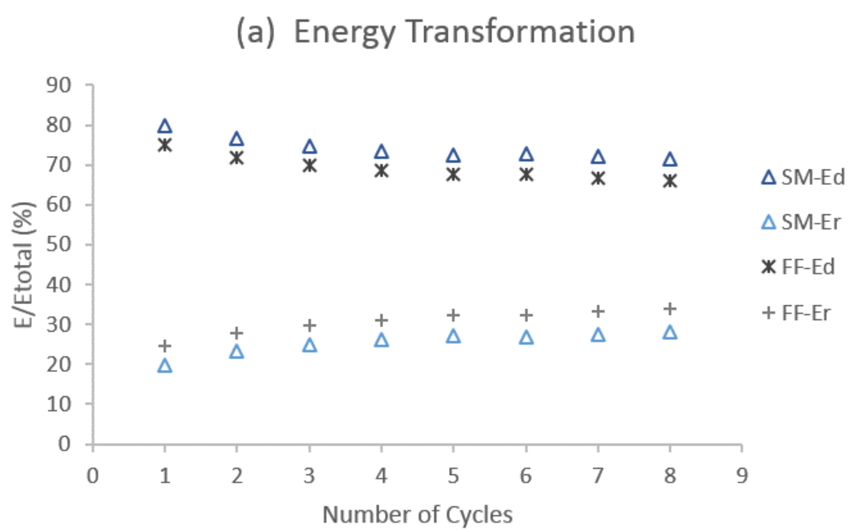

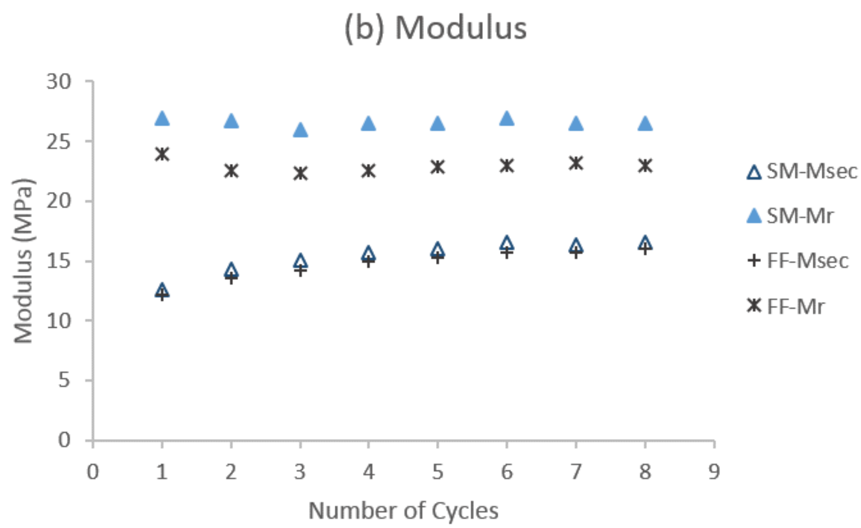
(b) Modulus
Modulus (MPa)
30
25
20
15
10
5
0
0
1
2
3
4
5
6
7
8
9
Number of Cycles
SM-Msec
SM-Mr
FF-Msec
FF-Mr

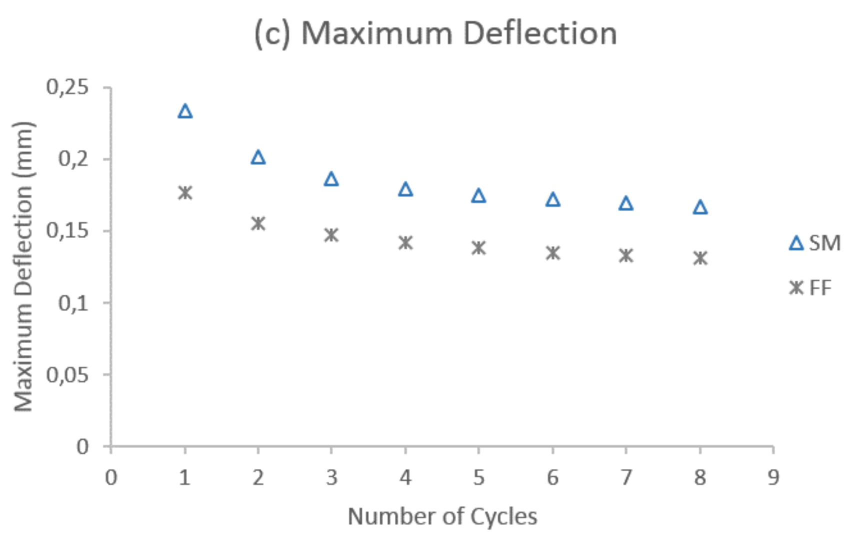
(c) Maximum Deflection
Maximum Deflection (mm)
0,25
0,2
0,15
0,1
0,05
0
0
1
2
3
4
5
6
7
8
9
Number of Cycles
SM
FF

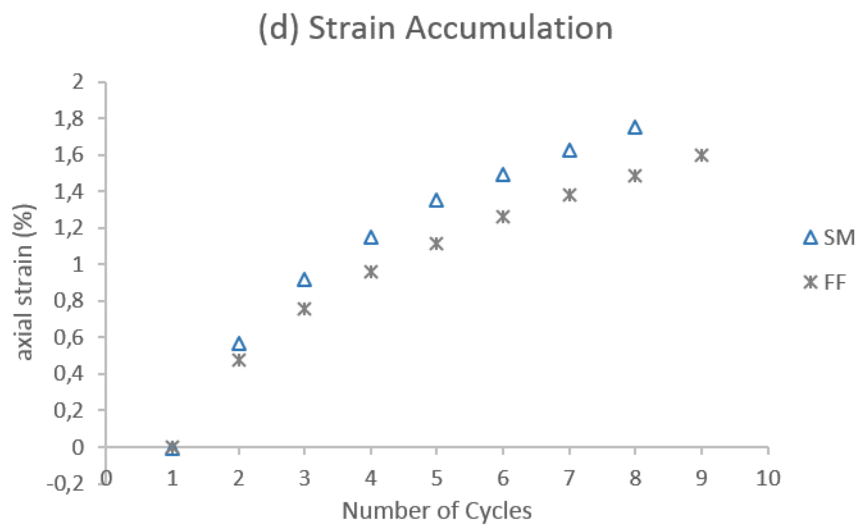

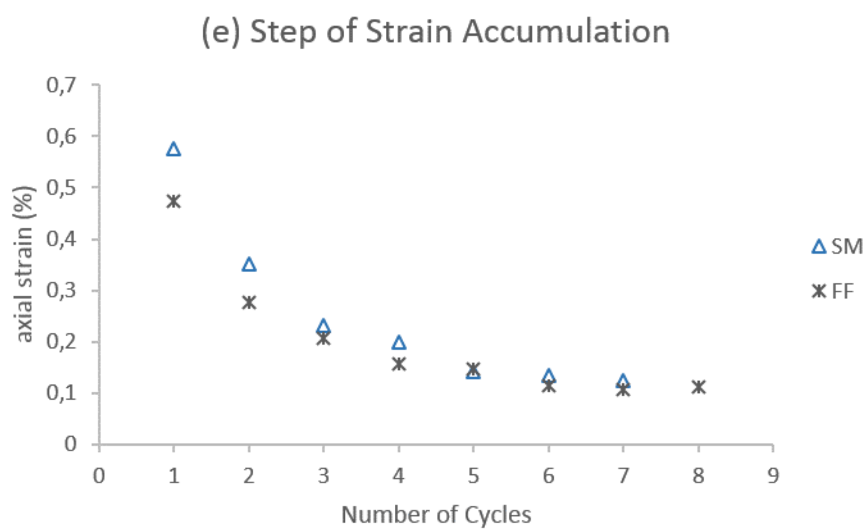

Figure 48. The combinations of carpet S, ceramic sand M and carpet F, ceramic sand F were examined under cyclic loading with 400 N/s loading rate. Those two combinations exist in real courts. Figure (a) refers to the percentage of energy transformation, (b) to the Modulus of the material (Secant, Resilient), (c) the maximum deflection, (d) to the percentage of strain accumulation and (e) to the step of percentage strain accumulation.

Strain accumulation effect

In Figure 49 the correlations of the percentage of energy dissipation and the secant modulus with the strain accumulation for the F ceramic sand in combination with three different carpets S, F and T were examined. As the strain accumulation increased with the number of cycles, the percentage of the dissipated energy decreased linearly (a) and the secant modulus increased linearly (b).

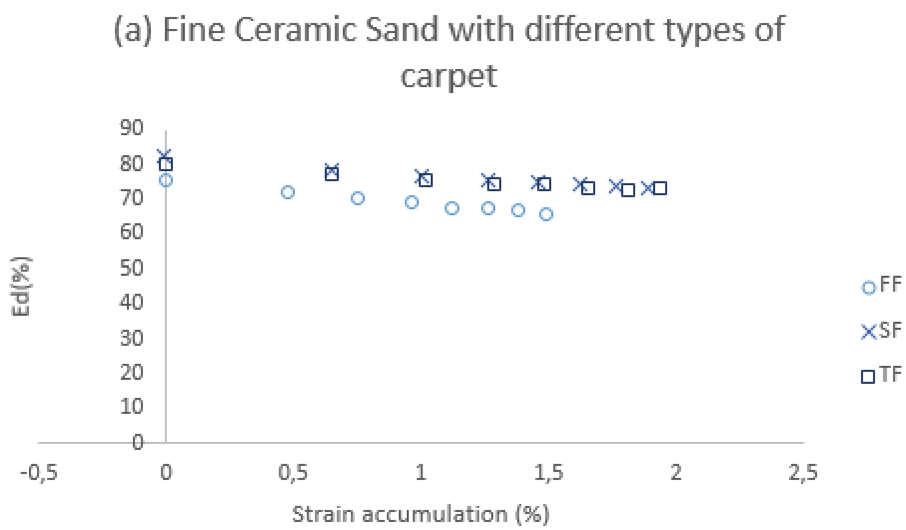

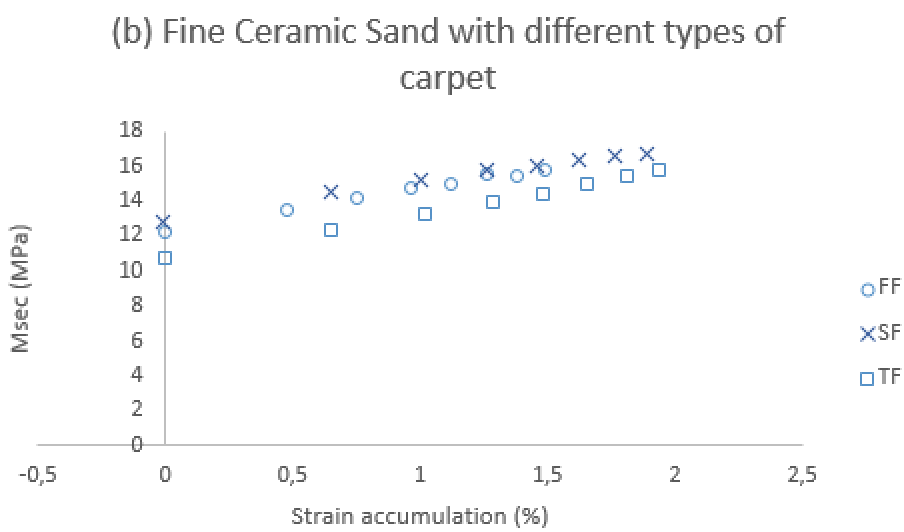

Figure 49. The ceramic sand F with the carpets S, F, T were examined under cyclic loading with 400 N/s loading rate. Figure (a) and (b) refer to the correlation of the energy dissipation and secant modulus with the strain accumulation, respectively.

In Figure 50, the correlations of the percentage of energy dissipation and the secant modulus with the strain accumulation for the S carpet in combination with three different ceramic sands C, F and M were examined. As the strain accumulation increased with the number of cycles, the percentage of the dissipated energy decreased linearly (a) and the secant modulus increased linearly (b).

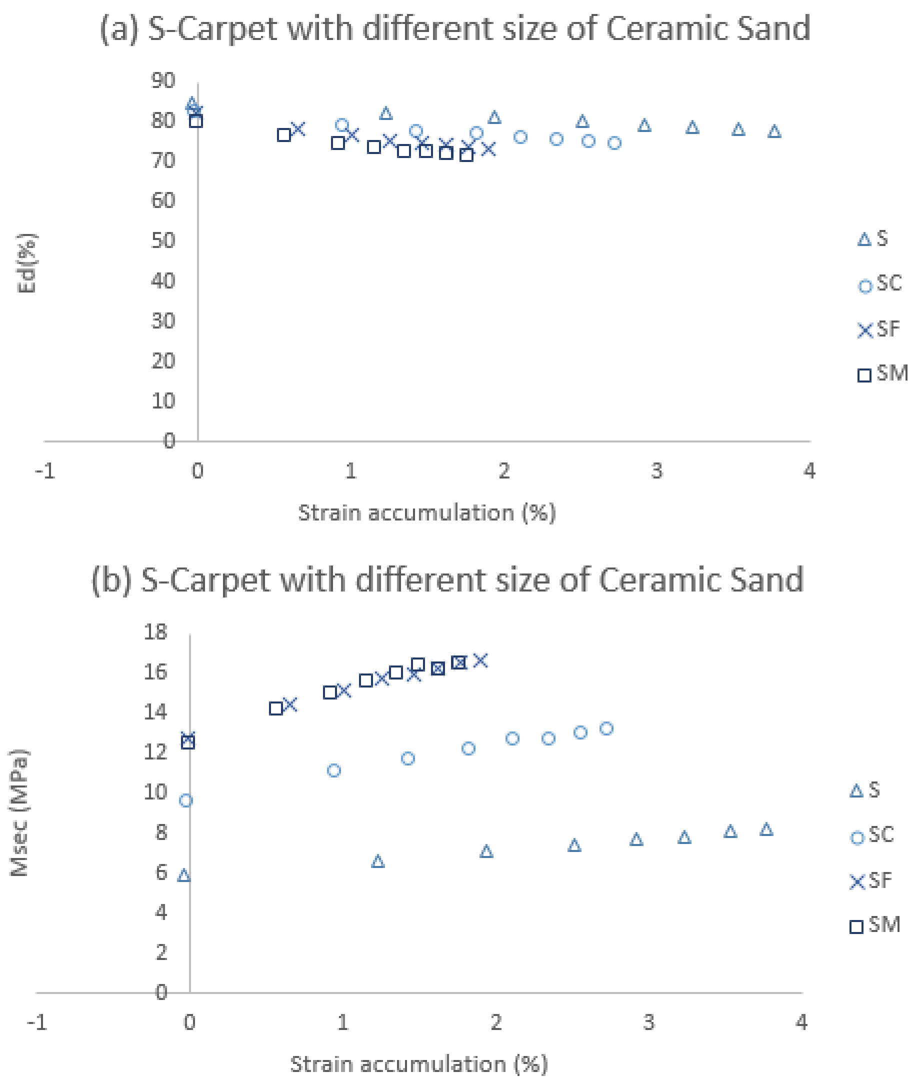

Figure 50. The carpet S with the ceramic sand C, M, F were examined under cyclic loading with 400 N/s loading rate. Figure (a) and (b) refer to the correlation of the energy dissipation and secant modulus with the strain accumulation, respectively.

6.2 Motion Capture System

The biomechanical measurements of the sliding movement were performed on two different clay courts by two different athletes, using both the Xsens Link and Awinda motion capture systems. However due to an error in the gravitational field of the left foot sensor of the Link system, only the data acquired by the Awinda system were considered reliable. Therefore, the following section refers to the Awinda system. In Figure 51 (a-f), the sliding with the right leg as dominant is described in six different moments, from the initial movement of the athlete to start the sliding (a) until the moment he lifted his foot to move towards the centre of the court (f).

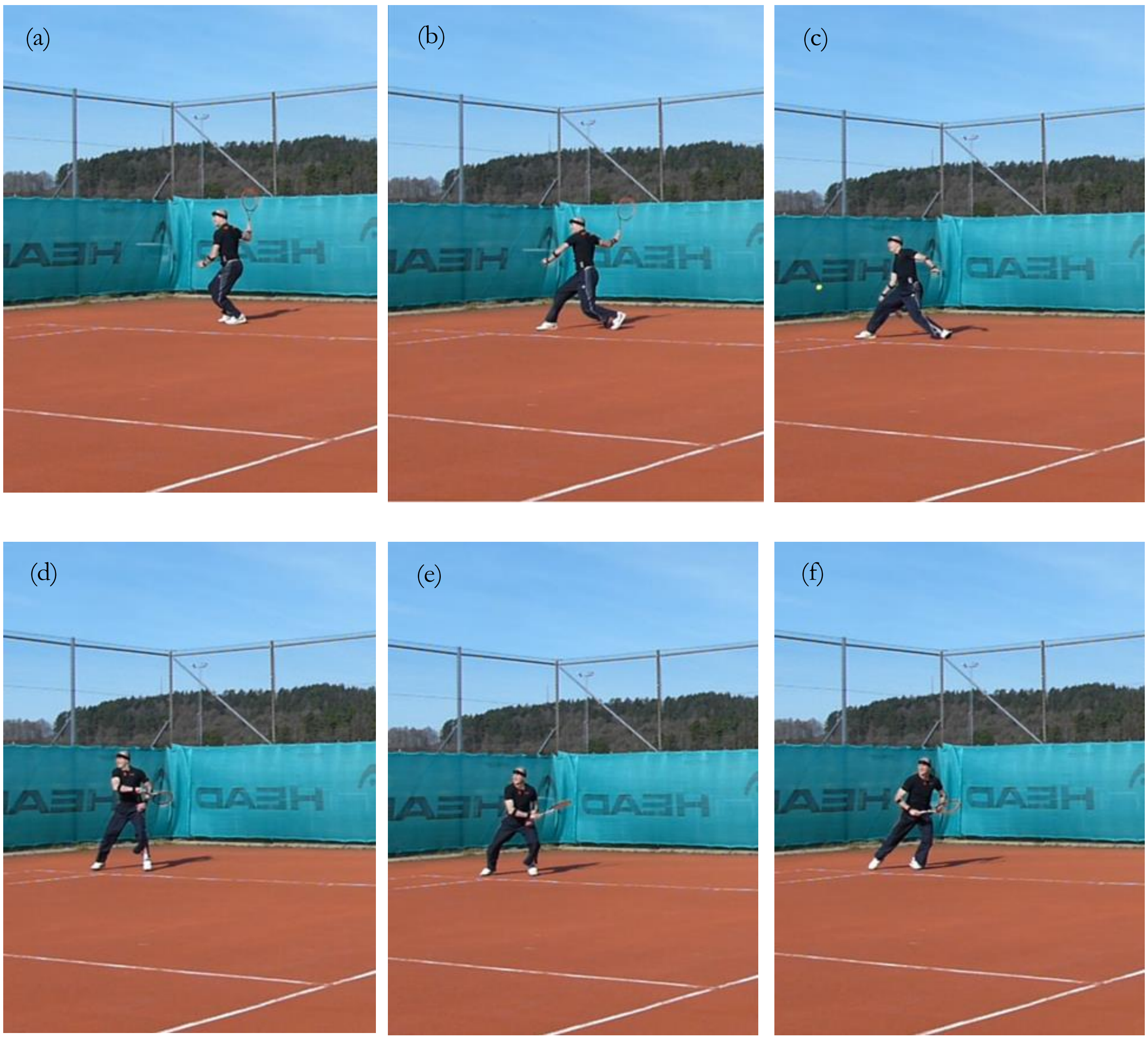

Figure 51. Sliding movement in the Lindome tennis court. Measurements were taken using the Xsens Motion Capture System. Figure (a) depicts the moment the athlete lifted his right leg in order to get prepared for the sliding movement. Figure (b) refers to the moment the athlete's right foot touched the court and the sliding movement was initiated. Figure (c) describes the moment the athlete finished the sliding and he was prepared to hit the ball. Figure (d) is when the athlete started to do a slight jump after the sliding and (e) when that jump was finished and the player's right foot was in propulsion mode. Figure (f) depicts the moment the player lifted his right foot and he started moving in the opposite direction.

In Figure 53 the kinematic data (displacement (a, b), velocity (c), acceleration (d)) of the athlete during sliding are depicted. The graphs can be separated in four regions (I-IV). The first region (I) is when the player was lowering his foot with the start corresponding to Figure 51 (a) and Figure 52 (a). During the lowering phase, the velocity of the toe was decreasing until the end of the region (I) where the player's toe touched the ground (Figure 51 (b), Figure 52 (b)). In the region (II) the player was sliding on the surface and the velocity of his toe was increasing until a point and then it started decreasing until it became zero (Figure 51 (c)). In the region (III) the athlete performed a small jump (Figure 51 (d, e)) during which the velocity remained stable and in the region (IV) the player started to move on the opposite direction (Figure 51 (f)). During this propulsion phase, it can be observed the lower vertical displacement and the higher acceleration while the velocity was increasing again.

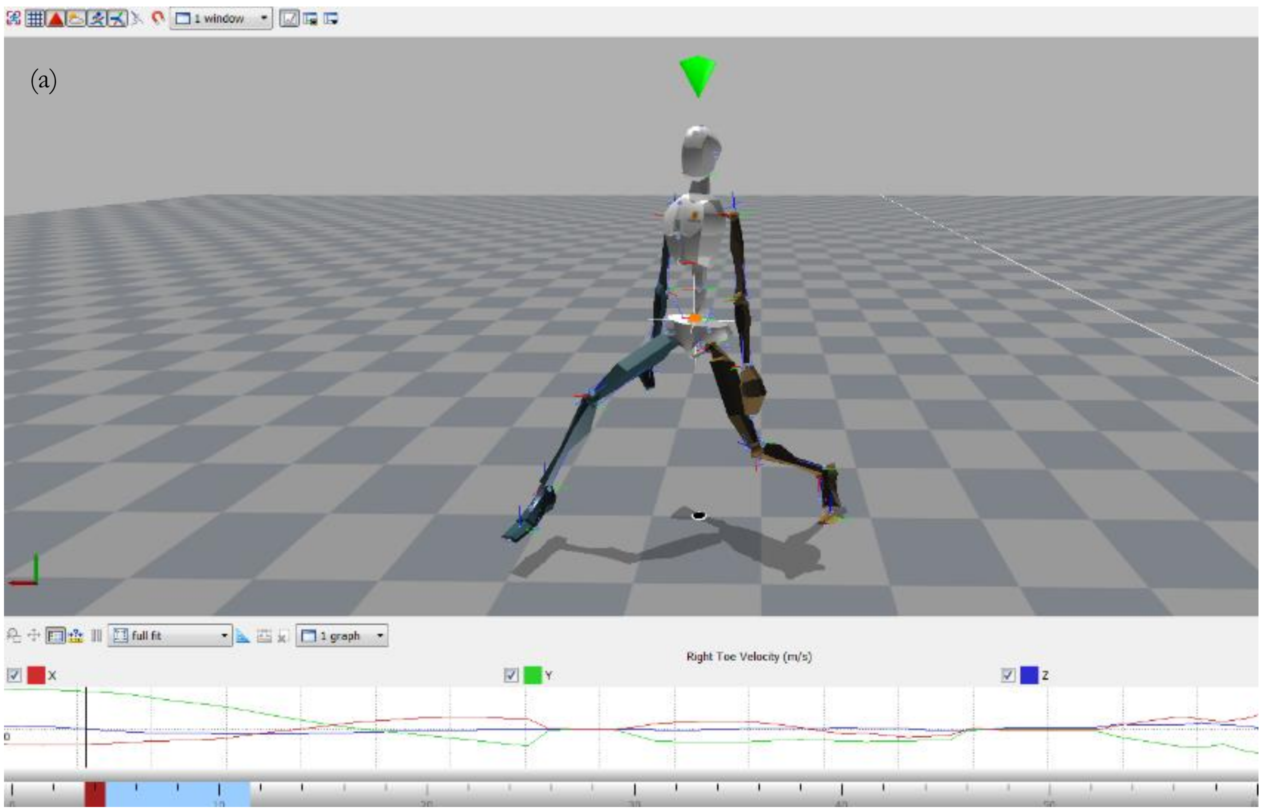

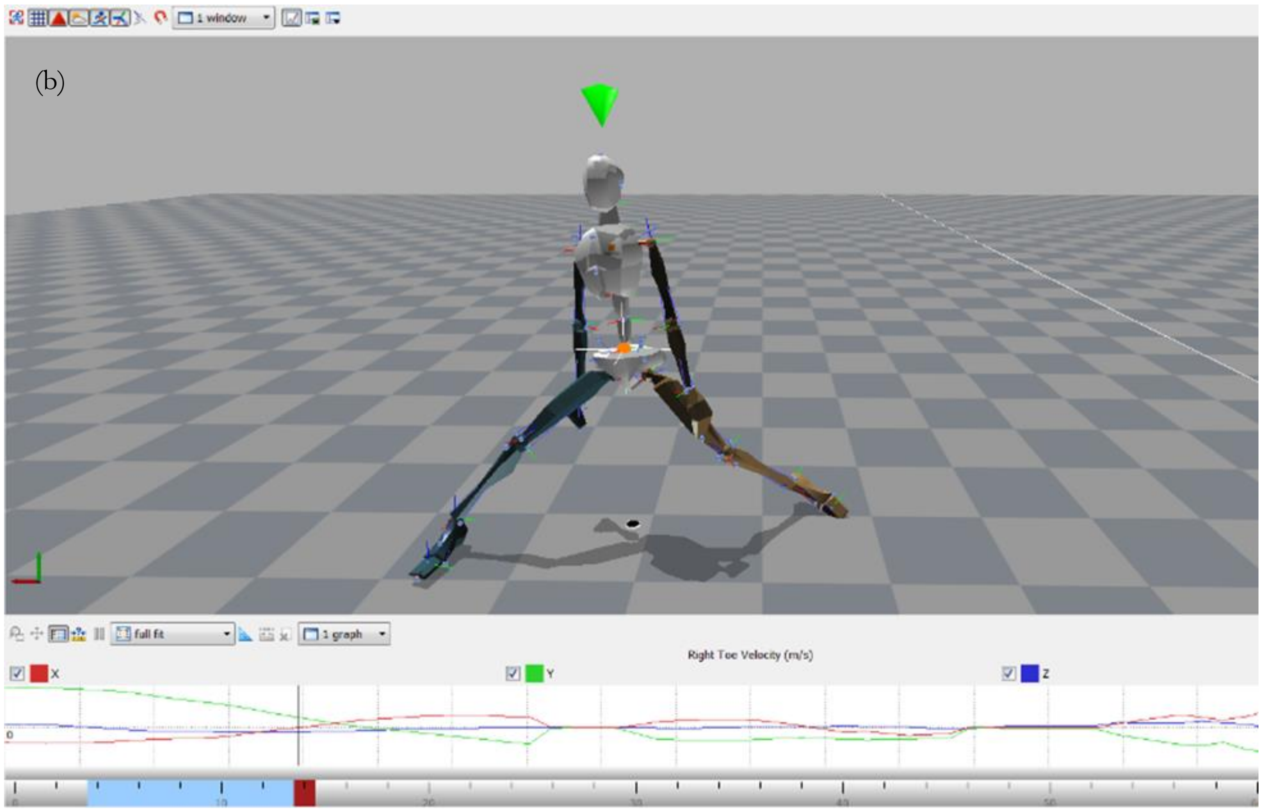

Figure 52. Sliding movement in the Lindome tennis court. Captures within the Xsens Biomech software. In figure (a), the moment the player started to lower his leg is depicted and in figure (b), the moment the athlete's foot touched the ground is presented.

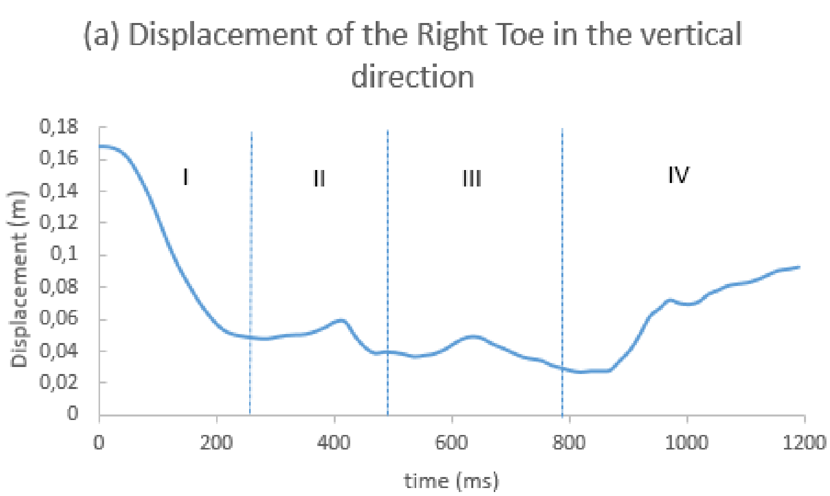

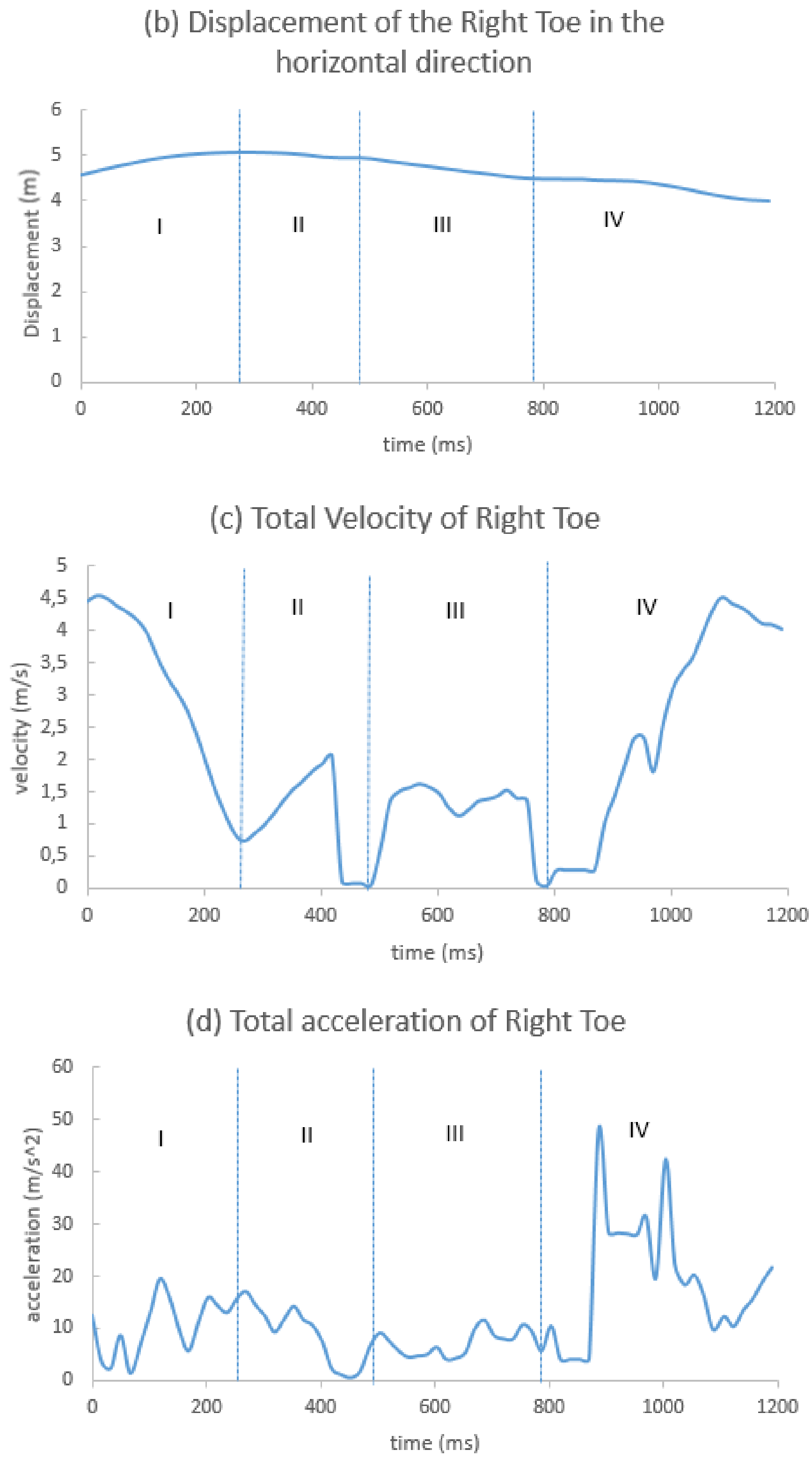

Figure 53. Kinematic data of a sliding movement in Lindome court. The figures refer to the right toe of the athlete. Figure (a) describes the displacement of the toe in the vertical direction (z-axis) while figure (b) refers to the horizontal displacement of the toe (x-y plane). Figure (c) analyses the total velocity of the toe and figure (d) the acceleration that was developed.

6.2 Friction Test

In Figure 54, the sliding movement is depicted. In (a) it was the starting position of the arm, while in (b) it was the moment the sample touched the ground. In (c) it was when the sample was sliding on the court and in (d) the moment it stopped. In (e) the arm started to return in its initial position and in (f) it can be noticed the trace of the shoe on the surface and the material aggregation at the end of the sliding phase.

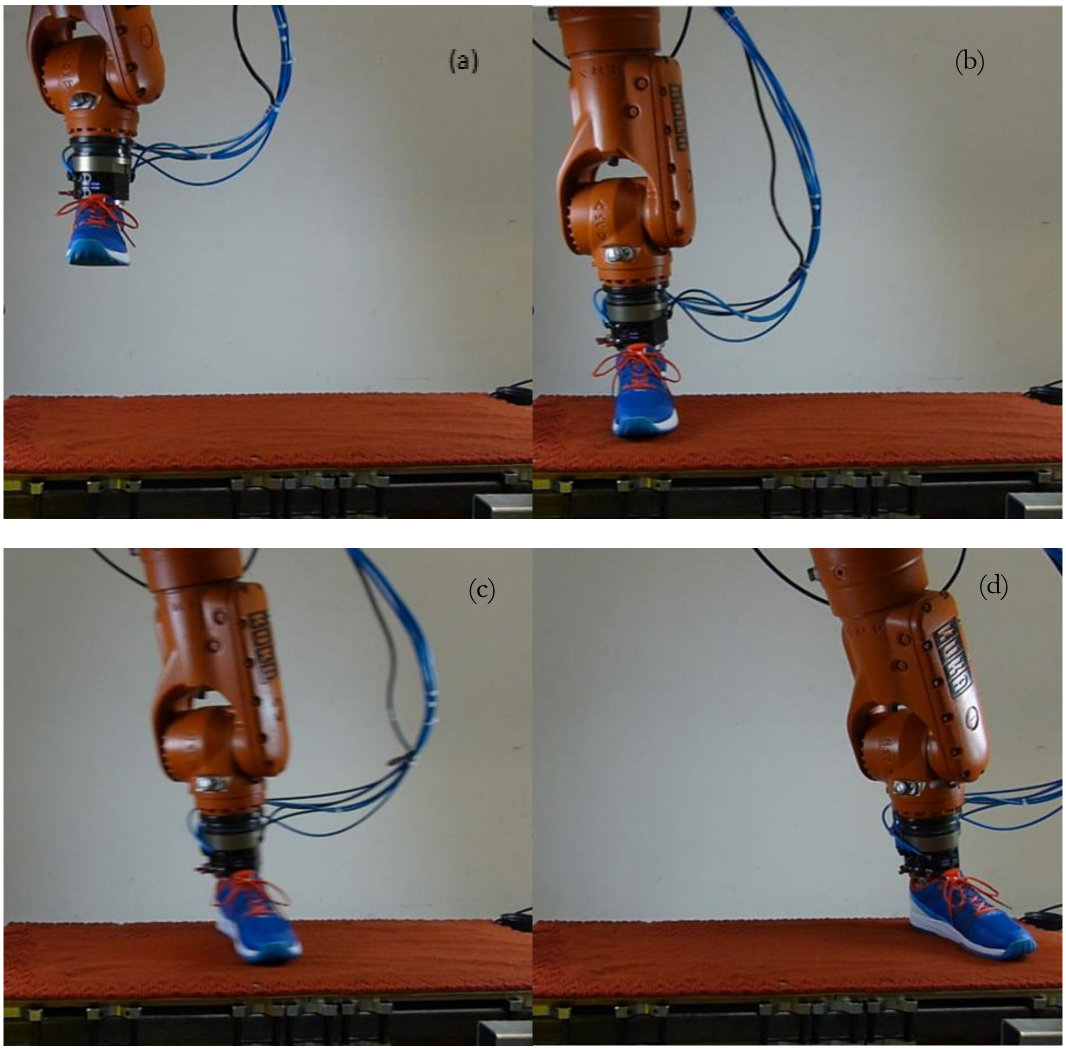

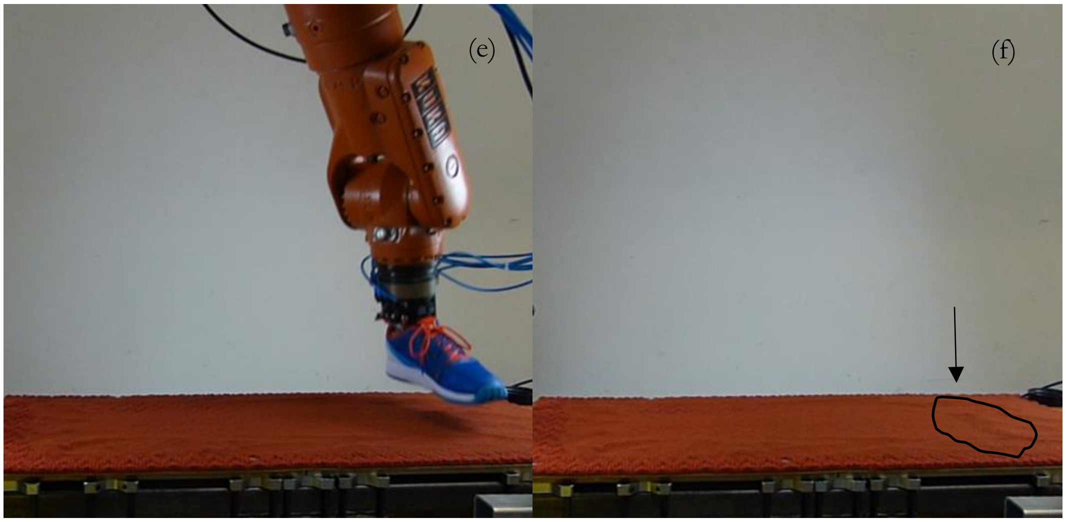

Figure 54. The sliding movement of the shoe-robot system in six frames (a-f).

In Figure 55, the shoe sample after repetitive testing is presented. It can be noticed that ceramic stand is stuck inside the shoe, which may affect the force results.

Figure 55. The shoe sample after repetitive testing.

In Figure 56, the forces developed on the shoe sample during a linear motion are presented. A Swiss Cross carpet and M ceramic sand were used with two different initial vertical forces, 480 N in the first test and 180 N in the second test. Initially, the sample was moved in the vertical direction where it was pressed upon the surface for 0.5 seconds and then it was dragged in the horizontal direction. When the movement started, shear force (F_{shear}) was developed with values lower than those of the vertical force. The movement stopped after 0.6 seconds. The test with the higher initial vertical force resulted in higher shear forces and in lower utilized coefficient of friction which became similar in both tests at the end of the motion. The ceramic sand had been distributed evenly with a brush after each experiment to assure similar testing surface. According to [21, 24], the transition between the static and dynamic area occurred when the utilized coefficient of friction was the maximum. Therefore, two areas of interest could be mentioned during the movement part and they are depicted in Figure 56. Area A, which is the area that the movement initiated, and area B, which is the area the shoe was sliding. In A during the first test, with the initial lower vertical force, the utilized coefficient reached its peak value of 0.8, whereas in the second test with the higher initial vertical force, the utilized coefficient was 0.7 and then it continued to rise. In B, the two tests exhibited similar behaviour with average utilised coefficients of 0.78 and 0.75 for the first and the second tests, respectively. In both tests the vertical (Fz) and shear forces (Fshear) developed were higher in A area compared to B area.

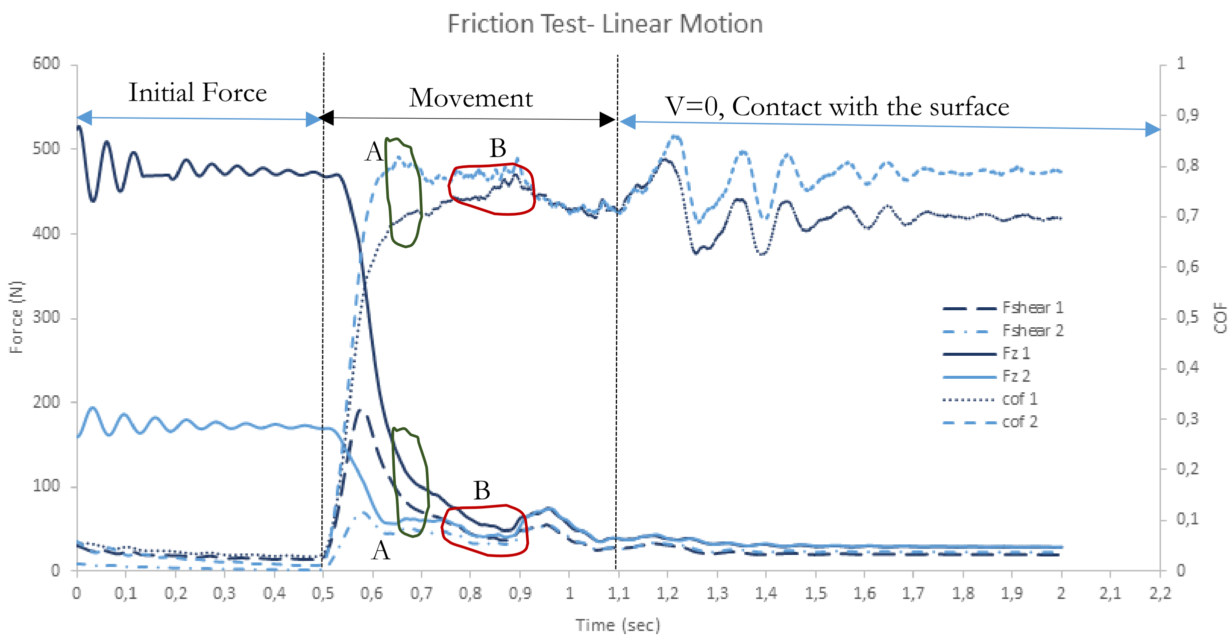

Figure 56. Linear Motion of the shoe sample with different initial vertical force, using S carpet and M ceramic sand.

In Figure 57, the forces developed on the shoe sample during a planar motion are illustrated. A Swiss Cross carpet and M ceramic sand were used with initial vertical force of 300 N. Similarly to the linear motion, the sample was initially moved in the vertical direction where it was pressed upon the surface for 0.57 seconds and then it was dragged in the horizontal direction. When the movement started, shear forces were developed with values lower than those of the vertical force. The movement stopped after 0.6 seconds. The utilized coefficient of friction in this case was ascending during the movement in contrast to the linear motion in which it started to decrease at the end of the motion. Two areas could also be noticed in that case, area A and B with 0.65 and 0.7 average coefficients of friction, respectively. In both tests the vertical (Fz) and shear forces (Fshear) developed were lower in A area compared to B area, which is the opposite of what occurred during the linear motion. The ceramic sand had been distributed evenly with a brush before the experiment to assure similar testing surface to the linear motion.

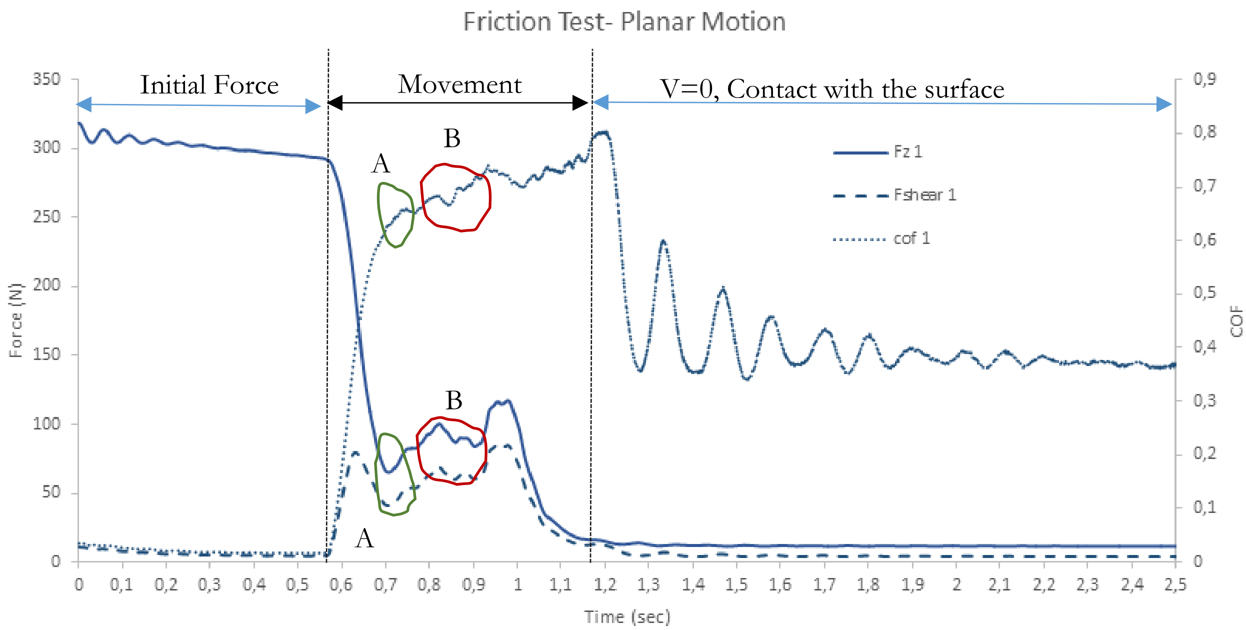

Figure 57. Planar Motion of the shoe sample, using S carpet and M ceramic sand.

In Figure 58, the forces developed on the shoe sample during a planar motion are depicted. A Swiss Cross carpet and M ceramic sand were used and the tests 2 and 4 were performed with two different initial vertical force values, 70 N and 140 N, respectively. Similarly to the previous movements, the sample was initially moved in the vertical direction where it was pressed upon the surface for 0.57 seconds and then it was dragged in the horizontal direction. When the movement started, shear force was developed with values lower than those of the vertical force. The movement stopped after 0.6 seconds. The ceramic sand had been distributed evenly with a brush before the first experiment and then the experiments were performed without adjustment of the sand. Therefore, in the second experiment the surface was covered with less ceramic sand compared to the first and during the fourth experiment there was very little sand still on the carpet because it was concentrated at the end of the sliding movement. Those consecutive sliding motions without sand's repositioning may imitate the court surface during long rallies while the court is not brushed. The utilized coefficient of friction in this case was decreasing during the movement and it started to increase at the end of the motion. Two areas could also be analysed in that case, areas A and B. For test 2, the utilized coefficients of friction were 0.82 and 0.74 for areas A and B, respectively while for test 4 they were 0.92 and 0.78. Additionally, the developed forces, in shear and vertical direction, presented a different pattern compared to the planar motion in which the shoe sample was sliding primarily on the ceramic sand and not on the carpet like it occurred to the second and fourth experiment.

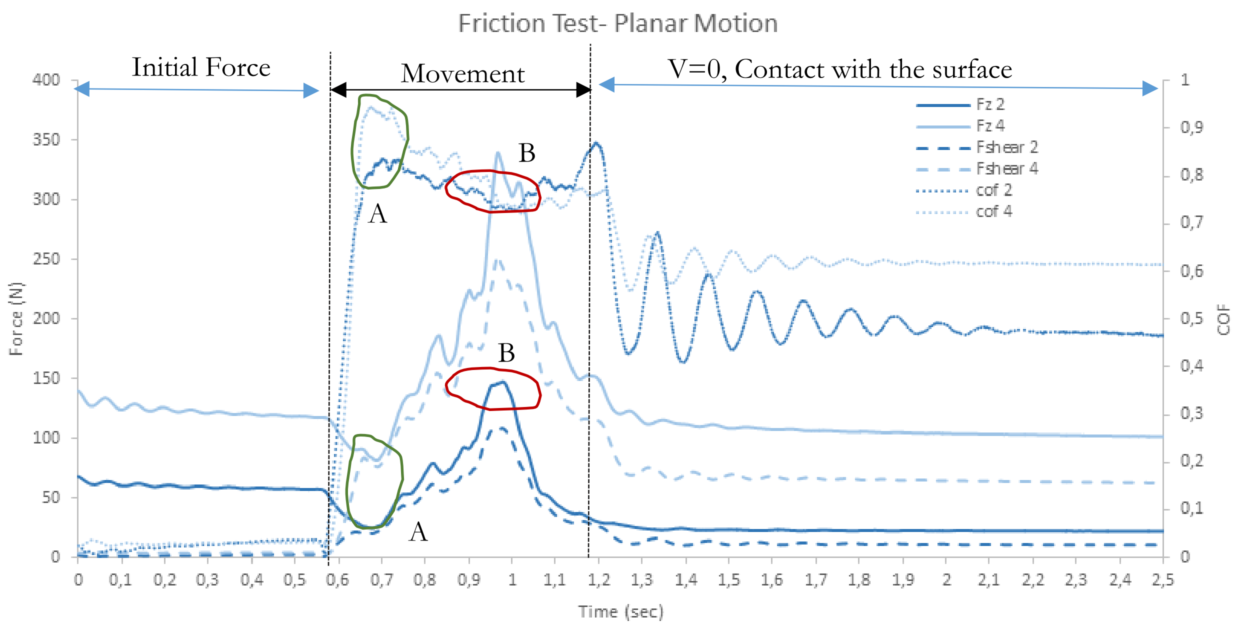

Figure 58. Planar Motion of the shoe sample with different initial vertical force, using S carpet and M ceramic sand.

6.3 Interview

The questions asked and the player's response are the following:

1. **Could you please compare the court with the Swiss Cross carpet and the 0.4-0.8 ceramic sand (SM) to the court with Fishbone Carpet and the 0.1-0.3 ceramic sand (FF) in terms of stiffness and slipperiness?**

– The Fishbone carpet may be a little stiffer compared to the Swiss Cross carpet but it is very smooth to run on. It has also a better ball bounce due to the slightly increased stiffness. The slipperiness is affected by the particle size and the moisture of the court. It is significantly lower for thinner sand and the optimal conditions are reached when the ceramic sand is slightly wet. Then it is not slippery at all. However, a problem occurs when the court is filled in with too much sand and it is very dry. Then, very good clay courts are needed otherwise the court may become very slippery.

2. **Which court requires more frequent maintenance?**

– When you play on the fishbone carpet with normal clay, much more maintenance is needed compared to the same carpet filled in with ceramic sand, where the required maintenance is very slight. The normal clay needs often watering and high pressure wash once per year.

3. **Could you please describe the importance of the court's slipperiness, stiffness, energy return, compaction from the player's perspective?**

– The most important parameter of the clay court is probably its slipperiness. The compaction can also be crucial because if the court is not appropriately compacted, the ball bounce will be insufficient causing problems to the game. After those, it is the energy return. However, the hierarchy depends also on the type of the player, his age and preferences. If a 60-year old player is asked, he would probably appreciate more the energy return. But playing on clay courts in generally better for your body compared to the game on hardcourts.

4. **What do you think that should be improved in the existing synthetic clay courts and where should the future research focus on?**

– The most important improvement of the existing synthetic clay courts would be the extension of the carpet's life. Right now, when the carpet is combined with normal clay, it wears out quickly due to the high compaction of the normal clay, which becomes like concrete. In addition, the courts should dry faster than they do today. Those problems do not exist when ceramic sand is used as the ceramic sand particles do not stick together. A possible future research topic would be the investigation of the infill material, how and if ceramic sand and normal clay could be combined so that the particles of the hybrid material would not stick together beyond a desirable point, the ball bounce would be still good, the court would not be slippery and the high pressure wash would be performed every 3-4 years.

7. Discussion

7.1 Compression Test

Force-Displacement curve

During cyclic loading the first cycle presented high non-linearity, possibly depending on the sample's initial state and the machine's characteristics. The behaviour cannot be predicted and it appeared in both dense and loose samples. The effect of the initial cycle was minimized after five consecutive cycles for samples with varying loading history. Furthermore, in the force-displacement graph (Figure 35 and Figure 38), it can be noticed that when the loading rate (N/s) was increased, the shape of the hysteresis loop changed, the inclination of the loading phase was raised and the consecutive cycles were more condensed inducing lower total strain accumulation. This can be explained if it is considered that when the loading rate was lower the material had more time to deform for the same forces [55]. In addition, the changes of the hysteresis loop showed how the properties of a surface were altered under repeated loading and the significance of compaction on sport surfaces [19].

For the same loading rate with the increasing number of cycles the percentage of energy dissipation was decreased and the secant modulus was increased. Similar behaviour was observed during cyclic loading of soils used for natural turf surfaces [19]. In addition, energy transformation occurred during the whole contact time and therefore, the loading frequency should be adjusted to be as close as possible to real measurements [13].

Carpet-Material combination

Regarding the carpet-material correlation, when the type of carpet was kept the same, the carpet-material combination with finer (F) and medium (M) ceramic sand had lower percentage of energy dissipation and stiffer response, potentially due to the denser state of the material. The C ceramic sand had also higher percentage of strain accumulation. When a type of ceramic sand was tested with different carpets, the combination with the F carpet provided the lowest percentage of energy dissipation and the lowest strain accumulation for both F and C ceramic sand, while the stiffness being at similar levels.

To sum up, based on the compression test results of this thesis, there is an indication that the response of the carpet-material combination will depend on the type of the carpet and the ceramic sand used, as well as the loading history and the loading rate of the sample. Additionally, the carpet selection will influence the percentage of energy transformation and the strain accumulation while the material alteration has an additional effect on the modulus of the system.

The results of compression tests could be initially used for a relative comparison between the different carpet-material combinations. Afterwards, they could potentially be combined with perception questionnaires or interviews with players who had previously played on the same surface and could rate how the surface responded according to their opinion. In this way, a reference table could be created with moduli and energy transformation values for the optimal surface based on the player's input and every new material-carpet combination will be tested in the lab and its values will be compared with the values of the optimal surface and then it could be decided if this combination is acceptable or not. Thus, surfaces which submit the player to significantly high loads or fatigue could be avoided.

Additionally, if data from a real court's usage, maintenance and weather conditions could be collected for a long term period, the form of cyclic loading could be adjusted to imitate those conditions. Subsequently, compaction and its effects for each carpet-material combination could be studied allowing the choice of a surface combination that demands less maintenance.

7.2 Motion Capture System

The motion capture system results offered an insight into the kinematic characteristics of the sliding movement based on the player's measurements. Those results were used to set up the robot-assisted friction test. Measurements of force or pressure during testing will enable a more spherical approach of the testing and will facilitate a straightforward comparison with the results produced by the robot. Additional movements [26], which may be critical for slipping to occur could also be studied and implemented by the robot. Biomechanical measurements could help the better understanding of the kinematics of the tennis player and the forces developed during dynamic movements and contribute to the development of bio-inspired mechanical test rigs with settings closer to those experienced by the athlete resulting in more realistic measurements [25].

7.3 Friction Test

The friction test through the robot arm provided an initial approach to the investigation of the friction mechanisms and of the forces exerted on the athlete during dynamic movements. The sliding experiments were performed at higher velocities compared other mechanical tests [21] and close to those the player in Figure 53 (c) experienced. Additionally, the normal force varied with time and it imitated the adaptations the human foot undergoes during motion [24, 26, 56], producing more realistic measurements.

The two different velocity profiles produced two different shear force profiles. The linear motion exhibited forces similar to a running forehand in [26] and the planar motion produced forces similar to a sliding movement in [24]. The developed forces were also different when there was a layer of ceramic sand under the shoe sample compared to the experiments where the main contact was between the shoe and the carpet. This may be explained by the different friction mechanisms developed during contact, which in the first case is rolling friction and in the second sliding friction [51]. Regarding the forces, a significant reduction of the vertical force can be observed in the start of the movement part and the robot's settings should be modified to avoid this drop.

The utilized coefficients of friction presented values higher than those in literature and in some cases their peak values did not coincide with the initiation of the sliding but they were developed during the sliding phase. This behaviour should be further investigated. It should be also mentioned that the measurements may be affected by the stiff base material. Moreover, the results suggested that different velocity profiles and varying amounts of ceramic sand create different force patterns. Therefore, further analysis should be carried out to analyse the parameters that affect the surface's response.

The results could be used to characterize surface slipperiness when a different carpet material combination is tested. The advantage of the robot is that it could be regulated to execute various movements that are produced by the tennis player, at various loads and speeds and therefore the results could exhibit what level of slipperiness each player may experience based on their playing and body characteristics and how the carpet-material selection may affect the results. Subsequently, the robot assisted frictional testing could be combined with players' perception data and create a reference table similar to the one mentioned in the compression tests, which could act as an evaluator of the new carpet-material combination.

7.4 Interview

The interview with Magnus Gustafsson, who is a former elite tennis player, contributed to the better understanding of the player's opinion of what it is expect from a synthetic clay court and aimed to cross check whether the results of the compression test are perceived similarly by the players or not and what characterizes a "good" surface.

The two main aspects of the court that were mentioned were its compaction level and its slipperiness which should be both optimised. Regarding the comparison of the two courts that exist in reality, his opinion is in line with the compression tests where the fishbone carpet with the finer ceramic sand (FF) had lower maximum deflection in every cycle compared to the swiss cross carpet with the medium ceramic sand (SM). However both combinations exhibited similar secant modulus and the SM combination had a higher resilient modulus, a result that requires a further examination. It was also mentioned that the fishbone-fine ceramic sand combination although it is a little stiffer it presents a very good ball bounce and it is pleasant to play on. Therefore, it may be assumed that the creation of a new clay court surface should be regulated to present properties similar to the FF combination.

7.5 Limitations

Compression Test

The results of the compression test are limited by the type of testing and the number of repetitions performed. The confined axial compression allows deformation only on the vertical axis and therefore, the shear deformations were not examined. In addition, the loading rate (N/s) was three orders of magnitude lower than those experienced by the player during dynamic movements in tennis and due to the dependence of the system's properties on the loading rate, loading rates closer to the real will provide a better understanding of the response and the properties of the surface. In addition, the sample preparation should be adjusted to imitate the actual tennis court at the furthest extent.

Motion Capture System

The results of the motion capture system are limited by the number of the repetitions, the number of the players and the type of the tested courts. Another limitation is the reproducibility of the sliding movement. More control points should be used to achieve a similar sliding movement.

Friction Test

The results of the friction test are limited by the sensor's and robot's functioning and safety range, the restricted possibility of analysis of the kinematic data from the robot, the number of the repetitions and by the use of only one carpet-material combination. In addition, adjustments should be made to the base of the carpet to imitate more the actual court.

8. Conclusion

8.1 General

The performed tests combined with the player's perspective, which was acquired by the interview with Magnus Gustafsson, who is a former professional tennis player, showed that the most significant properties of clay court from player's perspective are its compaction and slipperiness. The court should be sufficiently compacted to provide optimal ball bounce but not too compacted because then it loses its impact absorbing properties. Regarding the slipperiness of clay court, controlled sliding should be provided but the court should not be too slippery leading to loss of grip in critical phases such as direction change, and potentially in high injury risk. Additionally, the energy return of the surface is a factor that should be considered because it could potentially enhance comfort and performance of the player. The target is to reach a balance between those contradictive properties and produce the desirable surface.

During the compaction test, it was noticed that there were observable differences between different carpet material combinations which was confirmed also by the player during the interview. He stated that the Fishbone carpet-Finer ceramic sand combination (FF) was slightly stiffer compared to the Swiss Cross carpet- Medium ceramic sand combination (SM) which could be interpreted by the lower maximum deflection of the FF in each cycle although the secant moduli were the same in both cases. Moreover, the player claimed that FF combination was more "smooth" to run on, which could be explained by the higher percentage of energy return by FF compared to SM. As far as axial strain accumulation is concerned, it could correspond to the compaction rate of the surface and how often maintenance is needed but further investigation should be conducted. Additionally, according to the player the FF combination exhibits the optimal ball bounce and energy return feeling and therefore, this combination's values might be used as a reference for future tested surfaces.

8.2 Answers to the Research Questions

- **What are the parameters that influence the compressive behaviour of the clay court?**

In this thesis, it was observed that the response of the carpet-material combination during force controlled cyclic loading was dependent upon the loading rate of the force, the cycles' number, the carpet's characteristics and the texture, particle size and particle size distribution of the ceramic sand. This is in accordance with literature, where it is stated that compression test results are influenced by the loading magnitude and loading rate of the surface, the loading history of the surface and the material's properties.

- **Is it possible to quantify the compressive behaviour of the clay court with cyclic axial compression tests?**

Yes, the interview with the athlete showcased that the results produced by the cyclic axial compression tests have similarities to the properties perceived by the athlete while playing in similar courts. However, adjustments need to be made so that the results will reflect the values exhibited in reality. Higher loading rates, semi-confined tests and better court simulation in the sample are some of the alterations that would lead to that direction.

- **What are the parameters that influence the frictional behaviour of the clay court?**

In this thesis, one carpet-material combination was tested with varying initial normal force and two different velocity profiles. Additionally, consecutive experiments were carried out without brushing the material between the experiments, leading to testing with different infill volume. All the changes in the parameters resulted in different responses and further investigation is needed to derive the correlations. This is in accordance with literature where it is referred that the frictional behaviour of the surface depends on the loading conditions, the size of the material, the infill volume of the material and the moisture content, resulting in different frictional response when those parameters are varied.

- **Is it possible to measure the frictional properties of the clay court by using a robot?**

Yes, it has been shown in this thesis that the robot could be programmed to imitate various movements performed by the tennis players, and provide both kinematic and kinetic data with the assistance of a force sensor or potentially of a force plate. The velocities developed can be close to those experienced by the player, leading to results close to real values. Testing among distinct carpet-material combinations could help to identify how each component affects the results. Care should be given to the creation of the base where the tests are performed to be like a real tennis court and additionally, a procedure should be developed to assure the same initial conditions.

- **How does the carpet-material combination affect the response of the court and is it possible to choose the best combination from player's perspective?**

The compression test results suggested that the carpet selection will potentially influence the percentage of the energy transformation between the surface and the athlete and the strain accumulation on the carpet- material interface. The material change will additionally affect the modulus of the system. With the existing testing, it is not possible to identify which surface is better. However, the interview with the player assisted in creating a potential reference carpet- material combination, the FF.

8.3 Future work

The next steps in this area after this project should be the following:

Initially, further laboratory compression and frictional tests combined with in court biomechanical tests should be performed at loading rates similar to those developed during dynamic tennis movements. Additionally, shear compression tests and rotational friction tests should be conducted to investigate the system's response. Those experiments will help to achieve a better insight of the court's properties and response and to decide which carpet-material combination is the most appropriate.

Regarding the frictional test, the robot should be programmed based on measurements from motion capture systems. More measurements, at different courts, in various movements and with more athletes should be conducted to be able to simulate more accurately the response of the surface.

The friction and compaction tests should also analyse additional parameters that influence the system's response and weren't included in this thesis such as the effect of moisture content and weather conditions of the location, the influence of infill volume of the material and particles' size and their texture. A new hybrid material, a combination of natural clay and ceramic sand, could also be tested. Moreover, the properties of the carpet should be examined, the effect of its material, thickness, pattern and gluing process, and modifications may be performed. All the experiments should be combined with appropriate players' perception analysis to create reference tables and identify the values of the optimal surface. Combining all the aforementioned data, a model of the carpet- material combination can be created.

Another parameter that should be analysed is wear of carpets and methods to increase their durability. The robot arm can be used to replicate courts action allowing the examination of the carpets' wear under repetitive loading in various forms, by imitating a real court's traffic. Moreover, maintenance procedures of courts should also be analysed. Long term investigation in full scale courts can be conducted to examine the influence of maintenance tools, way of using the tools and frequency of each procedure, on the court's uniformity, response and deterioration. The aim will be to improve the procedure and/or the means used and create a maintenance manual.

References

1. Tennis, in Encyclopædia Britannica, B. Academic, Editor 2012.
2. (ITF), I.T.F. http://www.itftennis.com/technical/home.aspx.
3. Tennis Europe-Sweden. Available from: http://www.tenniseurope.org.
4. Federation, S.T. http://www.tennis.se.
5. Martin, C. and J. Prioux, Tennis playing surfaces: Effects of performance and injuries. Vol. 20. 2015. 6-14.
6. Pavitex, V., CLAYTECH- Clay Court Play- All year long (Brochure), 2015.
7. Kolitzus, H.-J., Criteria for the Development of Guidelines/Standards for Sports Surfaces. ISSS, 3rd Symposium on Sports Surfaces at the University of Calgary 2003.
8. Per Lindstedt, J.B., The value model: how to master product development and create unrivalled customer value. Nimba, 2003.
9. Young, C. and P. Fleming. A review of mechanical impact testing devices for sport surfaces. in STARSS 2007', proceedings of the first international conference of the SportSURF network, Loughborough University, UK. 2007.
10. Durá, H., Lozano, Martínez, The effect of shock absorbing sports surfaces in jumping. Sports Engineering, 1999. **2**(2): p. 103–108.
11. Kolitzus, H.J., Functional standards for playing surfaces. Sport Shoes and Playing Surfaces: Biomechanical Properties. (ed. Frederick, E.C.). Human Kinetics Publishers, 1984.
12. Farhang, B., et al., Landing impact analysis of sport surfaces using three-dimensional finite element model. Proceedings of the Institution of Mechanical Engineers, Part P: Journal of Sports Engineering and Technology, 2016. **230**(3): p. 180-185.
13. Baroud, B. Nigg, and D. Stefanyshyn, Energy storage and return in sport surfaces. Sports Engineering, 2002. **2**(3): p. 173-180.
14. ASTM F1976-13,Standard Test Method for Impact Attenuation of Athletic Shoe Cushioning Systems and Materials, 2013, ASTM International: West Conshohocken, PA.
15. Dixon, S.J. and V.H. Stiles, Impact absorption of tennis shoe-surface combinations. Sports Engineering, 2003. **6**(1): p. 1-9.
16. Carré, M.J., D.M. James, and S.J. Haake, Hybrid Method for Assessing the Performance of Sports Surfaces During Ball Impacts. Proceedings of the Institution of Mechanical Engineers, Part L: Journal of Materials: Design and Applications, 2006. **220**(1): p. 31-39.
17. Durá, J.V., A.C. García, and J. Solaz, Testing shock absorbing materials: the application of viscoelastic linear model. Sports Engineering, 2002. **5**(1): p. 9-14.
18. WANG, X., FLEMING, P.R. DIXON, N, Advanced measurement for sports surface system behaviour. Procedia Engineering, 2012. **34**: p. pp. 825 - 830.
19. Guisasola, I., et al., Dynamic behaviour of soils used for natural turf sports surfaces. Sports Engineering, 2010. **12**(3): p. 111-122.
20. Wang, X., P. Fleming, and S. Forrester, Advanced Measurement of Sports Surface System Behaviour under Player Loading. Vol. 72. 2014.
21. Clarke, J., et al., The development of an apparatus to understand the traction developed at the shoe–surface interface in tennis. Proceedings of the Institution of Mechanical Engineers, Part P: Journal of Sports Engineering and Technology, 2013. **227**(3): p. 149-160.
22. Starbuck, C., et al., The influence of tennis court surfaces on player perceptions and biomechanical response. Journal of Sports Sciences, 2016. **34**(17): p. 1627-1636.
23. Ura, D., et al., Influence of Clay Properties on Shoe-kinematics and Friction During Tennis Movements. Procedia Engineering, 2014. **72**: p. 889-894.
24. Starbuck, C., et al., Biomechanical responses to changes in friction on a clay court surface. Journal of Science and Medicine in Sport, 2017. **20**(5): p. 459-463.
25. Carré, M.J., et al., Friction at the Tennis Shoe-court Interface: How Biomechanically Informed Lab-based Testing can Enhance Understanding. Procedia Engineering, 2014. **72**: p. 883-888.
26. Damm, L., et al., Shoe-surface friction in tennis: influence on plantar pressure and implications for injury. Footwear Science, 2014. **6**(3): p. 155-164.
27. Damm, L., et al., The effect of surface traction characteristics on frictional demand and kinematics in tennis. Vol. 12. 2013. 389-402.
28. Ura, D., et al., Effect of Varying the Volume Infill Sand on Synthetic Clay Surfaces in Terms of the Shoe-surface Friction. Procedia Engineering, 2014. **72**: p. 877-882.

29. Evert, J. How to: Hit a Sliding Forehand. October 22, 2012; Available from: http://www.tennis.com/your-game/2012/10/how-hit-sliding-forehand/39861/.
30. Damm, L., et al., Biomechanical and mechanical testing of non-sliding and sliding tennis surfaces. Footwear Science, 2013. **5**(sup1): p. S117-S118.
31. Head, K.H., Manual of Soil Laboratory Testing, Volume 1 - Soil Classification and Compaction Tests (3rd Edition), Whittles Publishing.
32. Das, B.M., Geotechnical Engineering Handbook, J. Ross Publishing, Inc.
33. Ishihara, K., Soil Behaviour in Earthquake Geotechnics, Oxford University Press.
34. Sas, W., et al., Deformation Behavior of Recycled Concrete Aggregate during Cyclic and Dynamic Loading Laboratory Tests. Materials, 2016. **9**(9): p. 780.
35. Cambou, B., Behaviour of Granular Materials. 1998.
36. Rascol, E., Cyclic properties of sand - dynamic behaviour for seismic applications, 2009, EPFL.
37. Hübel, H., Basic conditions for material and structural ratcheting. Nuclear Engineering and Design, 1996. **162**(1): p. 55-65.
38. Wichtmann, T., A. Niemunis, and T. Triantafyllidis, Strain accumulation in sand due to cyclic loading: Drained triaxial tests. 2005. 967-979.
39. Karg, C. and W. Haegeman, Elasto-plastic long-term behavior of granular soils: Experimental investigation. Soil Dynamics and Earthquake Engineering, 2009. **29**(1): p. 155-172.
40. Titi, H.H., M.B. Elias, and S. Helwany, Determination of Typical Resilient Modulus Values for Selected Soils in Wisconsin. 2006-5.
41. Stolle, D., P. Guo, and Y. Liu, Resilient modulus properties of granular highway materials. Canadian Journal of Civil Engineering, 2009. **36**(4): p. 639-654.
42. Maher, A. and T. Bennert, Resilient Modulus Properties of New Jersey Subgrade Soils. 2000.
43. Liu, Y., et al., Stress-path dependency of resilient behaviour of granular materials. International Journal of Pavement Engineering, 2014. **15**(7): p. 614-622.
44. Ray, R.P. and R.D. Woods, Modulus and Damping Due to Uniform and Variable Cyclic Loading. Journal of Geotechnical Engineering, 1988. **114**(8): p. 861-876.
45. Lekarp, F., U. Isacsson, and A. Dawson, State of the Art. I: Resilient Response of Unbound Aggregates. Journal of Transportation Engineering, 2000. **126**(1): p. 66-75.
46. Darren J. Stefanyshyn, a.B.M.N., Energy and Performance Aspects in Sport Surfaces. ISSS, 3rd Symposium on Sports Surfaces at the University of Calgary, 2003.
47. Nigg, B. and B. Segesser, Biomechanical and orthopedic concepts in sport shoe construction. Vol. 24. 1992. 595-602.
48. Kramer, S.L., Geotechnical earthquake engineering. Upper Saddle River, N.J.: Prentice Hall., 1996.
49. Lin, M.-L., T.-H. Huang, and J.-C. You, The effects of frequency on damping properties of sand. Soil Dynamics and Earthquake Engineering, 1996. **15**(4): p. 269-278.
50. Ray Richard, P. and D. Woods Richard, Modulus and Damping Due to Uniform and Variable Cyclic Loading. Journal of Geotechnical Engineering, 1988. **114**(8): p. 861-876.
51. Mills, R., R.S. Dwyer-Joyce, and M. Loo-Morrey, The mechanisms of pedestrian slip on flooring contaminated with solid particles. Tribology International, 2009. **42**(3): p. 403-412.
52. Nigg, B.M., INJURY & PERFORMANCE ON TENNIS SURFACES The Effect of Tennis Surfaces On the Game of Tennis H. Calgary, Editor November 2003.
53. Svensk Standard SS-EN 933-1: Tests for geometrical properties of aggregates – Part 1: Determination of particle size distribution – Sieving method. 1997.
54. MVN User Manual User Guide MVN, MVN BIOMECH MVN Link, MVN Awinda, Document MV0319P, Revision Q. https://www.xsens.com/, April 2016.
55. Matešić, L. and M. Vucetic, Strain-Rate Effect on Soil Secant Shear Modulus at Small Cyclic Strains. Journal of Geotechnical and Geoenvironmental Engineering, 2003. **129**(6): p. 536-549.
56. Starbuck, C., PLAYER PERCEPTIONS AND BIOMECHANICAL RESPONSES TO TENNIS COURT SURFACES: THE IMPLICATIONS TO TECHNIQUE AND INJURY RISK, in Sport and Health Sciences2014, University of Exeter.

Appendix

Table 6 Compression Test Parameters

	Type of Carpet	Material	Size of material	Quantity of material	Force (N)	Force Rate (N/s)	Number of cycles	Loading History (cycles)	Preparation
Test 1	S	Ceramic Sand	0.4-0.8	43.1gr	0-2000	200	10	0	Material in the middle and then spread
Test 2	S	Ceramic Sand	0.4-0.8	43.1gr	0-2000	200	10	0	Material in the middle and then spread
Test 3	S	Ceramic Sand	0.4-0.8	43.1gr	0-2000	200	10	0	Brushing
Test 4A	S	Ceramic Sand	0.4-0.8	43.1gr	0-2000	200	5	0	Brushing
Test 4B							10	5	Immediately after 4A
Test 5A	S	Ceramic Sand	0.4-0.8	43.1gr	0-2000	200	5	0	Brushing
Test 5B							10	5	Immediately after 5A
Test 6A	S	Ceramic Sand	0.4-0.8	43.1gr	200-2000	200	5	0	Brushing
Test 6B							10	5	Immediately after 6A
Test 6C							10	5+10	Immediately after 6B
Test 7A	S	Ceramic Sand	0.4-0.8	43.1gr	200-2000	200	13	0	Brushing
Test 7B							30	13	Immediately after 7A
Test 7C							10	13+30	Immediately after 7B
Test 8A	S	Ceramic Sand	0.4-0.8	43.1gr	200-2000	200	10	0	Brushing
Test 8B							10	10	Immediately after 8A
Test 9A	S	Ceramic Sand	0.4-0.8	43.1gr	200-2000	200	10	0	Brushing
Test 9B							10	10	Immediately after 9A
Test 9C							10	10+10	Immediately after 9B
Test 10A	S	Ceramic Sand	0.4-0.8	43.1gr	200-2000	200	10	0	Brushing
Test 10B							10	10	Immediately after 10A

Test 10C							10	10+10	Immediately after 10B
Test 11A						200	10	0	Brushing
Test 11B	S	Ceramic Sand	0.4-0.8	43.1gr	200-2000	400	10	10	Immediately after 11A
Test 11C						400	10	10+10	Immediately after 11B
Test 12A							20	0	Brushing
Test 12B	S	Ceramic Sand	0.4-0.8	43.1gr	200-2000	400	10	20	Immediately after 12A
Test 12C							10	20+10	Immediately after 12B
Test 13A							20	0	Brushing
Test 13B	S	Ceramic Sand	0.4-0.8	43.1gr	200-2000	400	10	20	Immediately after 13A
Test 13C							10	20+10	Immediately after 13B
Test 14.1-10	S	Ceramic Sand	0.4-0.8	43.1gr	200-2000	400	10*10	0 (then consecutive sets of 10 cycles)	Brushing
Test F2A							20	0	Brushing
Test F2B	F	Ceramic Sand	0,1-0,3	43.1gr	200-2000	400	10	20	Immediately after .2A
Test F2C							10	20+10	Immediately after .2B
Test F3A							20	0	Brushing
Test F3B	F	Ceramic Sand	0,1-0,3	43.1gr	200-2000	400	10	20	Immediately after .3A
Test F3C							10	20+10	Immediately after .3B
Test F4.1-10	F	Ceramic Sand	0,1-0,3	43.1gr	200-2000	400	10*10	0 (then consecutive sets of 10 cycles)	Brushing
Test T1.1-10	T	Ceramic Sand	0.3-0.9	43.1gr	200-2000	400	10*10	0 (then consecutive sets of 10 cycles	Brushing
T1A T1B T1C	T	-	-	-	200-2000	400	20 10 10	0 20 20+10	Brushing in the beginning

T2A T2B T2C	T	-	-	-	200- 2000	400	20 10 10	0 20 20+10	Brushing in the beginning
F1A F1B F1C	F	-	-	-	200- 2000	400	20 10 10	0 20 20+10	Brushing in the beginning
F2A F2B F2C	F	-	-	-	200- 2000	400	20 10 10	0 20 20+10	Brushing in the beginning
S1A S1B S1C	S	-	-	-	200- 2000	400	20 10 10	0 20 20+10	Brushing in the beginning
S2A S2B S2C	S	-	-	-	200- 2000	400	20 10 10	0 20 20+10	Brushing in the beginning
TF1A TF1B TF1C	T	Ceramic Sand	0,1-0,3	43.1gr	200- 2000	400	20 10 10	0 20 20+10	Brushing in the beginning
TF2A TF2B TF2C	T	Ceramic Sand	0,1-0,3	43.1gr	200- 2000	400	20 10 10	0 20 20+10	Brushing in the beginning
FC1A FC1B FC1C	F	Ceramic Sand	0.3-0.9	43.1gr	200- 2000	400	20 10 10	0 20 20+10	Brushing in the beginning
FC2A FC2B FC2C	F	Ceramic Sand	0.3-0.9	43.1gr	200- 2000	400	20 10 10	0 20 20+10	Brushing in the beginning
SF1A SF1B SF1C	S	Ceramic Sand	0,1-0,3	43.1gr	200- 2000	400	20 10 10	0 20 20+10	Brushing in the beginning
SF2A SF2B SF2C	S	Ceramic Sand	0,1-0,3	43.1gr	200- 2000	400	20 10 10	0 20 20+10	Brushing in the beginning
SC1A SC1B SC1C	S	Ceramic Sand	0.3-0.9	43.1gr	200- 2000	400	20 10 10	0 20 20+10	Brushing in the beginning
SC2A SC2B SC2C	S	Ceramic Sand	0.3-0.9	43.1gr	200- 2000	400	20 10 10	0 20 20+10	Brushing in the beginning